

THESIS

SYSTEM DESIGN AND DEVELOPMENT OF FRONT-X: AN X-BAND
DUAL-POLARIZATION PHASED ARRAY WEATHER RADAR

Submitted by

Alexander Morin

Department of Electrical and Computer Engineering

In partial fulfillment of the requirements

For the Degree of Master of Science

Colorado State University

Fort Collins, Colorado

Spring 2019

Master's Committee:

Advisor: V. Chandrasekar

Margaret Cheney

Christine Chiu

Copyright by Alexander Morin 2019

All Rights Reserved

ABSTRACT

SYSTEM DESIGN AND DEVELOPMENT OF FRONT-X: AN X-BAND DUAL-POLARIZATION PHASED ARRAY WEATHER RADAR

The electronic beam steering capability of phased array weather radars has the potential to improve the temporal resolution of meteorological data and enable the development of multifunction radars, yet questions about their dual-polarimetric performance remain an ongoing topic of research. This thesis presents the system design and development of Front-X, an X-band dual-polarization phased array weather radar capable of both electronic and mechanical beam steering, whose purpose is to serve as a test-bed for implementing adaptive scan strategies, developing phased array radar calibration techniques, and exploring the efficacy of electronic scanning for weather applications. The design, development, calibration, and configuration of a system controller, antenna positioner, and signal processor are discussed. Furthermore, the system is demonstrated through a comparison of polarimetric electronic and mechanical scan weather data, including various electronic scan correction methods, and visually verified through a comparison to data collected with the proven CHILL X-band radar.

ACKNOWLEDGEMENTS

First, I would like to thank my advisor, Dr. V. Chandrasekar, and committee members, Dr. Christine Chiu, and Dr. Margaret Cheney. Thank you Chandra not only for the compelling work, guidance, advice, and priceless idioms, but also for enabling my addiction to world travel and providing me with an incredible and unique graduate school experience. Thank you Dr. Chiu and Dr. Cheney for the willingness to read my thesis and for the opportunity to defend it.

I want to thank my colleagues and friends at the CSU-CHILL Radar Facility, Chief Engineer Jim George, Facility Manager Pat Kennedy, and Dr. Francesc Junyent. Thank you Jim for being my mentor for the past three and a half years, you have been a firehose of knowledge and if they ever call me an engineer someday, I owe it to you. Thank you Pat for sharing your meteorological wisdom, invaluable radar user perspective, entertaining stories, and constant encouragement. Thank you Francesc for transmitting to me your X-band expertise and for teaching me the importance of a good, clean radar.

Thank you to Luke Sankey and the other engineers at the First RF Corporation for working with me to develop a phased array weather radar and generating some of the first polarimetric electronic scan weather data.

Finally, I want to thank my family and friends. Thanks to my parents for inspiring me to go back to school and providing me with aid and encouragement not only for the last three and a half years, but also the past 29. Thanks to my sister for leading by example and providing me with advice and guidance for navigating graduate school. And thanks to my friends and roommates for being there for my lows and for celebrating my highs.

TABLE OF CONTENTS

ABSTRACT	ii
ACKNOWLEDGEMENTS	iii
LIST OF TABLES	vii
LIST OF FIGURES	viii
Chapter 1 Introduction	1
1.1 Motivation	1
1.2 Objective	2
1.3 Thesis Organization	2
Chapter 2 Background Information	4
2.1 Introduction	4
2.2 Basic Principles of Polarimetric Doppler Weather Radar	4
2.2.1 Transmission and Reception of Dual-Polarized Pulses	4
2.2.2 Weather Radar Signal Processing	7
2.3 Parabolic Reflector versus Phased Array Antennas	8
2.3.1 Parabolic Reflector Antennas	8
2.3.2 Phased Array Antennas	9
Chapter 3 System Overview	12
3.1 Introduction	12
3.2 System Controller	13
3.3 Antenna Positioner	14
3.4 FRF166 Phased Array Antenna	15
3.5 Digital Exciter/Receiver	18
3.6 Signal Processor	19
Chapter 4 System Controller	22
4.1 Introduction	22
4.2 PARC Software Architecture	24
4.2.1 Master Thread	24
4.2.2 System Status Structure	27
4.2.3 Task-list	31
4.2.4 Subsystem Handler Threads	31
4.2.5 PARC Command-line Utility	33
4.3 Scan Mode Algorithms	36
4.3.1 Modular Structure	36
4.3.2 Electronic and Mechanical Volume Scan Modes	37
4.3.3 Electronic Scan Calibration Mode	40
4.3.4 Noise Calibration Mode	40
4.4 PARC Configuration	43

Chapter 5	Antenna Positioner	45
5.1	Introduction	45
5.2	Antenna Positioner Hardware Overview	47
5.2.1	Motion Control Computer	47
5.2.2	Encoders	47
5.2.3	Servo-drives and Motors	48
5.2.4	Pedestal	50
5.2.5	Radar Platform	52
5.2.6	Platform Leveling Measurement System	53
5.3	APC Software Architecture	56
5.3.1	Software Overview	56
5.3.2	Main Thread	56
5.3.3	APC Status Structure	57
5.3.4	Encoder Handler Thread	58
5.3.5	Servo-drive Handler Threads	59
5.3.6	APC Command-line Utility	61
5.4	APC Calibration and Configuration	62
5.4.1	Encoder Offsets	62
5.4.2	Position Control Loop	65
Chapter 6	Signal Processor	68
6.1	Introduction	68
6.2	Signal Processing Software Overview	69
6.2.1	Thread Pool Architecture	69
6.2.2	Offline Signal Processing Software	71
6.2.3	Signal Processing Platforms	72
6.3	Front-X Signal Processing Platform	72
6.3.1	Thread Pool Functionality	72
6.3.2	Single Polarization Autocovariance Processing Algorithm	74
6.3.3	Alternating Polarization Autocovariance Processing Algorithm	76
6.3.4	Electronic Scan Calibration Mode	79
6.3.5	Noise Calibration Mode	80
6.4	Downstream Software	81
6.4.1	Archiver	81
6.4.2	Binary-to-NetCDF Converter	81
6.4.3	Real-Time Display	83
6.5	Signal Processor Calibration and Configuration	84
6.5.1	Short-to-Long Pulse Transition	84
6.5.2	Radar Constant	85
6.5.3	Z_{dr} Bias Correction	87
6.5.4	Power Correction and Phase Rotation Tables	90

Chapter 7	System Operation and Demonstration	97
7.1	Introduction	97
7.2	July 27th, 2018: Electronic Scan versus Mechanical Scan	97
7.2.1	Reflectivity	98
7.2.2	Differential Reflectivity	102
7.2.3	Differential Phase	106
7.3	June 16, 2018: Front-X versus CHILL X-Band	108
Chapter 8	Summary and Future Work	115
8.1	Summary	115
8.2	Future Work	117
Bibliography	120

LIST OF TABLES

3.1	FRF166 phased array antenna specifications	15
3.2	Digital Exciter/Receiver specifications	18
3.3	Signal processing computer specifications	21
4.1	PARC system status structure fields	29
4.2	Functionality of the PARC command-line utility	34
5.1	Functionality of the APC command-line utility	62
6.1	System parameters and physical constants used to calculate radar constant	86
7.1	Scan parameters used to collect data for the July 27 weather event	98
7.2	Scan parameters used to collect data for the June 19 weather event	109

LIST OF FIGURES

2.1	Visualization of the basic principles of weather radar	6
2.2	Visualization of the basic principles of phased array antennas	11
3.1	Front-X system block diagram	12
3.2	Picture of the two-dimensional antenna positioner	14
3.3	Oscilloscope screenshot showing triggers and IF transmit signal to the FRF166	17
3.4	Spectrum analyzer screenshot showing IF transmit signal spectrum from the DXR	20
4.1	System controller block diagram	23
4.2	PARC master thread state machine diagram	26
4.3	PARC subsystem handler thread state machine diagram	33
4.4	Master thread flowchart for the electronic volume scan mode	38
4.5	Master thread flowchart for the mechanical volume scan mode	39
4.6	Master thread flowchart for the electronic scan calibration mode	41
4.7	Master thread flowchart for the noise calibration mode	42
5.1	Antenna positioner block diagram	46
5.2	Servo-drive current loop tuning in DriveWare	49
5.3	Antenna mechanical orientations	51
5.4	Plot of elevation motor current draw versus elevation angle	52
5.5	Plot of off-angle versus azimuth angle for unlevelled and levelled platform	54
5.6	PID position control loop block diagram	61
5.7	Azimuth encoder offset measurement and verification	64
5.8	PID position control system responses	66
6.1	Signal processor block diagram	70
6.2	Sample-time diagram of receive pulses in single polarization processing modes	74
6.3	Sample-time diagram of receive pulses in alternating polarization processing modes	77
6.4	Screenshot of the real-time display and command-line output	83
6.5	Comparison of uncalibrated versus calibrated short-to-long pulse transition	85
6.6	Comparison of dBZ for Front-X, using light rain bias correction, and CHILL X-band	88
6.7	Comparison of Z_{dr} for light rain, with and without a bias correction	89
6.8	Comparison of Z_{dr} for Front-X, using light rain bias correction, and CHILL X-band	91
6.9	Comparison of Z_{dr} for Front-X, using a -2 dB bias correction, and CHILL X-band	92
6.10	Electronic scan calibration results for horizontal power correction	94
6.11	Electronic scan calibration results for vertical power correction	95
6.12	Electronic scan calibration results for differential phase rotation	96
7.1	PPIs showing dBZ for electronic scan and mechanical scan on July 27	99
7.2	Difference in dBZ between electronic and mechanical scan at 5.7 km on July 27	100
7.3	Difference in dBZ between electronic and mechanical scan at 12.1 km on July 27	101
7.4	PPIs showing Z_{dr} for electronic scan and mechanical scan on July 27	103

7.5	Difference in Z_{dr} between electronic and mechanical scan at 5.8 km on July 27	104
7.6	Difference in Z_{dr} between electronic and mechanical scan at 10.0 km on July 27	105
7.7	PPIs showing Φ_{dp} for electronic scan and mechanical scan on July 27	106
7.8	Difference in Φ_{dp} between electronic and mechanical scan at 5.3 km on July 27	107
7.9	PPIs showing dBZ for Front-X and CHILL X-band on June 19	110
7.10	PPIs showing Z_{dr} for Front-X and CHILL X-band on June 19	111
7.11	PPIs showing Φ_{dp} for Front-X and CHILL X-band on June 19	112
7.12	PPIs showing velocity for Front-X and CHILL X-band on June 19	113

Chapter 1

Introduction

1.1 Motivation

The electronic beam steering capability of phased array antennas has several advantages over the mechanically steered parabolic antennas that are traditionally used for weather radar. While mechanical beam steering is limited by the ability of the antenna positioner to overcome the inertia of the antenna, electronic beam steering enables fast and flexible scanning through the electronic phase control of the radiating elements which compose the phased array antenna. Rapid, agile scanning allows for the collection of high temporal resolution data and opens up the possibility of multifunction radars capable of detecting weather and aircraft, among other targets. The collection of high temporal resolution weather data is crucial for improving the observations of short lived weather phenomena including the detection of hazardous weather, now-casting, and aviation guidance [1]. Scan strategies which adapt to the space-time variability of weather can be used to further reduce scan times without compromising data quality by collecting more samples from rapidly evolving regions [2]. Furthermore, a multifunction radar which saves cost by using one system to be solely responsible for weather sensing, air traffic control, and defense surveillance missions, is only possible with the agile scanning provided by electronic beam steering [3].

Phased array weather radars present many challenges, particularly the issue of dual-polarization performance required for useful meteorological observations. Dual-polarization capability is invaluable for weather radar as it provides meteorologists with data about the size, shape, orientation, density, and composition of hydrometeors. Because the differences in the returned horizontal and vertical signal from hydrometeors is typically very small, a well calibrated system which accounts for differences in the polarization paths is crucial for accuracy [4]. It has been shown that for phased array weather radars, in addition to poor cross-polar isolation for electronic scan angles far off boresight, the differences in the horizontal and vertical beams are dependent on electronic scan

angle which complicates the issue of weather radar calibration and measurement [5]. As a result, the investigation and calibration of dual-polarization phased array weather radars is an ongoing topic of research.

1.2 Objective

The Front-X weather radar is a dual-polarization X-band system which uses a phased array antenna for electronic beam steering and an antenna positioner for mechanical beam steering. As a result, Front-X is a system which can be used to self-validate electronic scan data with mechanical scan data, as well as provide a research test-bed for implementing adaptive scan strategies and phased array radar calibration techniques. The objective of this thesis is to provide a discussion of the system design and development of Front-X, in addition to the demonstration of the system by presenting a comparison of polarimetric weather data using electronic and mechanical scanning with various calibration and correction techniques.

1.3 Thesis Organization

This thesis presents the system design and development of Front-X, an X-band dual-polarization phased array weather radar, and is organized as follows:

Chapter 2 provides background information useful for understanding the topics discussed in this thesis, including the basic principles of polarimetric weather radar, parabolic antennas, and phased array antennas.

Chapter 3 presents a high-level overview of the Front-X radar system, with a brief hardware and software description of the radar subsystems, including the system controller, antenna positioner, phased array antenna, Digital Exciter/Receiver, and signal processor.

Chapter 4 discusses the design and implementation of the Front-X system controller referred to as PARC, or Phased Array Radar Controller, including the software architecture, scan modes, and software configuration.

Chapter 5 describes the antenna positioner hardware, discusses the design and implementation of the antenna positioner controller software, or APC, and the calibration and configuration of APC.

Chapter 6 presents an overview of the signal processor and downstream archiving and display software, details the implementation of the signal processing algorithms, and discusses the calibration techniques used to calculate the meteorological moments.

Chapter 7 provides a demonstration of the Front-X system by presenting and comparing polarimetric weather data collected using the electronic and mechanical scan modes, with different correction methods, as well as a visual comparison of the data with the CHILL X-band radar.

Chapter 8 summarizes the work presented in this thesis and discusses suggestions for future work.

Chapter 2

Background Information

2.1 Introduction

Polarimetric Doppler weather radars are remote sensing instruments which transmit and receive pulses of polarized microwave energy to detect and measure meteorological targets. These instruments use the measured amplitude, phase, and frequency of the returned signal from a weather target to calculate meteorological moments which enable meteorologists to estimate weather parameters including precipitation rate, precipitation type, air motion, turbulence, and wind shear [6]. In order to collect useful weather data, the beam formed by a radar antenna must be steered using either a traditional parabolic reflector antenna on a mechanical antenna positioner, or with electronic beam steering using a phased array antenna.

Phased array antennas are devices which use a multitude of small, phase-shifted antennas to form an electromagnetic beam and steer it electronically. Electronic beam steering has several advantages over mechanical beam steering, including faster scan times, flexible scanning, configurable beamshape, little to no mechanical wear, modularity, etc. However, phased array antennas are complex and expensive compared to traditional parabolic antennas, and questions about their dual-polarization performance make their application to weather an important topic of research.

This chapter will provide a review of the basic principles of polarimetric Doppler weather radar and a discussion of parabolic versus phased array antennas in the context of weather radar.

2.2 Basic Principles of Polarimetric Doppler Weather Radar

2.2.1 Transmission and Reception of Dual-Polarized Pulses

A pulsed-Doppler weather radar transmits a series of high power microwave pulses into the atmosphere in a narrow beam. The pulses are generated by a transmitter and have duration, or pulse width, on the order of microseconds and are separated in time by a pulse repetition time

PRT. A high-gain antenna forms a narrow conical beam, characterized by its relatively small beamwidth, radiating outward and steered in azimuth and elevation. The pulses travel along the beam axis and are partially scattered back to the antenna by a target at range r , computed by:

$$r = \frac{cT}{2} \quad (2.1)$$

where c is the speed of the and T is the time between when the pulse is transmitted and received by the radar. The target of interest for a weather radar are hydrometeors, the small water particles which compose clouds and precipitation. The signal received at the radar corresponds to the backscattered energy by hydrometeors enclosed in the resolution volume, the region of space bound by the antenna beam and the range resolution. The range resolution is computed by:

$$\Delta r = \frac{c\tau}{2} \quad (2.2)$$

where τ is the pulse width in units of time [7] and the resolution volume can be computed by:

$$V = \frac{\pi r^2 \theta_{bw} \phi_{bw} \tau}{16 \ln(2)} \quad (2.3)$$

assuming a Gaussian shape for the beam pattern, where θ_{bw} and ϕ_{bw} are the azimuth and elevation beamwidths [8]. The meteorological radar equation relates the received power from the scatterers in the resolution volume to the characteristics of the system :

$$P_{rx} = \frac{P_{tx} G_a^2 \lambda^2 \theta_{bw} \phi_{bw} c \tau G_r}{1024 \ln(2) \pi^2 r^2 L_r} \sum_{n=1}^N \sigma_n \quad (2.4)$$

where P_{tx} is the transmitted power, G_a is the antenna gain, λ is the operating frequency, G_r is the receiver gain, L_r is the receiver loss, and σ_n is the backscattering cross-section of the n -th scatterer in the resolution volume [9]. The Doppler frequency shift can be used to determine the velocity of the target:

$$f_{Doppler} = \frac{2v_r}{\lambda} \quad (2.5)$$

where v_r is the mean radial velocity of the scatterers within the resolution volume [10].

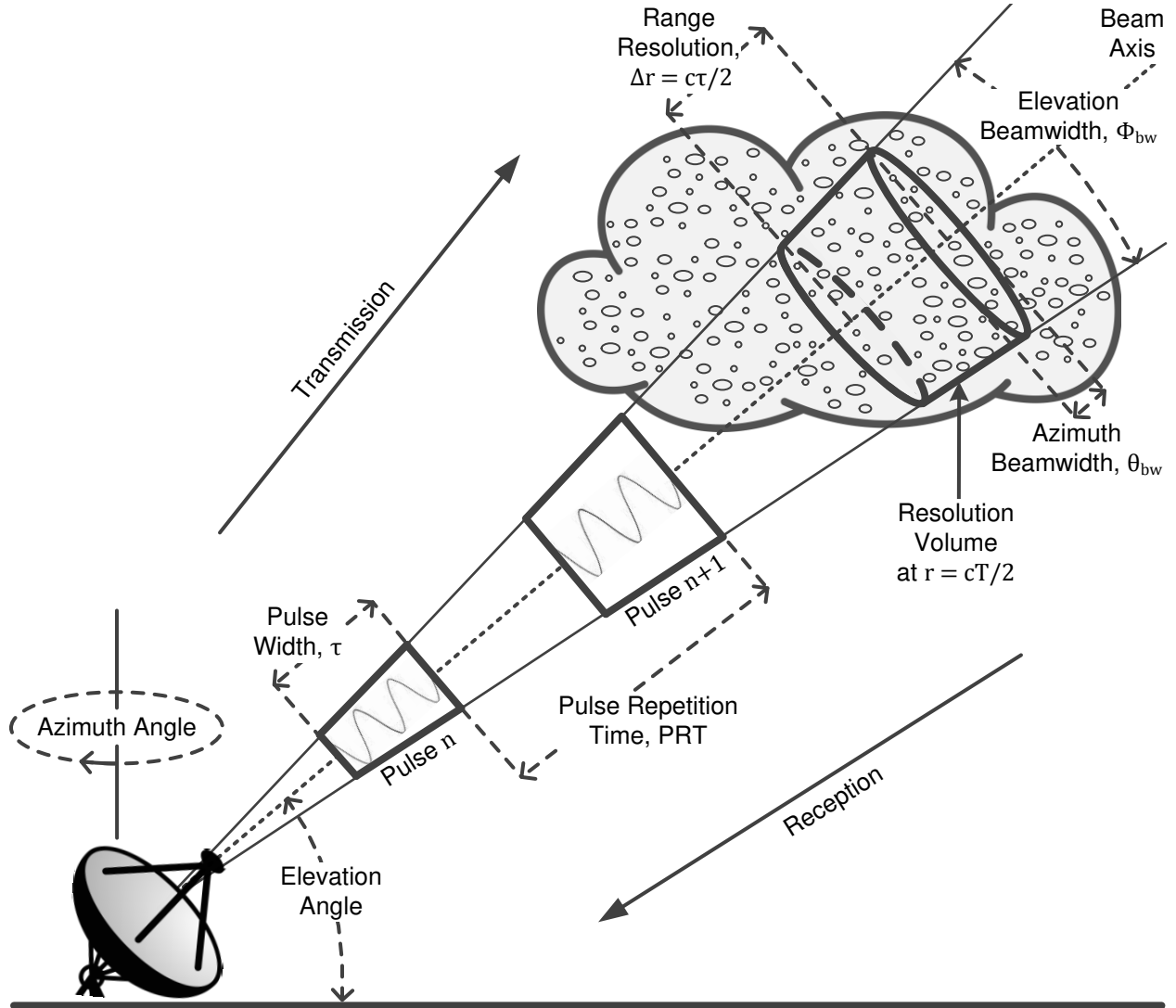


Figure 2.1: Visualization of the basic principles of weather radar: the transmission and reception of a steerable beam of electromagnetic pulses directed towards a weather target composed of reflective hydrometeors.

The pulses transmitted by a polarimetric weather radar are horizontally and vertically polarized in order to characterize the size, shape, orientation, density, and composition of hydrometeors in a resolution volume. The power and phase differences of the received signal between horizon-

tally and vertically polarized pulses due to characteristics of the scatterers can be used to derive improved rainfall rates and distinguish types of precipitation [11]. Depending on the capabilities of the radar system, two different polarization modes can be used: one in which horizontal and vertical pulses are transmitted and received simultaneously, and the other in which the pulses alternate between horizontal and vertical polarization. The simultaneous polarization mode requires two independent receive channels which can be used to measure the cross-polar signals in order to gain additional information about the scatterers and the polarization performance of the radar. The alternating polarization mode can be used in a radar system with just one receive channel, however a cross-polar measurement is only possible with two independent channels.

2.2.2 Weather Radar Signal Processing

A weather radar digitizes the received signal and processes the digital data to calculate the meteorological moments used to derive information about the weather. During the listening period after the transmission of a pulse:

$$T_{rx} = \text{PRT} - \tau \quad (2.6)$$

the antenna is connected to the receiver which samples the in-phase and quadrature components of the voltage of the received signal, generating a set of complex values versus range at equally spaced range bins. Due to the statistical uncertainty of the signal received by hydrometeors, one single sample at a given range bin is insufficient to estimate the meteorological moments [7]. Therefore, the antenna beam is steered such that a multitude of pulses are transmitted and received at the same elevation and azimuth angles in order to collect a statistically significant number of samples to estimate the meteorological moments at each of the range bins for a given ray.

The meteorological moments calculated by a polarimetric Doppler weather radar signal processor include reflectivity, velocity, spectral width, differential reflectivity, differential phase, specific phase, correlation coefficient, and linear depolarization ratio. A given value for a meteorological moment corresponds to the hydrometeors within one resolution volume at a particular range gate, and azimuth and elevation angle. The reflectivity represents the radar cross-section of the hydrom-

eteors per cubic meter in units of mm^6/m^3 , but is typically expressed on a decibel scale. The velocity is the mean radial velocity with respect to the radar of the hydrometeors in meters per second, while the spectral width is the variance of the velocity which corresponds to turbulence. The differential reflectivity is the ratio of horizontal reflectivity to vertical reflectivity in decibels, and gives information about the average hydrometeor shape which in turn can be used to determine rain drop size, rain rate, and precipitation type. The differential phase is the difference in phase, in degrees, between the received vertical and horizontal pulses due to hydrometeor shape. The derivative of differential phase is the specific phase, expressed in degrees per kilometer, which can also be used to determine rain drop size, rain rate, and precipitation type due to hydrometeor shape. The correlation coefficient represents the homogeneity of the hydrometeors in size and shape and can be used to determine precipitation type, particularly if it is mixed or not. Linear depolarization ratio, only calculable with two independent receive channels, is the ratio of the cross-polar vertical reflectivity normalized by the horizontal reflectivity, and can be used to determine canting angle of hydrometeors and thus gives more information about precipitation type [9]. The specific methods used to calculate the meteorological moments presented in this document are discussed in Chapter 6.

2.3 Parabolic Reflector versus Phased Array Antennas

2.3.1 Parabolic Reflector Antennas

An antenna is used in weather radar to convert a guided electromagnetic wave into a narrow beam which radiates towards a weather target and collects the scattered signal. One of the key characteristics of an antenna is its gain, which is the parameter used to describe how much of the input power is converted into useful radiated power in a particular direction, defined as:

$$G = \epsilon D_{max} \tag{2.7}$$

where ϵ is the antenna efficiency and D_{max} is its maximum directivity. The directivity of an antenna is the ratio of the radiated power intensity U , in watts per unit solid angle, to the total radiated power P_{rad} :

$$D(\theta, \phi) = 4\pi \frac{U(\theta, \phi)}{P_{rad}} \quad (2.8)$$

at a some non-range dependent point in space [12].

A parabolic reflector antenna is the most common type of antenna used for weather radar due to its simplicity in design and low cost in order to achieve high gain [10]. It is based on the principle of geometric optics that a beam incident on the surface of a reflective parabola, or dish, will converge to the focal point, and similarly that the rays incident on the dish emitted by a point source placed at the focal point of the parabola will form a collimated beam that is directed outwards [12]. The maximum directivity of a parabolic reflector antenna can be computed from the area of the antenna aperture A , and the operating wavelength λ :

$$D_{max} = \frac{4\pi A}{\lambda^2} \quad (2.9)$$

In order to perform the scans necessary to collect useful weather data, the beam of a parabolic reflector antenna is steered mechanically using an antenna positioner. The antenna positioner is typically based on a precise servo-mechanism which mechanically steers the antenna and uses feedback from sensors that measure the antenna position to accurately control the beam steering angle. In addition to mechanical maintenance and failures, the major drawback to mechanical beam steering is the inflexibility in scanning due to the relatively slow change in beam steering angle [10].

2.3.2 Phased Array Antennas

A phased array antenna is made up of a multitude of smaller, phase-controlled antennas whose combined radiation pattern forms a high gain beam that can be steered flexibly and rapidly, which can be used for collecting high temporal resolution data as well as for the development of multi-

function radars. By summing the field patterns f of each of the radiating elements that make up the array, the total field pattern F of the phased array antenna can be determined:

$$F(\theta, \phi) = \sum_{n=0}^{N-1} w_n f_n(\theta, \phi) e^{j \frac{2\pi}{\lambda} \hat{r} \cdot \mathbf{r}_n} \quad (2.10)$$

where \mathbf{r}_n is the position vector of the n -th element, \hat{r} is the unit vector in the direction of any point in space (R, θ, ϕ) , and w_n is a complex weight of the form:

$$w_n = |w_n| e^{j\psi_n} \quad (2.11)$$

applied to the field pattern of the n -th element [13].

The magnitude of the weights can be chosen in order to specify the beamshape, while the phase ψ is used to electronically steer the beam formed by the constructive interference of the radiation from the array. In the simple case of a linear array of identical elements with spacing d , 2.10 can be simplified to:

$$F(\theta, \phi) = f(\theta, \phi) \sum_{n=0}^{N-1} |w_n| e^{jn(\frac{2\pi}{\lambda} d + \psi)} \quad (2.12)$$

where if ψ is chosen to be:

$$\psi = \frac{2\pi}{\lambda} d \sin \theta_{scan} \quad (2.13)$$

the array field pattern will have a maximum at an angle θ_{scan} off the antenna boresight, referred to as the electronic scan angle. The summation term in 2.12 which defines the geometry, weighting, and phase shifting of the array is referred to as the array factor A , and can be used to compute the total directivity of the phased array antenna:

$$D_{tot}(\theta, \phi) = |A(\theta, \phi)|^2 D(\theta, \phi) \quad (2.14)$$

where D is the directivity of a single identical element in the array [14].

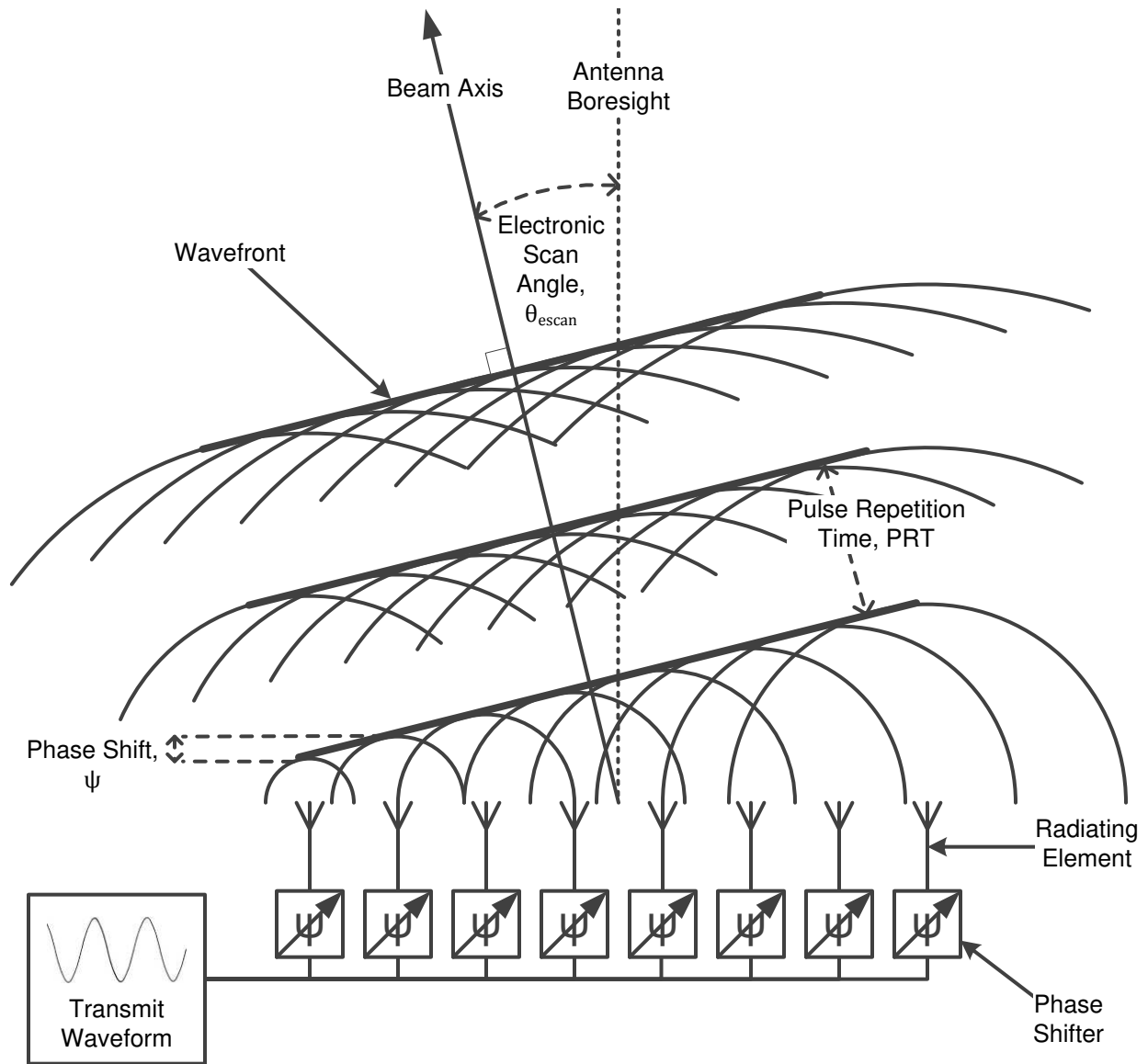


Figure 2.2: Visualization of the basic principle of a phased array antenna: the transmission and reception of an electronically steerable beam of electromagnetic pulses using an array of phase shifted radiating elements.

Chapter 3

System Overview

3.1 Introduction

Front-X is an X-band dual-polarization phased array weather radar capable of both electronic and mechanical beam-steering for executing radar scans. The system is composed of four subsystems: the antenna positioner, the phased array antenna, the Digital Exciter/Receiver, and the signal processor. A system controller is responsible for coordinating the radar subsystems to run scans and configure the system based on user commands from a system control client. This chapter will provide an overview of the system controller and radar subsystems.

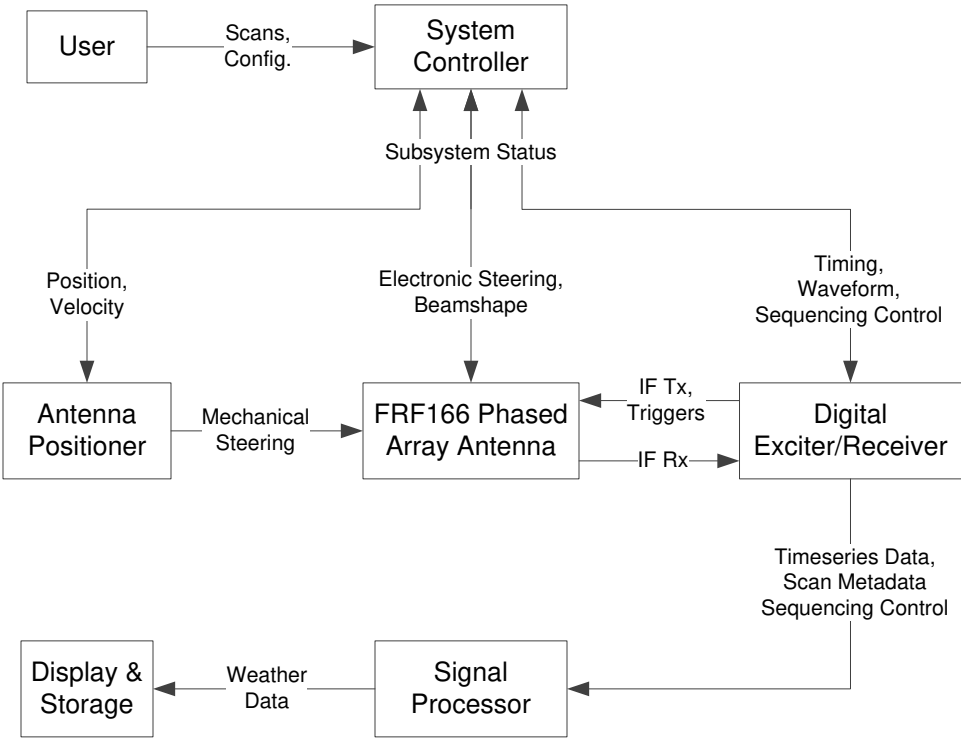


Figure 3.1: Block diagram of the Front-X radar system.

3.2 System Controller

The system controller software which runs on a Linux machine that hosts the Digital Exciter/Receiver hardware, responds to commands from a client to configure the system and execute scans by coordinating the radar subsystems. The client uses a command-line interface for a user to input radar tasks, system configuration, and system status queries, which are sent to the system controller using a TCP/IP interface over an Ethernet link. Radar tasks fall under two categories, data collection scans and calibration scans. Two data collection scan modes have been implemented: a mechanical scan mode which mechanically steers a beam to illuminate targets, and an electronic scan mode which uses the phased array antenna to electronically steer a beam. In addition, two calibration modes have been implemented: an electronic scan calibration mode which measures power and phase differences between electronic scan angles to generate power and phase correction tables for calculating weather moments, and a noise calibration mode which measures the noise floor for calculating signal-to-noise ratio and performing noise subtractions.

The system controller uses a multi-threaded architecture to asynchronously coordinate the radar subsystems to execute a radar task. A master thread interprets high-level system commands from the client and breaks them down into subsystem level commands which are sent using queues to the subsystem handler threads. Three independent subsystem handler threads maintain a connection to the control software of their corresponding subsystem and send them the subsystem level commands: the FRF166 handler thread maintains a serial connection to the phased array antenna, the DXR handler thread maintains a TCP/IP connection to the Digital Exciter/Receiver, and the APC handler thread maintains a TCP/IP connection to the Antenna Positioner Controller. The subsystem handlers are also responsible for receiving subsystem status updates which are used to update the overall status of the system, which can be queried by the client. Additionally, sequencing control packets sent to the DXR through the DXR handler thread are output to the signal processor for coordination of the data processing.

3.3 Antenna Positioner

The antenna positioner receives commands from the system controller to move the antenna, in azimuth and elevation, to a specified position and/or velocity. When the system uses the mechanical scan mode, the antenna positioner is commanded to move the antenna to a start position and when reached, sweep the antenna at a constant velocity to an end position. In the electronic scan mode, the antenna positioner is simply commanded to hold a fixed position. The hardware which composes the antenna positioner is an SCR-584 pedestal to which the phased array antenna is mounted and can be rotated about boresight, a trailer which serves as the radar platform, a platform leveling system, two 16-bit optical encoders for measuring position in the two axes, two servo drive/motor pairs to provide torque to the gearboxes in the pedestal to move the antenna in the two axes, and a motion control computer which hosts the Antenna Positioner Controller software that communicates with the system controller and manages the positioner hardware.

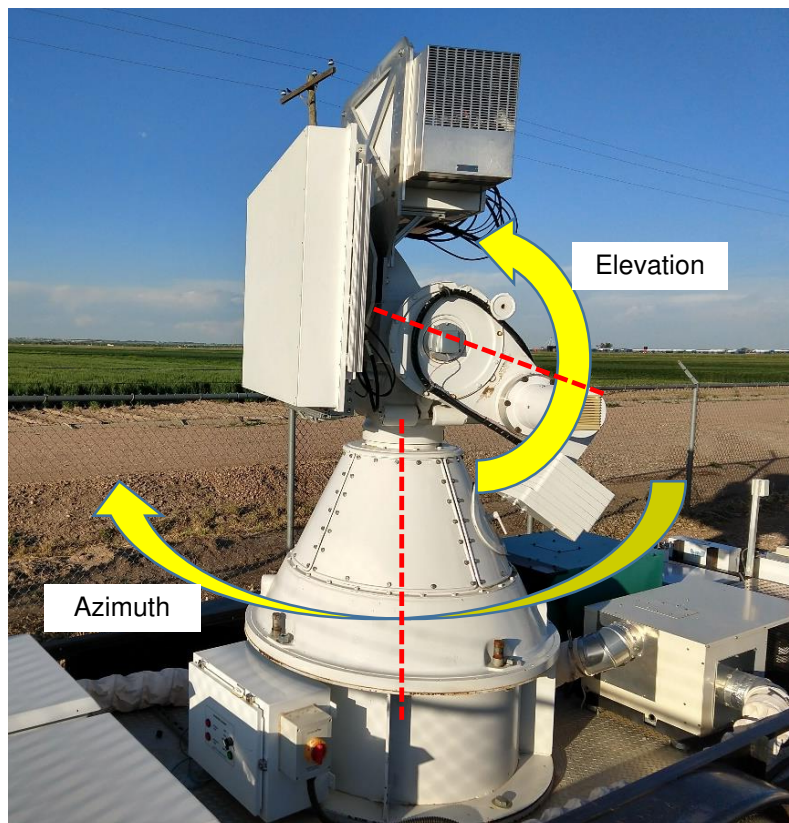


Figure 3.2: Picture of the antenna positioner highlighting azimuth and elevation motion.

The Antenna Positioner Controller software, or APC, uses a multi-threaded architecture to respond to the positioning commands from the system controller. A connection handler thread receives commands using TCP/IP over Ethernet from the system controller which contain target positions and velocities. An encoder handler thread calculates and stores the current position and velocity of the antenna from the the encoder values it reads from an FPGA over a serial interface. Two servo-drive handler threads maintain a serial connection with the servo-drives and close a PID position loop in each axis using the target position from the system controller and the current position from the encoder handler.

3.4 FRF166 Phased Array Antenna

The FRF166 is an X-band, dual-polarization phased array antenna developed by the First RF Corporation in Boulder, Colorado. It uses a linear array of 64 dual-polarization antennas distributed across eight transmit/receive (T/R) modules to transmit and receive horizontally and vertically polarized pulses in a beam that can be electronically steered in one dimension. The polarization modes include horizontal-only, vertical-only, and alternating horizontal and vertical pulses. The antenna can be configured to use different beamshapes in order to control sidelobe levels, including uniform, Taylor, and cosine-pedestal beamshape modes. A loopback mode which enables a path to channel the transmit signal after frequency conversion but before the T/R modules to the antenna's IF output can be used to characterize nonlinearities in the frequency converter. Additionally, several debug modes allow for the individual radiating elements of the antenna to be tested including an isolated element mode which transmits horizontal and vertical pulses for each element individually. Table 3.1 summarizes the RF performance and electrical specifications of the antenna from the FRF-166 Prototype PTWR Antenna User's Guide [15].

Table 3.1: Specifications of the FRF166 Phased Array Antenna.

Parameter	Value
Input Voltage	48 to 65 VDC
Operating Current	9 to 15 A

Output Power	72 W
Operating Frequency (center)	9.41 GHz
RF Bandwidth	400 MHz
Intermediate Frequency (center)	60 MHz
IF Bandwidth	30 MHz
System Noise Figure	7 to 9 dB
Maximum Pulse Width	50 μs
Maximum PRF	6.5 kHz
Non-E-Scan Axis Beamwidth	2.5°
E-Scan Axis Beamwidth (boresight)	1.5°
E-Scan Axis Beamwidth (off-boresight)	$1.2 * (1.5^\circ / \cos(\theta_{escan}))$
Non-E-Scan Axis Sidelobe Level (all beamshapes)	-22 dB
E-Scan Axis Sidelobe Level (uniform beamshape)	-13 dB
E-Scan Axis Sidelobe Level (taylor, cosine beamshapes)	-22 dB
Electronic Scan Range	-45° to 45°
Electronic Scan Power Loss	$\cos(\theta_{escan})^{3/2}$
Electronic Scan Speed	1 $m s$ beam-to-beam

The FRF166 interacts with the system controller software for beam steering and configuration using an RS-422 serial interface over a CAT5 Ethernet cable to the system controller's host computer. This connection allows the antenna to receive commands to load an electronic scan angle sequence for electronic beam steering and set the beamshape, loopback mode, and debug mode. The FRF166 uses "Ack" and "Nack" messages to reply to the system controller when a scan sequence or setting was either successfully or unsuccessfully received, respectively. When the last electronic scan angle for a given sequence is transmitted and received by the antenna, an end of scan message is sent to the system controller. Additionally, the antenna can be commanded to return its health status which includes its current configuration, temperature, and the number of T/R modules which are reporting to the antenna control unit.

The FRF166 receives triggering logic and the transmit IF waveform and returns the received IF signal to and from the DXR. The antenna handles two types of triggers using differential signaling over a CAT5 Ethernet cable: polarization triggers and transmit/receive triggers. The polarization triggers are used to transmit horizontally or vertically polarized pulses when the signal is low or high, respectively. The transmit/receive triggers put the antenna in transmit mode when high, and receive mode when low. The signal which is frequency up-converted to X-band and transmitted by the antenna is sent by the DXR at IF (60 MHz) over coaxial cable. Similarly, the FRF166's received signal is down-converted to IF and sent to the DXR over coaxial cable.

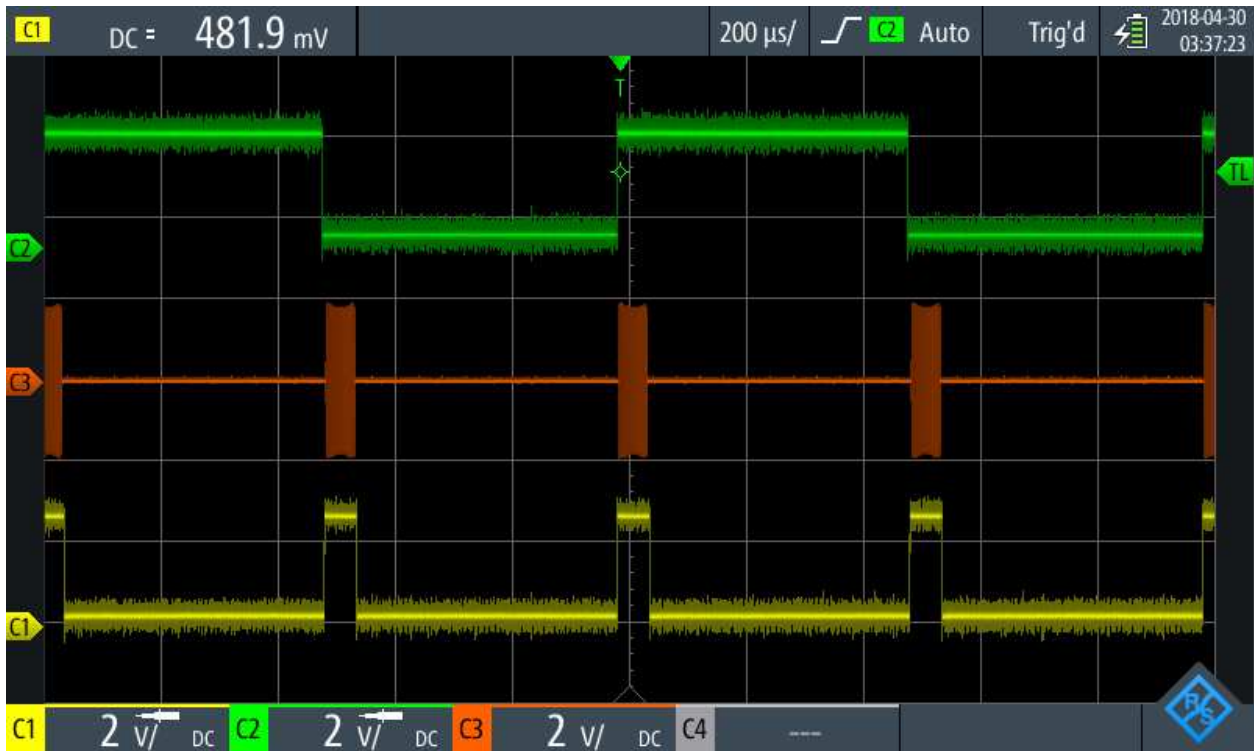


Figure 3.3: Oscilloscope screenshot showing triggers and IF transmit signal to the FRF166. The C1 trace shows the transmit/receive triggers, the C2 trace shows the polarization triggers in alternating mode, and the C3 trace shows the IF transmit waveform.

3.5 Digital Exciter/Receiver

The Digital Exciter/Receiver, or DXR, receives commands from the system controller to generate the radar triggering and IF pulse compression waveform for the FRF166, to digitize and filter the IF receive signal from the FRF166, and to output timeseries data, metadata, and sequencing control to the signal processor. The DXR, composed of timing, ADC, and DAC subsystems, is based on a Pentek 71620 XMC board which includes three ADC channels and two DAC channels controlled by a Virtex-6 FPGA. The FPGA logic implements the timing subsystem which generates the transmit/receive and polarization triggers that are sent to the antenna, in addition to synchronizing the DAC and ADC subsystems. The ADC subsystem uses three 200 MHz 16-bit ADCs to digitize the received IF signal from the antenna, which is then frequency downconverted and passed through a 480-tap complex valued pulse compression filter operating at an input data rate of 5 MSPS. Each channel has two independently programmable subchannels which are used to process the ADC output with two different configurations in parallel: one for a long pulse and the other for a short pulse. The DAC subsystem generates the pulse compression waveform at IF with an input data rate of 200 MHz interpolated up to 800 MHz over two independent channels. DAC waveforms are stored in 256 MB DDR3 memory used for pulse-to-pulse waveform switching. Table 3.2 summarizes the specifications of the DXR [16].

Table 3.2: Specifications of the Digital Exciter/Receiver.

Parameter	Value
Number of ADC Channels	3
ADC Sampling Rate	200 MHz
Number of DAC channels	2
DAC Sampling Rate	800 MHz
IF Range	10 to 80 MHz
Input Signal Max. Power	+8 dBm
Output Signal Max. Power	+4 dBm
Timing Resolution	5 ns
Output Data Rate (without Pulse Compression)	1-10 MSPS

Output Data Rate (with Pulse Compression)	1-5 MSPS
Bandwidth	80% of $f_{sampling}$
Dynamic Range (without Pulse Compression)	> 90 dB
Dynamic Range (with Pulse Compression)	> 110 dB
Number of Pulse Compressor Filter Taps	480

The IF waveform generated by the DXR uses combination of a long and short pulse: a linearly frequency modulated $49 \mu s$ pulse with a bandwidth of 2.5 MHz centered at 65 MHz is used for high sensitivity at long range, followed by a $1 \mu s$ pulse centered at 55 MHz used to cover the blind range of the long pulse. Figure 3.4 shows the measured spectrum of the transmit waveform at IF using a spectrum analyzer.

The DXR is controlled by the Acquisition Daemon software which runs on a Linux machine that hosts the DXR hardware. The Acquisition Daemon receives commands from the system controller using TCP/IP over Ethernet to configure the radar timing and signal processing parameters, load pulse compression waveforms and filters, and broadcast metadata and sequencing control. Adjustable radar timing and signal processing parameters include PRF, samples per ray, sampling rate, and decimation rate. The Acquisition Daemon outputs the timeseries data, metadata, and sequencing control using TCP/IP over a 10 Gb/s Ethernet link to the signal processor for weather moment calculation and to the timeseries archiver for raw data storage.

3.6 Signal Processor

The signal processing software, running on a Linux machine whose specifications are shown in Table 3.3, ingests the timeseries data, metadata, and sequencing control output by the DXR over a 10 Gb/s Ethernet link and calculates weather moment variables using a thread-pool architecture. An assigner thread sets the processing mode based on incoming scan mode packets and forms work units of timeseries data which represent one ray of unprocessed data which are sent to

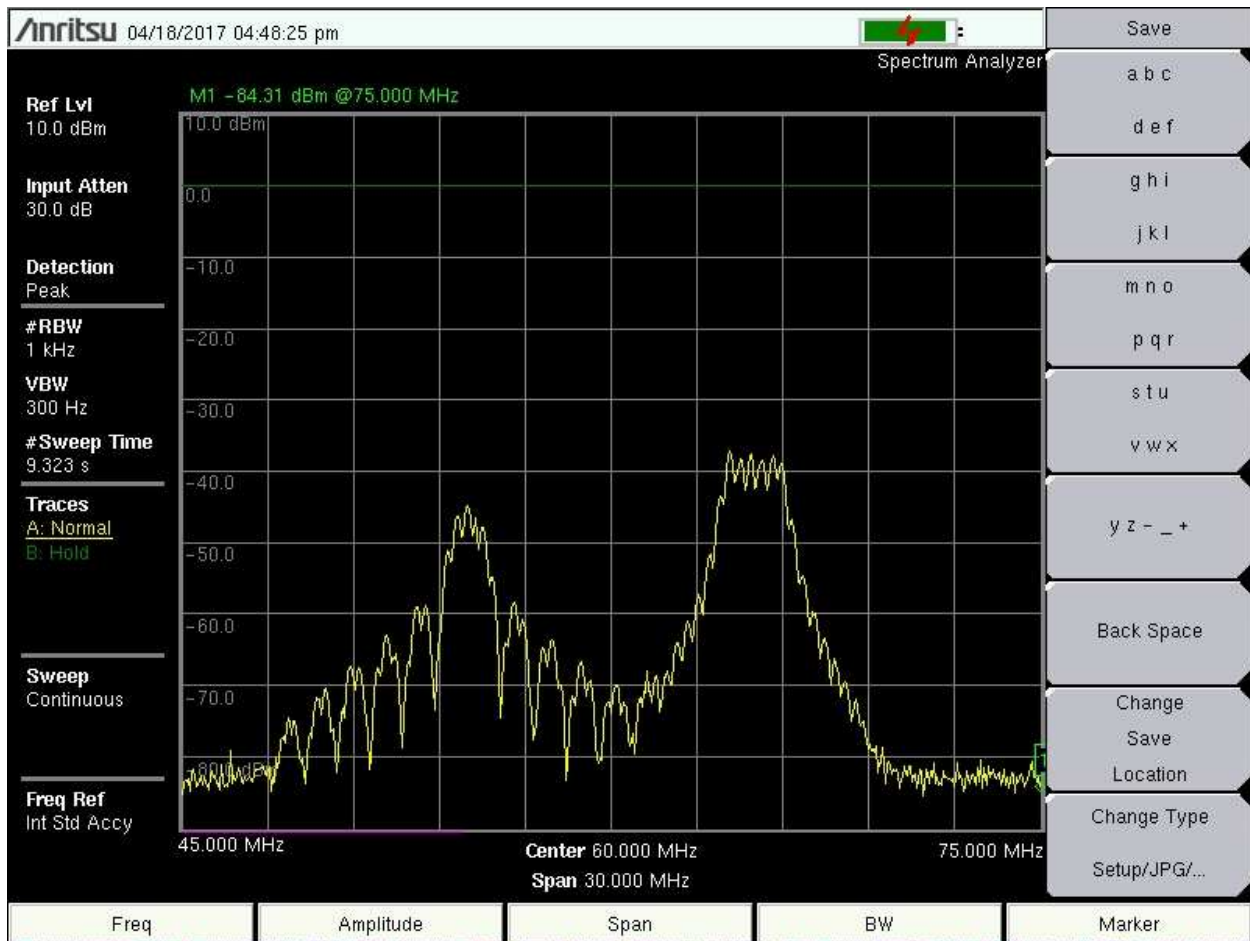


Figure 3.4: Spectrum analyzer screenshot showing the IF transmit signal generated by the DXR. The spectrum centered about 65 MHz corresponds to the linearly frequency modulated $49 \mu s$ long pulse, and the spectrum centered about 55 MHz corresponds to the $1 \mu s$ short pulse.

available worker threads. The thread-pool is made up of several worker threads which process the work units using the algorithm specified by the processing mode. Four processing algorithms have been implemented which use autocovariance processing: single polarization mechanical scan, single polarization electronic scan, alternating polarization mechanical scan, alternating polarization electronic scan. Additionally two calibration modes have been implemented including electronic scan calibration and noise calibration. Using the algorithms implemented in the processing modes, the following moments can be computed: signal-to-noise ratio, reflectivity, doppler velocity, normalized coherent power, spectral width, differential reflectivity, differential phase, and correlation coefficient. A collector thread receives the processed data from the worker threads, orders them,

and sends them to connection handler threads which in turn send the data to client software using TCP/IP over Ethernet.

Table 3.3: Specifications of the signal processing computer.

Specification	Part
Operating System	CentOS Linux v7
CPU	3.6 GHz Intel Xeon E3-1270 Quad-core Skylake Processor
Memory	2 x 16 GB Micron DDR4 SDRAM
Data Storage	8 x 2 TB Seagate 2.5" SAS 7200 RPM HDD

Archivers store both the processed moment and raw timeseries data files and a display plots the moment data in real-time. Multiple instances of the archiver software can be run to collect both moment and timeseries data by connecting over Ethernet to the signal processor software in moment mode and to the DXR in timeseries mode as TCP/IP clients. The archiver uses sequencing control packets to open new files, write the data, and close the file when a radar task is finished, writing the files to a RAID storage system. A real-time display finds newly written moment files on the RAID storage and plots the data on a scan-by-scan basis.

Chapter 4

System Controller

4.1 Introduction

The Phased Array Radar Controller software, or PARC, is the system controller which is responsible for receiving and responding to client commands over Ethernet to execute radar scans, manage a task-list, configure the system, and maintain the status of the system. PARC runs on a Linux machine that hosts the DXR hardware and utilizes a multi-threaded architecture to manage and coordinate the radar subsystems. A master thread interprets high-level client commands and breaks them down into subsystem specific commands which are sent to each subsystem controller via subsystem handler threads. Three separate subsystem handler threads maintain connections to the antenna positioner, Digital Exciter/Receiver, and FRF166 phased array antenna and are responsible for sending commands to the subsystem controllers and updating the status of their corresponding subsystem in a radar system status structure.

PARC uses a modular scan mode structure to run different types of data collection and calibration tasks. Two types of data collection scan modes have been implemented: electronic volume scan which utilizes the electronic beam-steering capability of the phased array antenna to complete sweeps in a volume, and mechanical volume scan which utilizes only the boresight beam and steers it mechanically with the antenna positioner. Additionally, two calibration modes have been implemented: an electronic scan calibration mode to measure horizontal and vertical power biases as well as differential phase for each electronic scan angle to correct reflectivity, differential reflectivity, and differential phase; and a noise calibration mode to measure the noise floor of the system to calculate signal-to-noise ratio and to perform noise subtractions.

This chapter will detail the design and implementation of the PARC software architecture and the scan mode algorithms used for electronic and mechanical volume scans and the electronic scan and noise calibration modes.

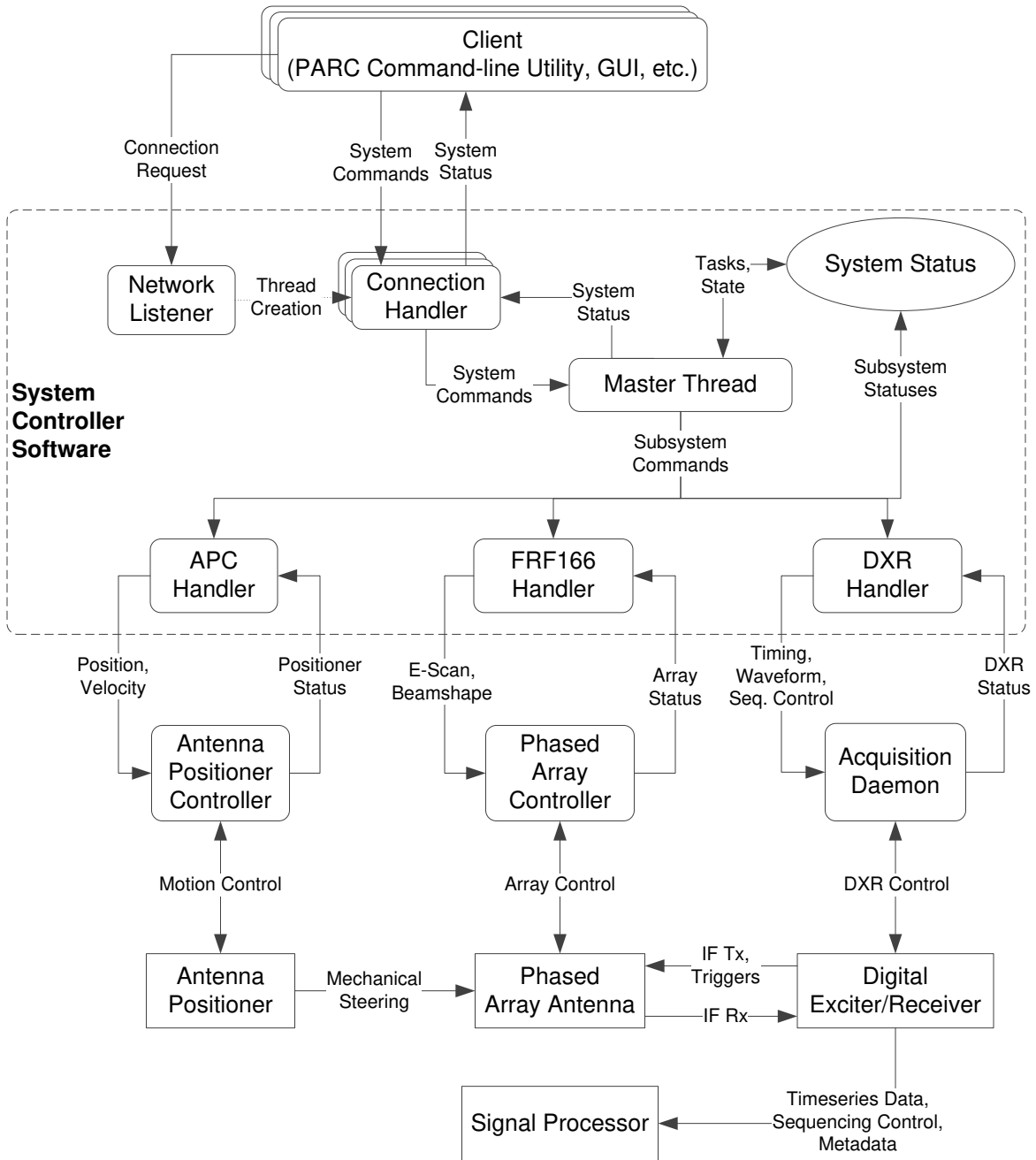


Figure 4.1: Block diagram of the system controller software and interaction with the radar system.

4.2 PARC Software Architecture

4.2.1 Master Thread

The master thread is the first process to run when executing PARC and is responsible for configuring the software using a configuration file, initializing and managing the system status structure, the task-list, and the subsystem handler threads, and interpreting high-level client commands to coordinate the actions of the subsystem handlers to control the radar system. When the software is executed the master thread first reads the command-line for a path to a configuration file. If a filepath is not specified by the user, a default configuration file is used. The configuration file is read and its values, including default waveform and matched filter filepaths, network interface settings, queue settings, timer values, update periods, and general system information are stored in a configuration structure for read access by the rest of the software.

Data structures are initialized including the system status structure, the task-list, the distribution list, the system command queue, and the subsystem handler thread command queues. In addition to the status of the radar's subsystems, the system status structure includes general system information, such as radar name and location, which is initialized by the master thread using the values set in the configuration file. This general information is emitted in a radar information packet with every scan for ingestion and interpretation by downstream processing software. The task-list is used to store and manage radar tasks, including scan and calibration tasks. The distribution list is used to manage TCP/IP client connections and can be used to broadcast packets to all connected clients. The system command queue is used to pass client commands from the network interface to the master thread which are then broken down into subsystem specific commands and added to the subsystem command queues to pass to the subsystem handler threads.

The master thread initializes the network interface and the three subsystem handler threads: the FRF166 handler, the DXR handler, and the APC handler. Each subsystem handler thread is passed a pointer to the configuration structure and pointers to their respective command queue, subsystem status structures within the system status structure, and mutexes to manage reading and writing to the shared resources with the master thread. The listener thread, which initializes the rest of

the network interface, is passed a pointer to the configuration structure along with pointers to the distribution list, command queue, the system status, and subsystem status handler mutexes.

After setting up the data structures and launching the other threads, the master thread enters a state machine which dictates the actions of PARC based on client commands, the task-list, radar state, and subsystem statuses. The master thread first enters the INIT state where it sends commands to the subsystem handler threads to set the initial conditions of each subsystem: the beam-shape, converter gain, loopback mode, debug mode, local oscillators for the FRF166 are initialized, the DXR is sent a reset command and triggering is disabled, and the APC is commanded to stop antenna motion.

After initialization has been completed, the master thread enters the IDLE state where it checks an idle timer, checks for subsystem faults, processes commands, and checks the radar state. The idle timer measures how long the system has been idle, and if it passes a configurable threshold, a command is sent to the APC handler thread to disable the servo-drives to reduce unnecessary stress on the antenna positioner. Fault flags corresponding to each subsystem in the system status structure, which are set by the subsystem handler threads, are checked; if a fault is encountered the master thread enters the FAULT state. Otherwise, the system command queue is checked for new commands to process, including adding or removing tasks from the task-list, starting or stopping the task-list, as well as configuring individual subsystems.

If PARC receives a start task-list command or it is in the process of executing the task-list as reflected by the radar state, the master thread will enter the SCAN state where it calls the appropriate scan mode function depending on the current radar task. If the scan mode function returns with a value indicating that the task is done, the next task will become the current task. While executing a task, the master thread alternates between the SCAN and IDLE states in order for PARC to be able to respond to commands while scanning. Using a scan timer, if the time it takes to complete a task exceeds a configurable time limit, the master thread will abort the task-list and enter the FAULT state.

When the master thread enters the FAULT state, it sends commands to the DXR handler thread to disable triggering and to the APC handler thread to stop antenna motion. The fault flags will then be monitored until they are reset by the subsystem handler flags, at which point the INIT state will be re-entered where the system is reinitialized and the state machine is reset. In the FAULT state, the master thread will only process some limited commands which do not depend on the faulted subsystem to be carried out.

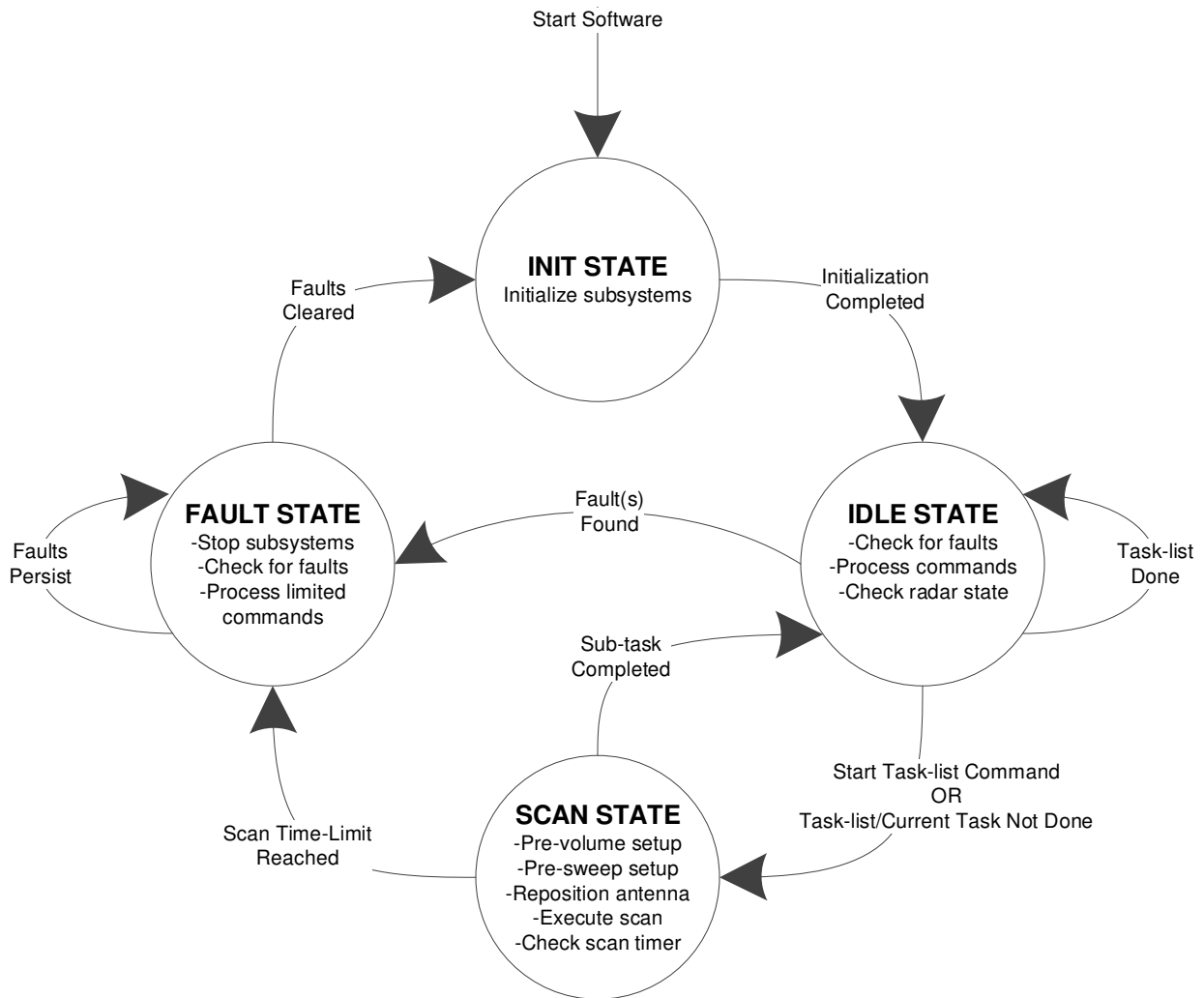


Figure 4.2: Diagram of the state machine governing the PARC master thread.

4.2.2 System Status Structure

The system status structure contains the values which reflect the status of each of the three directly controlled subsystems in addition to the array orientation, radar state, and current task. The network interface has read access to the system status structure in order for the connection handlers, which each manage a TCP/IP client connection, to respond to system status queries. Each subsystem handler thread has read/write access only to its corresponding subsystem status structure within the system status structure which it updates as it receives status packets from the subsystem server to which it is connected. The FRF166 subsystem status structure contains the antenna converter gain, beam-shape, loopback mode, debug mode, local oscillators, end of scan flag, flipped polarization flag, antenna temperatures, number of T/R modules connected, and FRF166 fault flag. The DXR subsystem status structure contains the system timing, platform timing, radar timing, waveform and matched filter, trigger state, flipped polarization flag, and DXR fault flag. The APC subsystem status structure contains the azimuth and elevation axis mode, target position, target velocity, max-speed flag, current position, current velocity, at-target position and velocity flags, motor current consumption, limit switch state, emergency stop switch state, servo-drive power bridge state, axis fault state, and APC fault flag. The array orientation field is used to represent the mechanical orientation, either horizontal or vertical, of the phased array antenna in order for the DXR and FRF166 handler threads to set their "flip polarization" flags.

The radar state indicates what stage of a task is in progress in order to keep track of the status of a task for a given scan mode when the master thread alternates between the IDLE and SCAN states. The radar state can be one of the following: IDLE, PRE-VOLUME, PRE-SWEEP, REPOSITION, and SCAN. In the IDLE state, the system is not currently executing any tasks because the task-list is either empty or has been completed. In the PRE-VOLUME state, a volume scan task has just begun and the setup commands associated with the task are in progress. In the PRE-SWEEP state a new sweep within the volume scan has begun and the setup commands for the sweep are in progress. In the REPOSITION state, the antenna positioner is currently moving the antenna to the

desired position for the start of a sweep. In the SCAN state, DXR transmit/receive and polarization triggering is active and the radar is transmitting and collecting data.

Table 4.1: PARC system status structure fields.

System Status Fields	Description
Radar state	Current operating state of the radar: IDLE, PRE-VOLUME, PRE-SWEEP, REPOSITION, or SCAN.
Array orientation	Mechanical orientation of the phased array antenna: horizontal (for E-PPIs) or vertical (for E-RHIs).
Current task	The task currently running or to be run when task-list is started.
Current task index	Index in the task-list corresponding to the current task.
DXR Status Structure	
System Timing	Timing parameters used internally by the acquisition daemon common to all radar platforms using the DXR, including ADC and DAC delays.
Platform Timing	Front-X specific timing parameters including polarization mode, pulse-width, and mute delay.
Radar Timing	Task specific timing including pulse repetition time, pulse to integration, samples per ray, and range gate spacing.
Waveform	Transmit waveform used by the system.
Filter	Matched filter corresponding to the waveform.
Trigger state	DXR outputting triggers: enabled or disabled.
Flip polarization flag	Flag indicating that the antenna is vertically oriented and polarization triggers should be flipped.
DXR fault flag	Flag indicating a fault in the DXR or DXR handler thread.
FRF166 Status Structure	
Converter Gain	Antenna gain mode: high or low.
Beam-shape	Antenna receive beam-shape: uniform, cosine pedestal, taylor, taylor-left, or taylor-right.
Loopback mode	Loopback path: enabled or disabled.
Debug mode	Antenna debug mode: normal operation, isolated element, all element cycle, or single element cycle.
Local oscillator	Local oscillator selection: L-band internal/external, X-band internal/external.
End of scan flag	Flag indicating that an end of scan signal was

received from the antenna.

Health status	Antenna temperatures and number of T/R cards connected.
Flip polarization flag	Flag indicating that the antenna is vertically oriented and polarization should be flipped.
FRF166 fault flag	Flag indicating a fault in the FRF166 or FRF166 handler thread.
APC Status Structure	
Velocity	Measured azimuth and elevation antenna velocity.
Position	Measured azimuth and elevation antenna position.
Motor current	Current draw for azimuth and elevation motors.
Target velocity	Target azimuth and elevation velocity.
Target position	Target azimuth and elevation position.
Axis mode	Control mode for azimuth and elevation: idle, stop, velocity, or position.
Max-speed flags	Flags indicating if maximum configured speed is being used for azimuth and elevation.
At-target velocity flags	Flags indicating target azimuth or elevation velocity is reached.
At-target position flags	Flags indicating target azimuth or elevation position is reached.
Bridge-enable flags	Flags indicating if azimuth and elevation servo-drive power bridge are enabled.
Limit-switch status	Flags indicating if positive or negative limit switch is triggered in elevation axis.
Emergency-stop switch status	Flag indicating if emergency stop switch is triggered.
Servo-drive fault flags	Flags indicating a fault within the azimuth or elevation servo-drive.
APC fault flag	Flag indicating a fault in APC or APC handler thread.

4.2.3 Task-list

The task-list contains the radar tasks which are to be run by the system, to which a user can add and remove individual tasks in addition to clearing the entire list. The task-list uses a linked list structure to simplify the insertion and deletion of tasks. Each task is a structure which contains a scan mode packet structure, final instruction field, and task name. Each scan mode uses a scan mode specific structure which defines the values that specify how the scan will be run, for example, pulse repetition time, pulses to integrate per ray, samples to collect per ray, electronic scan angles, start and end antenna positions, scan speed, etc. When PARC executes the current task in the task-list, the PRE-VOLUME and PRE-SWEEP state functions refer to the scan mode packet structure within the current task to set up the scan. When the task is complete the master thread reads the final instruction field telling PARC how to proceed, which gives the user more control on how to automate the execution of the task-list. If the final instruction variable is set to "repeat", the same task is repeated; if set to "next", the next task is executed; and if set to "stop", the task-list is aborted. Finally, the task name is a string which the user sets for a given task which is written to data files corresponding to the scan by downstream archiving software.

4.2.4 Subsystem Handler Threads

The subsystem handler threads include the FRF166 phased array antenna handler, the Digital Exciter/Receiver handler, and the antenna positioner handler, which are responsible for maintaining a connection with, sending subsystem specific commands to, and receiving and responding to data from the servers controlling their respective subsystems. The subsystem handlers use a state machine to dictate their functionality and are in one of the following states: CONNECT, IDLE, COMMAND, or INGEST.

Upon initialization, the subsystem handler threads enter the CONNECT state in which a connection with the respective subsystem server is established. The FRF166 handler thread opens a serial connection with the antenna controller software using a configurable baud rate, the DXR handler thread opens a socket and requests a TCP/IP connection with the Acquisition Daemon,

and the APC handler thread opens a socket and requests a TCP/IP connection with APC on the motion control computer. If an error occurs while connecting to a server, the subsystem handler thread sets its fault flag which gets read by the master thread, and continues trying to connect. If successful, the fault flag is cleared and the subsystem handler thread enters the IDLE state.

In the IDLE state, the subsystem handler thread checks its command queue for new commands from the master thread and checks its server connection for incoming packets. If a new command has been received by the master thread, the subsystem handler will enter the COMMAND state where it will write the command packet to the serial port in the case of the FRF166 handler, or a socket in the case of the DXR and APC handlers. If any error occurs during the write, the thread will return to the CONNECT state and attempt to re-establish the server connection. If pending data from the connected server is detected, the thread will enter the INGEST state and read in the data from the serial port or socket. If an error occurs during the read, the thread will return to the CONNECT state. If the data corresponds to any of the subsystem status fields the thread locks the field using the subsystem handler specific mutex to avoid read/write conflicts with the master thread and connection handlers, and overwrites the field with the updated value. After sending the command in the COMMAND state or reading and responding to the server packet in the INGEST state, the thread will return to the IDLE state. Because the FRF166 antenna controller sends an acknowledgment, or "Ack", specific to the message sent to it, the thread stores the sent message and clears it only when the corresponding "Ack" is received from the FRF166. If the time it takes to receive the acknowledgment exceeds the FRF166 handler's configurable update period or the FRF166 sends a "Nack" response, indicating that there was an error receiving the message, the thread will return to the CONNECT state and attempt to reset the connection to the server.

Additionally, when in the IDLE state the FRF166 and APC handler threads periodically send a status query to their connected server to maintain updated subsystem statuses. When a status query is sent to the server, the thread starts a timer and will only send another status query when the timer reaches the configurable subsystem specific update period. It is important for the APC handler thread to use a short update period, around 100 ms, because near real-time monitoring of

the at target position flags in the APC status packets is critical to the functioning and performance of PARC's scan modes. The DXR handler thread does not use a periodic status query because any changes made to the DXR is broadcast to all of the Acquisition Daemon clients, including the DXR handler thread.

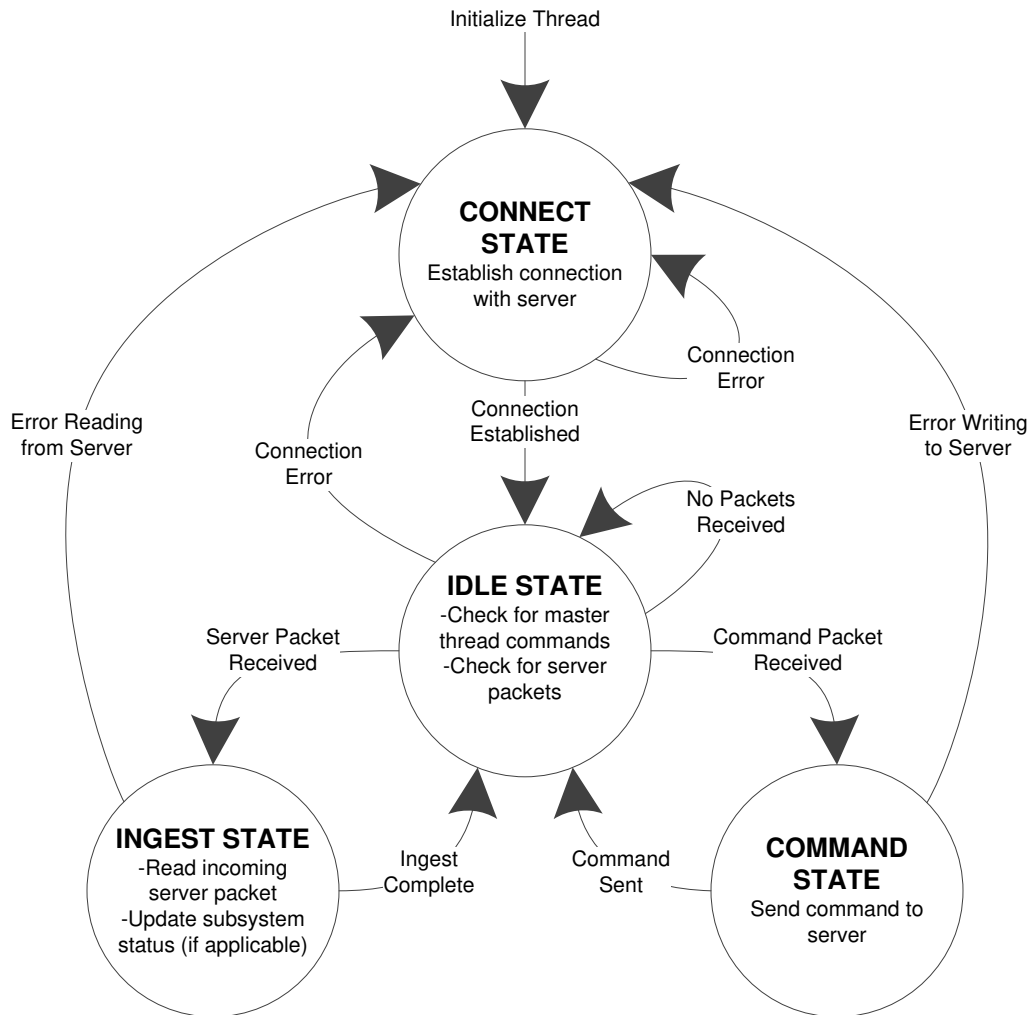


Figure 4.3: Diagram of the state machine governing PARC's subsystem handler threads.

4.2.5 PARC Command-line Utility

The PARC command-line utility is used to send commands to PARC over the network which query the status of the system, configure the radar subsystems, and populate, execute, and abort

the task-list. Table 4.2 shows all of the command-line arguments of the utility, the parameters they accept, and their functionality. The command-line utility reads text files edited by a user to form and send large packets to PARC, for example radar tasks, DXR waveform, timing, etc. A system status display script, which calls the PARC command-line utility several times per second, is used to show the status of the system in real-time.

Table 4.2: Command-line arguments and functionality for the PARC command-line utility.

Argument	Parameters	Functionality
General PARC Functions		
-help	None	Returns usage information.
-server	Hostname : port	Specifies the PARC computer hostname and listening port.
-timeout	Timeout (seconds)	Sets time after which no response from PARC gives a timeout error.
-version	None	Returns the PARC version number.
-status	None	Returns the connection status of each of the subsystem servers.
-radar_state	None	Returns the radar state (IDLE, PRE-VOLUME, PRE-SWEEP, REPOSITION, SCAN).
-system_status	None	Returns the full system status.
-array_orientation	Orientation	Get/set the phased array antenna orientation: "h" (horizontal) or "v" (vertical).
FRF166 Specific Functions		
-statusfrf166	None	Get the health status of the FRF166.
-convgain	Converter gain	Get/set the converter gain: "high" or "low".
-beamshape	Beam shape	Get/set the beam shape: "uniform", "cosine_pedestal", "taylor_full", "taylor_left6", "taylor_right6".
-debugfrf166	Debug mode	Get/set the debug mode: "normal", "isolate", "all_cycle", or "single_cycle".
-loopback	Loopback enable	Get/set the loopback mode: "on" or "off".

-clearscansequences	None	Clears loaded electronic scan sequences
-pdufrf166	Power command	Commands FRF166 power supply to turn: "on", "off", or "reboot".
DXR Specific Functions		
-system_tmg	Filepath	Get/set DXR system timing variables.
-platform_tmg	Filepath	Get/set DXR platform timing variables.
-radar_tmg	Filepath	Get/set DXR radar timing variables.
-reinit_dxr	None	Reinitialize the DXR.
-triggers	Trigger state	Get/set trigger state: on or off.
-waveform	Filepath	Get/set waveform file.
-filter	Channel, subchannel filter spec, filepath	Get/set filter coefficients for a channel, subchannel, filter spec with a specified file.
APC Specific Functions		
-status	None	Queries APC for status.
-target	Az. axis mode, Az. target position, Az. target velocity, Az. max-speed flag, El. axis mode, El. target position, El. target velocity, El. max-speed flag, Command bitmask	Sends a motion command to APC. Axis mode can be "s" (stop), "i" (idle), "v" (velocity), and "p" (position). The bitmask indicates to the APC which parameters, if any, to ignore.
-goto	Az. target position, El. target position	Sends a command to APC to move the antenna to the specified position using the maximum configured speed.
-setidle	None	Disables the power bridge circuit on the servo-drives.
Task-list Functions		
-start_tasklist	None	Execute the task-list.
-stop_tasklist	None	Abort the task-list (mid-task).
-clear_tasklist	None	Clear the task-list.
-add_task	Filepath, index	Add a task at a specified index.
-remove_task	Task index	Remove task at a specified index.

4.3 Scan Mode Algorithms

4.3.1 Modular Structure

PARC uses a modular algorithm to execute scans which facilitates the implementation of new scan modes in addition to enabling the system to respond to new client commands during a scan. Two data collection scan modes have been implemented: electronic volume scan and mechanical volume scan. Volume scans are broken up into four functions, each corresponding to one of the non-idle radar states: PRE-VOLUME, PRE-SWEEP, REPOSITION, and SCAN. When executing a task, the master thread checks its scan mode and calls the function corresponding to the next state for the given mode. Between calls to each of the four state functions, the master thread returns to its internal IDLE state in which it can respond to new client commands. The four state functions for each scan mode are stored in separate source files with an associated header file. Implementing a new scan mode requires adding a source file which defines the four state functions for the mode and a corresponding header file to be included by the master thread. A library of functions which set up subsystem specific commands and send them to the appropriate subsystem handler thread can be used to simplify the implementation of a new scan mode.

The scan mode packets which define how a scan is run contain radar timing, beam steering information, and scan type which refers to either PPI or RHI. The radar timing includes pulse repetition time, range gate spacing, number of pulses to integrate, number of samples to acquire per ray, and polarization mode which can be horizontal-only, vertical-only, or alternating polarization. The beam steering information specifies where the beam will be pointed for the duration of the scan which differs depending on the electronic or mechanical scan modes. For electronic scans, a list of angles specifies the electronic beam steering and can either be generated using a start angle, increment, and number of angles, or entered manually. A list of azimuth and elevation angles specify where the antenna will physically point for fixed angles in the volume, using the first azimuth and the list of elevation angles for PPIs and the first elevation and list of azimuth

angles for RHIs. For mechanical scans, lists of start and end angles for azimuth and elevation are specified, where the first start and end azimuth and list of elevation angles are used for PPIs and the first start and end elevation and list of azimuth angles are used for RHIs. An antenna velocity is specified for the speed of the sweeps.

4.3.2 Electronic and Mechanical Volume Scan Modes

The PARC master thread uses four major functions, PRE-VOLUME, PRE-SWEEP, REPOSITION, and SCAN, to execute the electronic and mechanical volume scans. Starting with the PRE-VOLUME function, the radar state is changed to PRE-VOLUME, the scan timer is started, and a command is sent to move the antenna to the first starting position of the volume followed by commands for the DXR to broadcast a "start task" event packet, a radar information packet, a task information packet, a scan mode information packet, and a "start sweep" event packet. The event packets are used by downstream software to determine the beginning and end of sweeps and volumes, for example used by the NetCDF converter to separate the data for a given volume into individual sweeps. Then a command to load the electronic scan angles is sent to the FRF166 handler thread, using the specified list for electronic scan and using 0° angles for mechanical scan. The radar state is then changed to REPOSITION.

The REPOSITION function checks the status of APC; if the antenna has not yet reached its target position then the radar state remains in REPOSITION and the function exits. If the target position has been reached, this indicates to the master thread that the antenna is physically pointing at the starting position for the sweep and a command is sent to the DXR to start triggering. The radar state is then changed to SCAN.

The SCAN function checks if the sweep has completed, which differs between the electronic and mechanical scan modes. In the electronic scan mode the end of scan flag is checked to see if the FRF166 completed its loaded scan sequence, while in the mechanical scan mode the APC status is checked to see if the end position has been reached. The end of scan flag is also checked in the mechanical scan mode to see if another set of 0° angles needs to be loaded. In both modes,

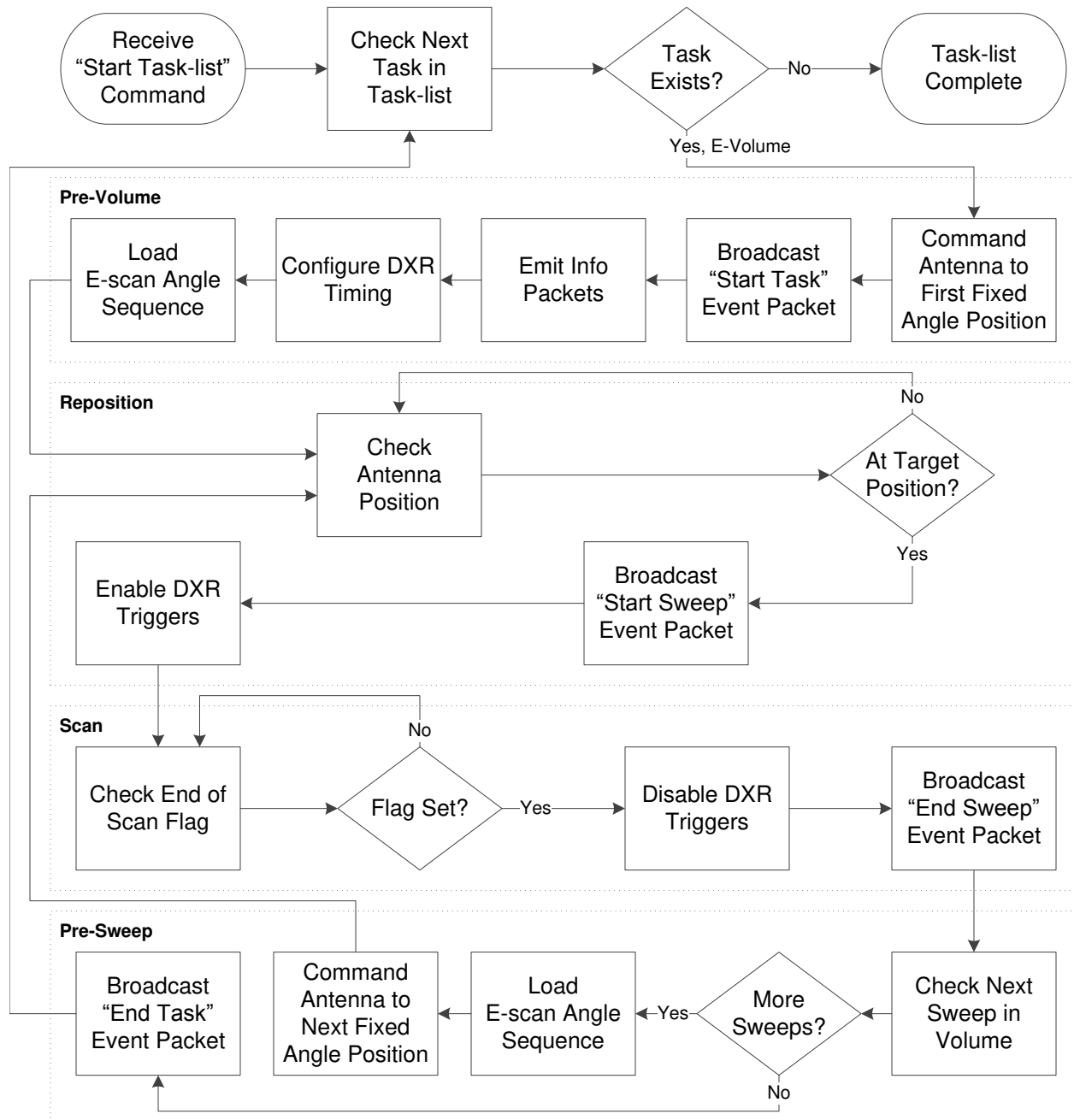


Figure 4.4: Flowchart diagram used by the PARC master thread when executing the electronic volume scan mode with steps labelled by radar state.

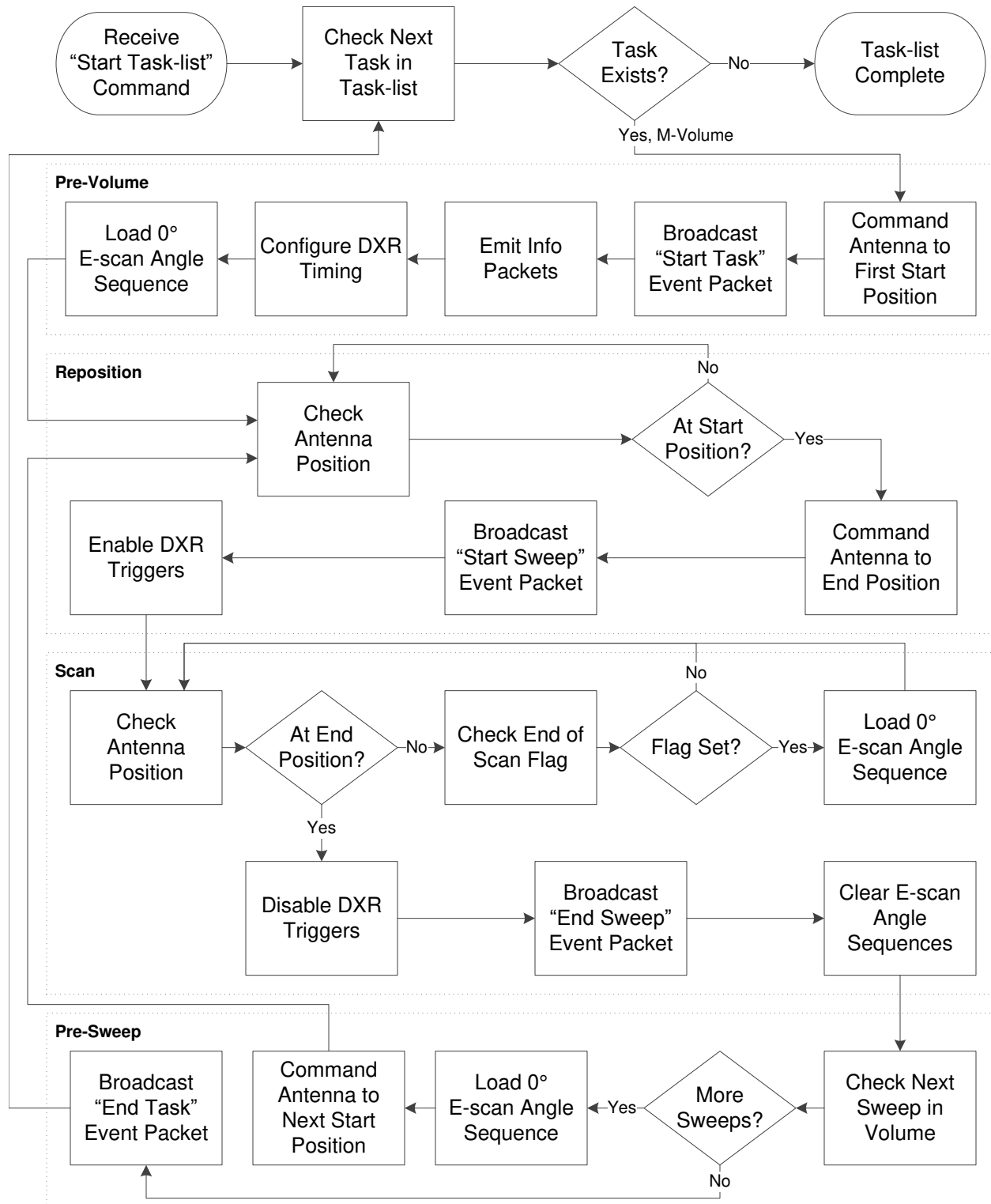


Figure 4.5: Flowchart diagram used by the PARC master thread when executing the mechanical volume scan mode with steps labelled by radar state.

when the sweep is complete commands are sent to stop DXR triggering and broadcast an "end sweep" event packet. The radar state is then changed to PRE-SWEEP.

The REPOSITION function sets up a new sweep in the volume scan if another fixed angle exists in the volume, otherwise a command is sent to broadcast an "end task" event packet and the radar state is changed to IDLE. If there is another fixed angle in the volume scan, commands are sent to broadcast a "start sweep" event packet and reposition the antenna to the starting position for the next sweep. The radar state is changed to REPOSITION and the cycle continues until all sweeps in the volume are complete.

4.3.3 Electronic Scan Calibration Mode

The electronic scan calibration mode is used to measure differences electronic scan beams for horizontal power, vertical power, and differential phase for use by the signal processor to correct electronic scan data, including reflectivity, differential reflectivity, and differential phase data. Fixed angle pointing is used to to transmit and receive pulses, using a range of electronic scan angles, at a user specified azimuth and elevation where a calibration target can be placed. To make measurements for each beam, the antenna is moved mechanically to offset the electronic scan angle of the beam in order to maintain the same pointing angle. Because the antenna is repositioned for each electronic scan angle, this calibration mode functions similarly to a volume scan using the four state functions: Pre-Volume, PRE-SWEEP, REPOSITION, and SCAN. The difference comes when loading electronic scan angles, as only one angle is loaded per fixed angle "sweep". The scan mode packet includes the range, in meters, of the calibration target for use by the signal processor to calculate the horizontal and vertical received power and differential phase.

4.3.4 Noise Calibration Mode

The noise calibration mode is used to measure the noise floor of the system to store in the signal processor for calculating signal-to-noise ratio and noise subtractions. Fixed angle pointing is used to collect a user specified number of samples to average over at a single elevation angle of 90° to avoid echo from ground targets. Because only one elevation angle is used, only three state

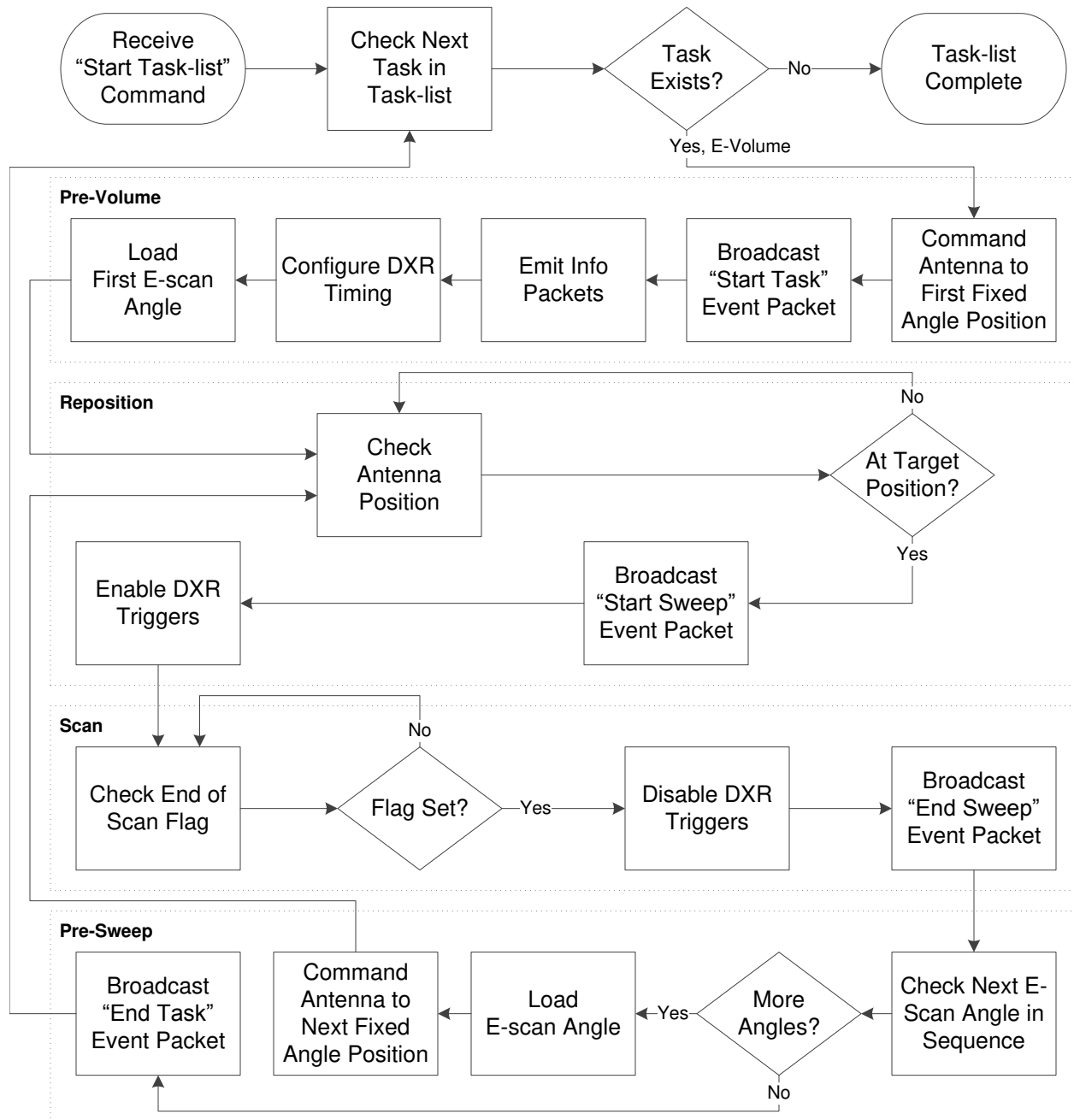


Figure 4.6: Flowchart diagram used by the PARC master thread when executing the electronic scan calibration mode with steps labelled by radar state.

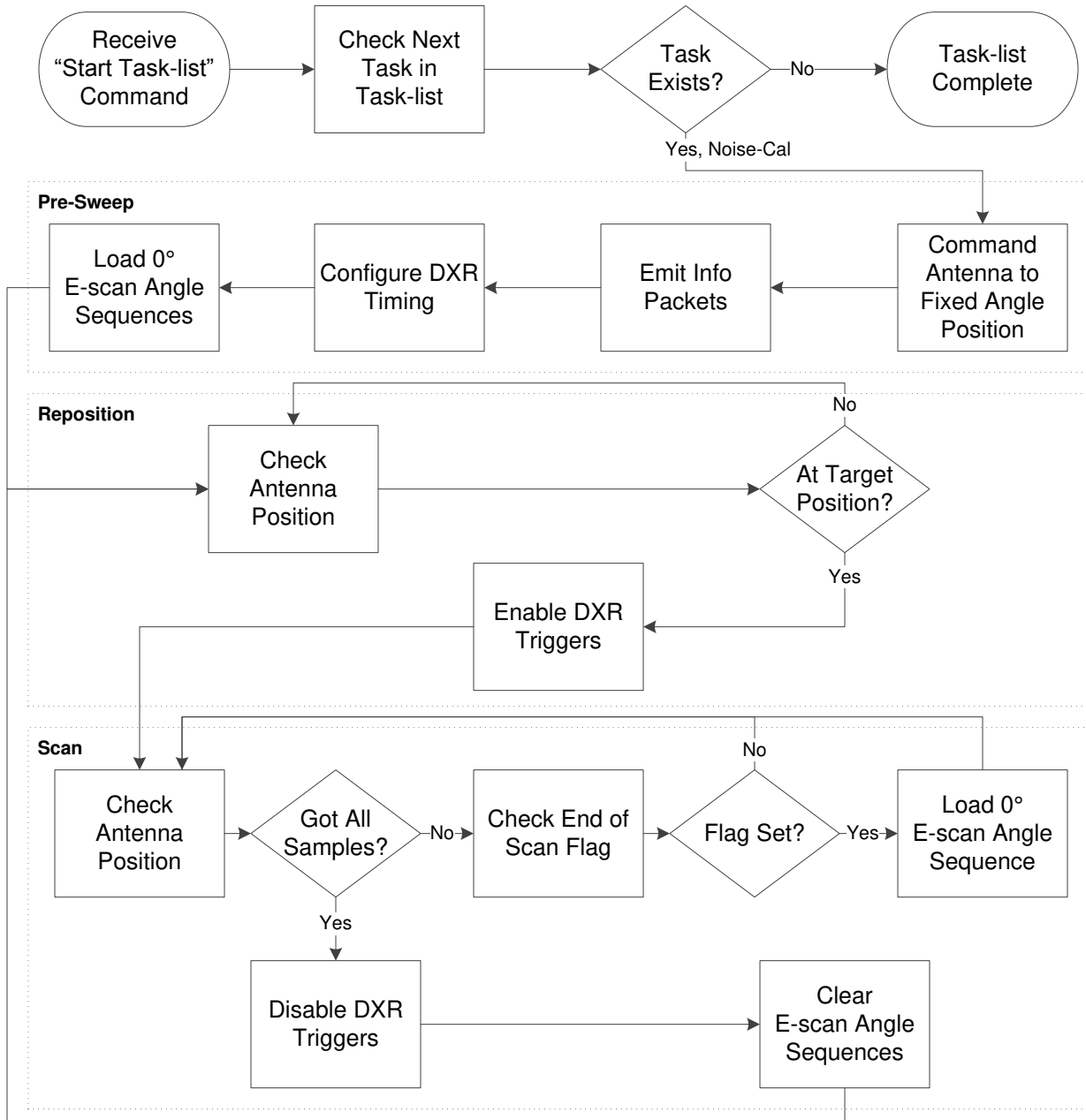


Figure 4.7: Flowchart diagram used by the PARC master thread when executing the noise calibration mode with steps labelled by radar state.

functions are used: PRE-SWEEP, REPOSITION, and SCAN. During PRE-SWEEP, the scan timer is started and commands are sent to reposition the antenna to the fixed pointing position, configure the DXR timing, and broadcast the scan mode packet which signals to the signal processor to start its noise calibration processing mode. In REPOSITION, as with the volume scan modes, PARC waits for the APC status to indicate that the target position has been reached. When the target position is reached, the SCAN state starts which enables triggering. The number of transmitted pulses is counted by incrementing a counter for every end of scan signal received from the FRF166 and multiplying it by the number of 0° angles in the electronic angle sequences sent to the FRF166. When the number of pulses reaches the user specified value, triggering is disabled and the radar returns to the IDLE state.

4.4 PARC Configuration

The PARC configuration file is used to set values which dictate how PARC functions including the waveform and filter filepaths, APC and Acquisition Daemon IP address or hostname and port, APC and ACU handler update periods, system idle time limit, scan time limit, and general radar information. The APC and ACU update periods dictate how often the APC and ACU handler threads request the status of their subsystems and update the system status structure. It is critical that the APC update period is set small enough (<200 ms) to ensure that the system status structure accurately reflects the current, real-time status of the antenna positioner so that there is fast response time after antenna reposition commands. The DXR handler thread does not require an update period because the Acquisition Daemon automatically broadcasts every change made to the DXR configuration. The system idle time limit sets the amount of time that the radar remains in the IDLE state before disabling the servo-drives and braking the motors, in order to prevent unnecessary wear on the antenna positioner. The scan time limit sets the maximum amount of time that the radar will perform a task before entering the FAULT state, in order to halt the system in the event that a scan failed without any subsystem throwing a fault. The general radar information, which is used by PARC to send information about the system to downstream software with every

scan, includes radar name, latitude, longitude, altitude, azimuth and elevation beamwidth, operating frequency, and antenna gain. The data archivers write this information to each data file output by the system.

Chapter 5

Antenna Positioner

5.1 Introduction

The antenna positioner subsystem is responsible for precisely and accurately positioning the phased array antenna in the azimuth and elevation axes for fixed mechanical pointing during electronic scans and to sweep the antenna beam during a mechanical scan. The software which controls the antenna positioner subsystem responds to motion commands and status queries from the system controller over the system network. The dual-axis antenna positioner consists of two encoders which measure the antenna position, two servo-drive and motor pairs which actuate the positioning, the pedestal which provides support and enables mechanical rotation of the antenna, the radar platform which supports and levels the pedestal, the platform leveling measurement system which facilitates the leveling of the radar platform, and the motion control computer which runs the Antenna Positioner Controller software, or APC.

APC manages the antenna positioner hardware and uses a network interface to respond to motion commands and status queries of the antenna positioner by clients using TCP/IP over Ethernet, which includes the system controller for radar operations, the APC command-line utility for testing, and the platform leveling measurement system. APC can control the positioner to move the antenna to within 0.1° of a specified target position by closing a position control loop that uses feedback from the high precision encoders as input to a PID control algorithm to calculate motor velocity commands that it sends to the servo-drives to actuate the motors.

This chapter will provide an overview of the antenna positioner hardware, detail the design and implementation of APC, and discuss the procedures used to calibrate and configure the antenna positioner subsystem using APC.

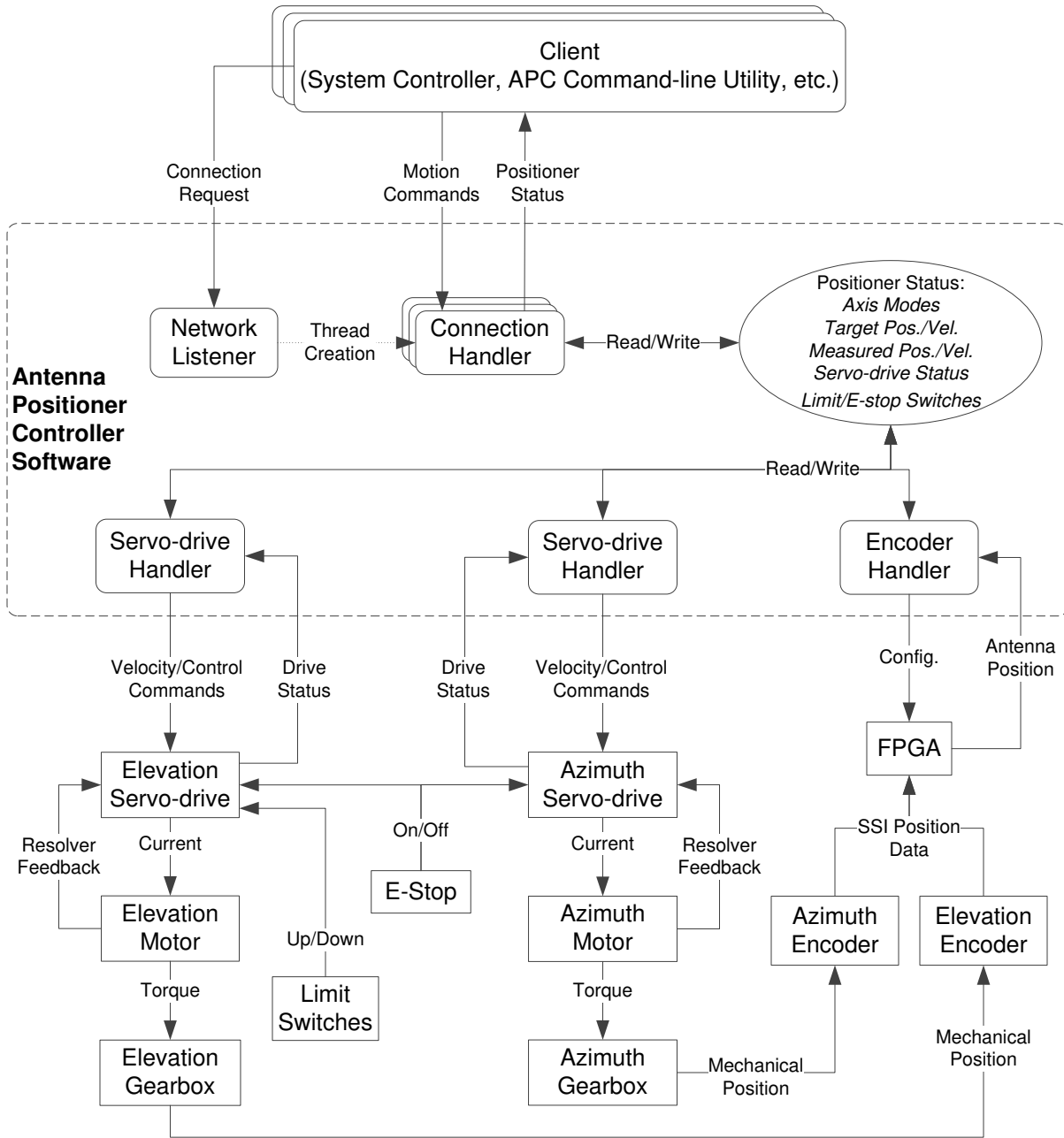


Figure 5.1: Block diagram of the antenna positioner.

5.2 Antenna Positioner Hardware Overview

5.2.1 Motion Control Computer

A motion control computer interfaces with the antenna positioner hardware and runs APC which controls the servo-system. The computer consists of a Technologic Systems TS-4710 embedded ARM processor computer-on-module (COM) and a Xilinx 3S50A FPGA. The TS-4710 meets several important constraints including low-power consumption by the CPU, ability to handle a wide temperature range, low cost, Linux support, two serial ports for communication with the servo-drives, and an Ethernet port for network communication. It uses a Marvell PXA166 processor with ARMv5TE architecture which runs the Debian distribution of Linux, booted from an SD card. The serial ports used for controlling the servo-drives utilize the RS-422 standard for serial communication. Additionally, the TS-4710 implements a 16-bit parallel bus, with multiplexed address and data which it uses to communicate with an FPGA. The Xilinx 3S50A FPGA is used to read raw antenna position data from the encoders at high speeds in order to minimize the time between antenna position measurement by the encoders and usage of the position data by APC to close the position loop. The FPGA communicates with the encoders using the Synchronous Serial Interface (SSI) via two differential TTL transceivers.

5.2.2 Encoders

Two optical absolute encoders, manufactured by SICK-Stegmann, are used to precisely measure the azimuth and elevation angles of the antenna which are used by APC to calculate antenna velocity and as feedback to the position control loop. They rely on a 24 VDC power supply and an SSI data link which uses differential TTL signals terminated by 120 ohms. The SSI link consists of a clock signal sent from the motion control computer to the encoders and 16-bit serial data sent back from the encoders to the motion control computer. Unlike relative encoders, absolute encoders do not need to be homed to start measuring absolute position if their power supply is cycled or interrupted. The azimuth encoder is mounted in the central cavity of the pedestal coupled to the

azimuth bull-gear and the elevation encoder is mounted inside the elevation head coupled to the main elevation gear. Both encoders turn 1-to-1 with the antenna in their respective axes.

The FPGA in the motion control computer needs to be configured in order to communicate with and receive accurate position data from the encoders. When each encoder is initially mounted to the pedestal, their shafts are at an arbitrary angular position with respect to the antenna and so an offset is measured and configured in the FPGA, which it uses to correct the raw position data. Additionally, the time it takes between the transmission of a clock signal from the FPGA to the encoders and receiving serial data from the encoders back must be determined so that the FPGA can sample the incoming serial data correctly.

5.2.3 Servo-drives and Motors

Two pairs of servo-drives and motors are used to move the antenna in azimuth and elevation by receiving velocity commands from APC and closing a velocity control loop. One servo-drive per axis is responsible for delivering current to its respective motor which in turn generates torque used to drive the gearbox of its respective axis. The two brushless motors, manufactured by Parker, are capable of applying up to 8.3 Nm of peak-torque drawing 11.8 A, and are rated for continuous stall torque of 2.9 Nm drawing 3.7 A. The azimuth motor is mounted in the central cavity of the pedestal with the shaft coupled to the azimuth gearbox and the elevation motor is mounted to the elevation arm with the shaft coupled to the elevation gearbox. The motors use internal resolvers which are used for approximate shaft position feedback to the servo-drives for closing the velocity loop and auto-commutating the motors. The digital servo-drives, manufactured by Advanced Motion Controls (AMC), rely on a 230 VAC power supply to deliver current to the motors. Each servo-drive uses an RS-422 serial connection to communicate with the motion control computer and also has programmable digital inputs which are used for the elevation limit switches and emergency stop switch.

An AMC proprietary software tool called DriveWare was used to configure the servo-drives which includes auto-commutating the motors, tuning the current and velocity control loops, setting

up the digital inputs, and setting the acceleration limits. Performing an auto-commutation of a motor causes the servo-drive to automatically detect the resolver feedback and polarity of the motor and configures the servo-drive such that the optimal angle between the permanent magnets on the rotor and the electric field generated by the current in the stator windings is maintained when driving the motor [17].

DriveWare is used to tune the current and velocity loops implemented by the servo-drives to smoothly and reliably actuate the motors at a commanded velocity. The servo-drives use a PI controller for the current loop and a PID controller for the velocity loop. Tuning the current and velocity loops consists of using the servo-drive to input a square wave to the respective loop, measuring and displaying the output, and tweaking the gains such that the output best matches the input square wave as shown in Figure 5.2. When tuning the current loop, the motor is decoupled from

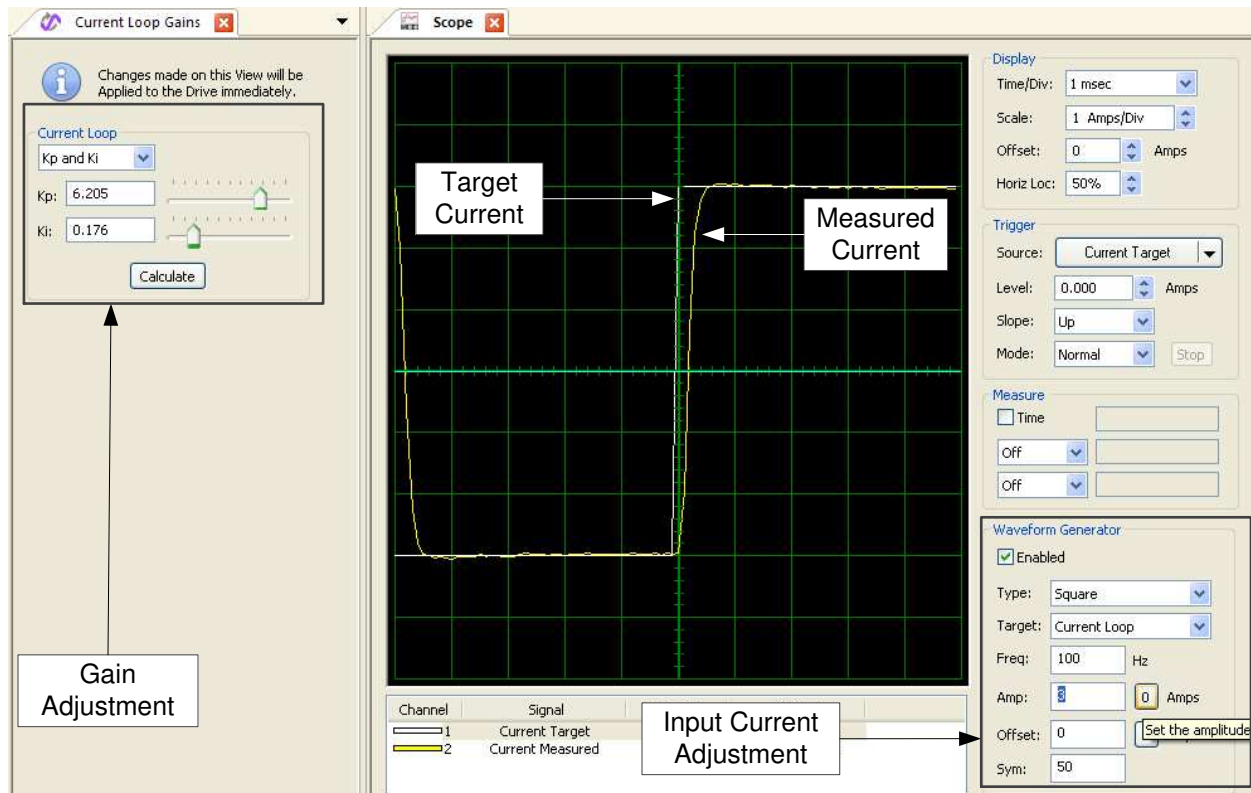


Figure 5.2: Tuning the servo-drive current loop using DriveWare.

the positioner because the purpose of this loop is to ensure that the servo-drive is outputting the desired amount of current, which is independent of the mechanical output of the motor. However when tuning the velocity loop, the motor is coupled to the positioner because the velocity of the motor shaft is dependent on the load to which it is providing torque.

The servo-drives are configured to respond to digital input from a pair of elevation limit switches and an emergency stop switch. Because the elevation axis of the pedestal is only able to move along limited range of angles, approximately -5° to 95° , before the antenna interferes with the pedestal, two limit switches are used to sense when the positioner is close to either of these mechanical limits. The limit switches are mounted in the elevation head and wired to two pairs of digital input terminals on the elevation servo-drive. When a limit switch is mechanically triggered, the elevation servo-drive receives a signal to stop motion and only respond to motion commands which will move the pedestal away from the triggered limit. Additionally, an emergency stop switch is mounted on the platform in an easily accessible location away from the pedestal and is connected to a pair of digital input terminals on both the azimuth and elevation servo-drives. When the emergency stop button is pressed, both servo-drives receive a signal and respond by stopping motion and ignoring any motion commands until the emergency stop switch is reset.

5.2.4 Pedestal

The pedestal, originally from an SCR-584 radar, has been repurposed for this phased array antenna positioner. The mechanical interface between the phased array antenna and the pedestal is a rigid frame made from 80/20 aluminum parts which allows the antenna to rotate on a large bearing about boresight. Figure 5.3 demonstrates how the antenna can be locked in two possible configurations: with the linear array parallel to the horizon for electronic PPI scans, or perpendicular to the horizon for electronic RHI scans. Also on the rotating upper-portion of the pedestal, adjacent to the antenna, is the antenna mounted electronics enclosure which houses the DXR, IF electronics box, and host computer running the system controller and the Acquisition Daemon. Network communication from subsystems on the rotating portion of the pedestal to the rest of the

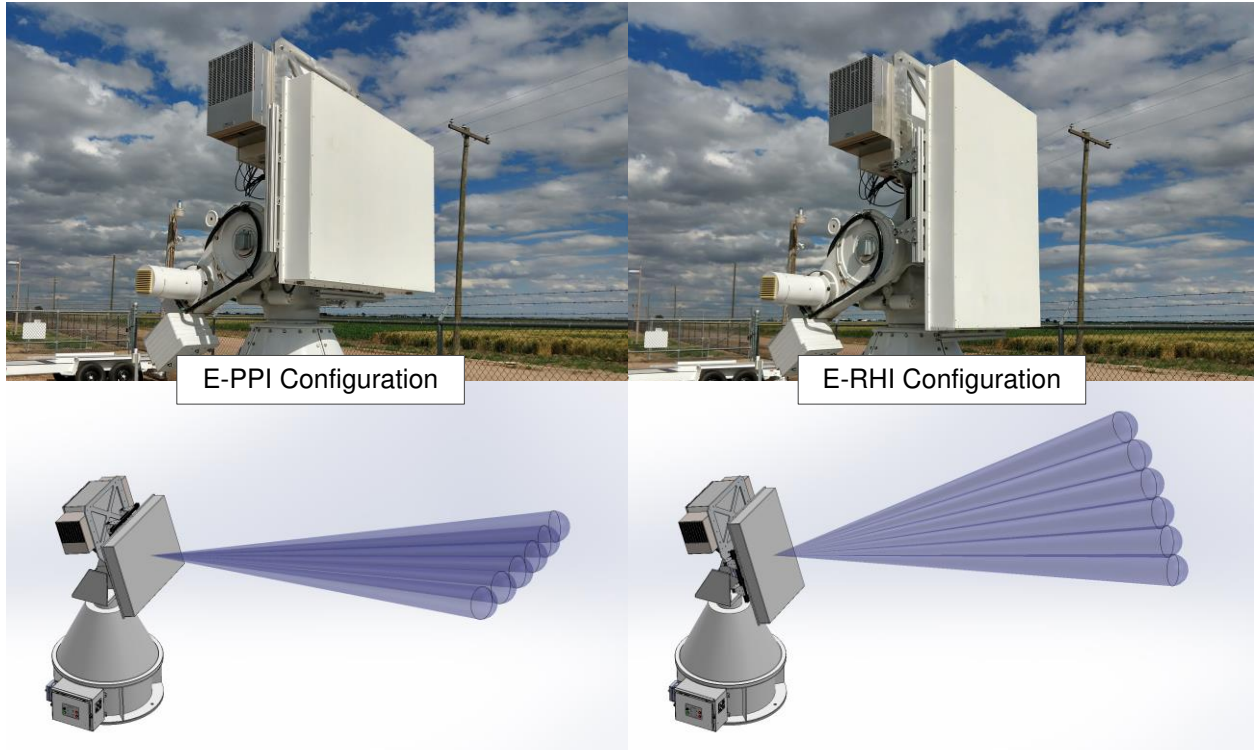


Figure 5.3: Antenna in the two mechanical configurations: electronic PPI and electronic RHI

system is done through a fiber-optic rotary joint capable of 10 Gb/s speeds. All other signals are passed through a set of slip-rings.

A counterweight system was designed and implemented to improve the static balance of the pedestal which helps reduce the load on the elevation motor during operation and also facilitates moving the antenna by hand in the case that the motion control system is disabled. The counterweight position on the elevation arm of the pedestal was chosen because it both minimized the net torque applied to the elevation motor shaft while also providing a convenient and safe point to mount without physically interfering with the rest of the system. Eight 6.25 kg steel plates were fabricated to mate to the threaded mounting rods screwed into the elevation arm. In order to determine optimal mass which reduced the net torque applied to the elevation motor shaft, the current draw of the motor was monitored while statically pointing the antenna at different elevation angles. Figure 5.4 demonstrates that when using all eight plates at 50 kg for the counterweight, compared

to four plates at 25 kg, and no weight at all, the elevation motor current draw is reduced for almost all elevation angles, particularly the lower angles.

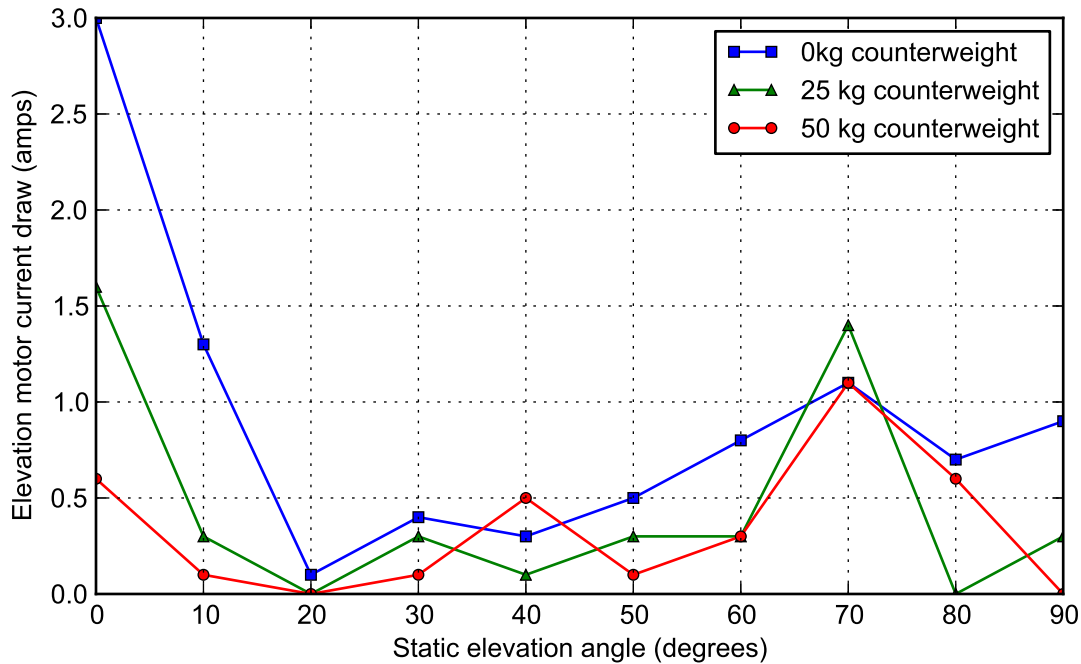


Figure 5.4: Elevation motor current draw versus static elevation angle for different counterweight masses.

The pedestal has two oil reservoirs in which the positioner gears are submerged which helps maintain lubrication and cooling of the mechanical system. The azimuth reservoir is located below the central cavity with a drain plug that can be accessed from underneath the pedestal, and the elevation reservoir and drain plug is located on the elevation arm. Each reservoir has an approximate capacity of two quarts and is refilled with gear oil every six months, using higher viscosity oil during the hotter part of the year.

5.2.5 Radar Platform

The radar platform on which the pedestal and all other electronics enclosures are intended to be mounted is a steel frame, tandem axle trailer designed and manufactured by Maxey Trailer Co. in Fort Collins, Colorado. The trailer design had to meet several constraints including sufficient load

capacity and bed-space, ease of shipping, rigidity, and leveling capability. The trailer has a load capacity of 5000 lbs with 150" x 54" of usable bed space. In order to fit into a standard 20-foot shipping container for ease of deployability, the overall size of the trailer is 210" x 77". The bed is made of 3/8" steel and is supported by eight steel cross-beams to maximize rigidity under the load of the antenna positioner at all azimuth and elevation angles. The trailer is fitted with four leveling jacks, each mounted onto an outrigger which extends out 28" past the bed of the trailer.

5.2.6 Platform Leveling Measurement System

The platform leveling measurement system consists of an A20-OLinuXino-LIME single board computer which is connected through USB to a SparkFun 9DoF Razor inertial measurement unit, or IMU, both of which are mounted inside a small weather-proof enclosure and in turn mounted to the antenna frame such that the IMU is near and parallel to the antenna. The IMU includes a 3-axis accelerometer which is used to measure the direction of acceleration due to gravity with respect to the IMU and the antenna. The A20 computer is connected to the system network through an Ethernet connection to a spare port on the antenna mounted electronics enclosure leading to a network switch. Using this Ethernet connection, a power over Ethernet injector located in the antenna mounted electronics enclosure provides 5 VDC power to the platform leveling measurement system. This design requires only one physical connection for both power and communication which is useful because of the limited number of spare ports on the antenna mounted electronics enclosure.

The A20 computer runs software which uses the accelerometer data to calculate and display the angle between the azimuth axis of the pedestal and gravity as a function of antenna azimuth position, which informs the user how to adjust the leveling jacks on the radar platform. The leveling measurement software opens a virtual serial port to read data from the IMU and connects to APC. A command is sent to APC to reposition the antenna to a specified starting position, followed by another APC command which moves the antenna at a specified constant velocity in azimuth. Once motion has started, the software continually queries APC for the current azimuth position

as it reads raw 3-axis accelerometer values from the IMU serial port, applies a correction, and averages a specified number of samples in order to reduce variability in the measurements caused by vibrational noise. The angle between the measured gravity vector and the azimuth axis vector, which is assumed to be reasonably aligned with one of the axes of the IMU, is calculated below:

$$\theta = \cos^{-1}(v_{az} \cdot \vec{g}) \quad (5.1)$$

The off-angle result and corresponding antenna azimuth angle is written to a file which can be read by a simple plotting program used to visualize the data.

Figure 5.5 shows two sets of data collected by the platform leveling measurement system: the first taken while the platform was in an unlevelled state and the second taken after the platform was leveled. The pre-leveling data forms a sinusoidal curve whose peak amplitude indicates that the

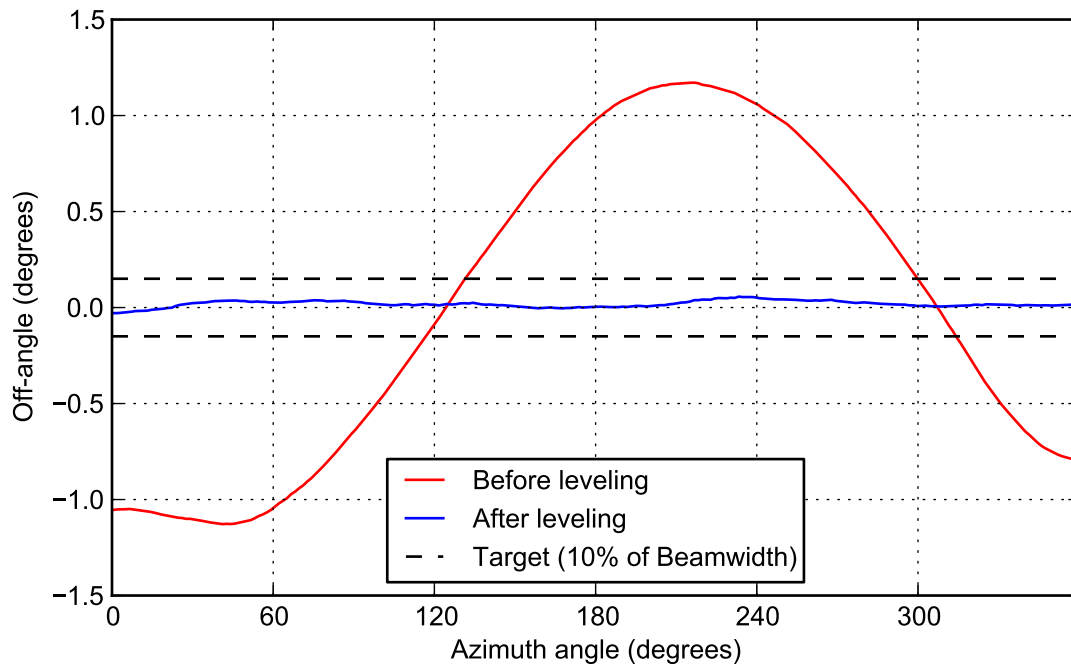


Figure 5.5: Off-angle versus antenna azimuth angle before and after leveling the platform.

platform was unlevelled at a maximum of approximately 1.2° near 40° and 220° in azimuth. The

post-leveling data shows that the off-angle is within the target leveling of 10% of the minimum antenna beamwidth, or 0.15° , for all azimuth angles. Note that the plotted data has been smoothed by a Savitzky Golay filter in order to filter out high frequency noise and preserve the shape of the curve [18].

Prior to running the platform leveling measurement software, the 3-axis accelerometer must be calibrated in order to correct the inherent sensor error. Calibration consists of measuring the offset and gain for each axis of the accelerometer and storing them in the leveling measurement software where they are used to correct the raw data from the IMU [19]. The actual accelerometer value, in units of g (9.8 m/s), is calculated by:

$$A_{actual} = \frac{A_{out} - A_{offset}}{G} \quad (5.2)$$

The gain G and offset A_{offset} are calculated using (5.3) and (5.4), where A_{+1g} is the raw measurement of a 1-axis accelerometer parallel to and in the same direction as the gravitational field, and A_{-1g} is the same but in the opposite direction:

$$A_{offset} = 0.5 * (A_{+1g} + A_{-1g}) \quad (5.3)$$

$$G = 0.5 * \frac{A_{+1g} - A_{-1g}}{2} \quad (5.4)$$

In practice, A_{+1g} and A_{-1g} are measured by placing the IMU on a surface that has been determined to be level, oriented such that the accelerometer axis in question is parallel to the direction of gravity, observing the output of the accelerometer for the first value, then rotating the IMU 180° about an axis perpendicular to the accelerometer axis in question and observing the output of the accelerometer again for the second value; the positive value will be A_{+1g} and the negative value will be A_{-1g} .

5.3 APC Software Architecture

5.3.1 Software Overview

APC controls the antenna positioner subsystem using a multi-threaded design to handle each I/O device in the subsystem independently and a global status structure to coordinate actions between threads. The main thread creates the following threads: a listener thread which in turn creates one connection handler thread per client requesting a TCP/IP connection; an encoder handler thread which communicates with the FPGA to configure the encoders, read antenna position, and calculate velocity; and a pair of servo-drive handler threads which communicate with the servo-drives to actuate the motors and receive information about their status.

APC maintains a global structure containing a set of values which together make up the status of the antenna positioner subsystem, including measured antenna position and velocity, target position and velocity, motor current, and emergency-stop and limit switch status. The individual threads all have read and write access to the APC status structure in order to update values pertaining to their I/O device and to read status values relevant to their function. Connection handlers receive commands from a client and update the axis mode and target position and velocity variables in the APC status structures accordingly, which are monitored and fed into a control algorithm by the servo-drive handler threads. Clients can also query APC to receive a packet which contains the most recent antenna positioner status.

5.3.2 Main Thread

The main thread is the first process to run when executing APC and is responsible for ingesting a configuration file, establishing communication with positioner hardware, initializing the global APC status structure and associated mutexes, and creating the other threads which make up the rest of the APC software, including the network interface and hardware handler threads.

The first task done by the main thread is to read a configuration file using a default filepath if one is not specified as a command-line argument. The configuration file contains a list of variables which set up the network interface, PID control parameters, position and velocity command lim-

its, servo-drive communication information, encoder configuration information, and general APC behavior. The configuration variables are stored into a structure by the main thread, a pointer to which is passed to the other threads when they are created.

The main thread initializes connections to the FPGA and the azimuth and elevation servo-drives. Communication with the FPGA, which is physically connected to the COM board via a 16-bit parallel multiplexed address and data bus, is established by mapping the FPGA registers to the COM memory using `/dev/mem`, to which a pointer is created. Serial communication is established with each of the servo-drives using configurable baud rates. By default the servo-drives are configured for their maximum serial communication speed which is 115200 baud.

The main thread initializes the global APC status structure and associated mutexes for managing global read and write access and creates the other threads: the network listener, encoder handler, and servo-drive handler threads. Pointers to the configuration variable structure, the APC status structure, and the mutexes are passed to each one of the created threads. Additionally, the encoder handler thread is passed a pointer to a structure containing the information needed for communication with the FPGA and the servo-drive handlers are passed pointers to the structures containing the information needed for serial communication with their respective servo-drives.

5.3.3 APC Status Structure

The APC status structure is used to store the values which represent the current state of the antenna positioner subsystem. It contains four structures: the azimuth and elevation target structures and the azimuth and elevation measured status structures. The target structures contain variables which represent how the antenna positioner is being commanded, consisting of the axis mode, target position, target velocity, and a max-speed flag used to indicate whether the maximum configured speed will be used for reaching a target position. The measured status structures contain variables which reflect the current measured state of the antenna positioner, consisting of the current position, velocity, at-target position and velocity flags, motor current consumption, limit switch state, emergency stop switch state, servo-drive power bridge state, and axis fault state.

Read and write access to the APC status structure is global so that each thread can update the status of the APC and read the fields it needs to complete a task for which it is responsible. The connection handler threads receive packets from clients which contain either motion control information used to write to the target structures or status queries to which a connection handler responds with a copy of the APC status structure. The servo-drive handler threads read both the target and measured status structures for inputs to the control system and to update the measured status structures with at-target position and velocity flags in addition to the information it receives from the servo-drives which includes motor current consumption, switch states, servo-drive power bridge state, and axis fault state information. The encoder handler thread updates the measured status structures with current antenna position and velocity. One mutex per axis is used to manage the global access of the APC status structure in order to prevent multiple threads from reading or writing to a field simultaneously.

5.3.4 Encoder Handler Thread

The encoder handler thread is responsible for configuring the FPGA to properly handle communication with the encoders, calculating antenna position and velocity from raw encoder position, and updating the APC status structure with measured position and velocity. The encoder handler thread uses the pointers passed to it from the main thread to read and write to the registers on the FPGA in order to send configuration information receive encoder data.

The FPGA is configured by setting the encoder offsets and specifying the clock period and sample edge delay for SSI communication with the encoders. Because both encoders are installed with their shafts at an arbitrary starting position with respect to the position of the antenna, an offset for both axes is determined and included in the configuration file so that the encoder handler thread can write the appropriate values to the offset registers in the FPGA. The clock period dictates the rate at which data is received by the FPGA and is set to the maximum data output rate of the encoders. The sample edge delay is the time it takes between the transmission of a clock signal

from the FPGA to the encoders and receiving serial data back to the FPGA, which is the aggregate of delay due to slew rate, propagation delay, and encoder logic.

After configuring the FPGA, the encoder handler thread reads the azimuth and elevation encoder position registers in the FPGA every 100 milliseconds and calculates the current antenna position and velocity. The raw encoder data is in units of encoder steps which is a function of the number of bits of precision the encoders have. The conversion from encoder position in steps P_s to degrees P_d for an n -bit encoder is calculated by:

$$P_d = \frac{360}{2^n} * P_s \quad (5.5)$$

For the 16-bit encoders used in this system, there are 65536 steps per revolution of the encoder shaft. Velocity is calculated simply by taking the difference between successive position reads, applying the step-to-degree conversion (5.5), and dividing by the 100 millisecond position read period. The case where the encoder passes the 0-th count between successive position reads is taken into account when calculating velocity for azimuth and elevation. Finally, the encoder handler thread uses the position and velocity values it calculated to update the appropriate fields in the APC status structure.

5.3.5 Servo-drive Handler Threads

There are two servo-drive handler threads, one for azimuth and one for elevation, which are responsible for communicating with their respective servo-drive to control the motion of the antenna and update the servo-drive and motor information in the APC status structure. They each use the serial port file descriptor passed to them by the main thread to send commands to and receive status from a servo-drive.

The servo-drive handler threads utilize a state machine structure which reflects one of the four modes in which the axis mode in the APC status structure is set: idle, stop, velocity-hold, and position-hold. In idle mode, the servo-drive power bridge is disabled, which disconnects power to the motor and applies the brake. In stop mode, the motor is stopped but remains powered and un-

braked. In velocity-hold mode the motor moves the antenna at the target velocity in the APC status structure. In position-hold mode, the motor moves the antenna to the target position in the APC status structure. Because the servo-drives are only capable of closing a velocity loop, the motors are actuated by velocity commands to the servo-drives from the servo-drive handler threads which implement a PID control system to close the position loop.

When in position-hold mode, a servo-drive handler thread iterates through a loop in which it calculates the position error and PID terms, then sums them and sends the result to the servo-drive as the target velocity. To calculate the position error, the difference is taken between the target position and the current position:

$$e = P_{target} - P_{actual} \quad (5.6)$$

If the absolute value of the error is less than that of the configurable position error tolerance value then the at-target position flag in the APC status structure is set. The proportional term is calculated simply by multiplying the configurable P-gain by the error:

$$P_n = K_p * e_n \quad (5.7)$$

This term is stored, along with a timestamp, to calculate the derivative term in the next iteration of the loop. The derivative term is calculated by taking the difference between the current position error and the most recent previously calculated error, dividing the result by the difference between the current time and the aforementioned timestamp, and multiplying the result by the configurable D-gain:

$$D_n = K_d \frac{e_n - e_{n-1}}{t_n - t_{n-1}} \quad (5.8)$$

The integral term is calculated by multiplying the position error by the time-delta, multiplying the result by the configurable I-gain, and adding it to a stored accumulator which is set to zero whenever a new target position is set:

$$I_n = K_i(t_n - t_{n-1}) + I_{n-1} \quad (5.9)$$

The I-term has a configurable maximum value to limit large and sporadic velocity commands caused by a nonzero steady-state error. Finally, the sum of the PID terms is computed and sent to the servo-drive as a target motor velocity after being capped by the configurable speed limit for the appropriate axis [20].

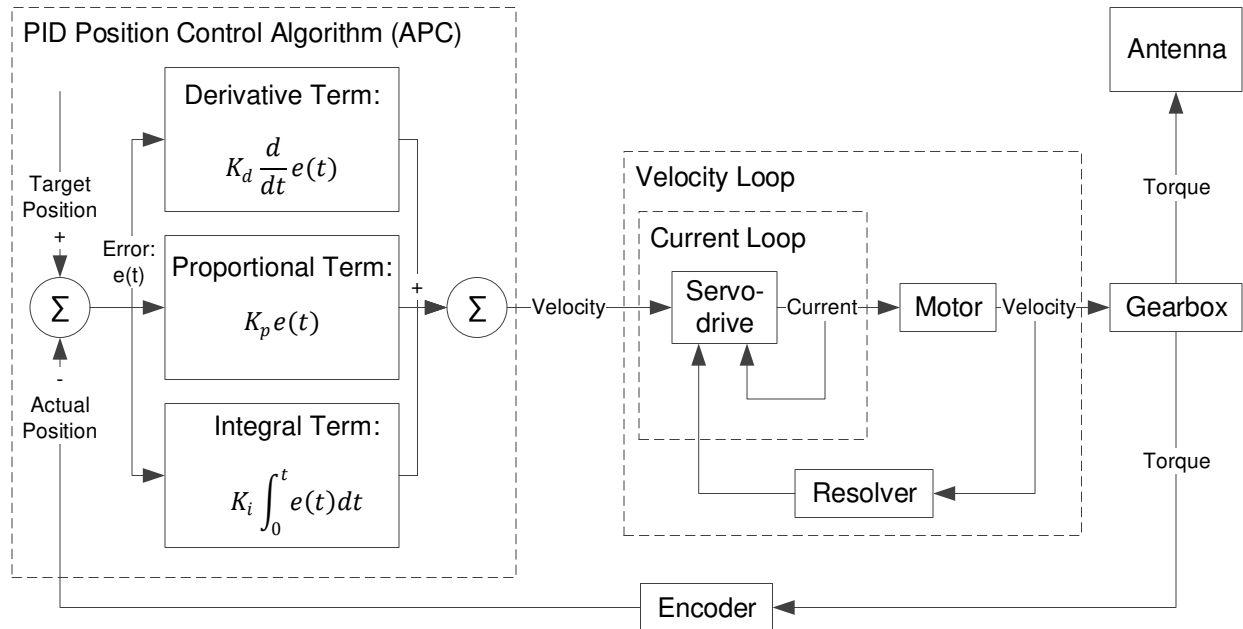


Figure 5.6: Block diagram of the position control loop, highlighting the PID algorithm implemented by the servo-drive handler threads.

The servo-drive handler threads are also responsible for updating several fields in the APC status structure which correspond to the status of their respective servo-drive and motor. The servo-drives are queried for status which provides information to APC, including motor current consumption, limit switch state, emergency stop switch state, motor brake state, servo-drive power bridge state, and fault state.

5.3.6 APC Command-line Utility

The APC command-line utility is a simple program which is used to send commands directly to APC over the network from a separate host computer for APC development and testing purposes or

if the system controller is disabled. It takes command-line arguments which allow the user to query APC for status, send motion commands, disable the servo-drives, clear any faults within APC, and write position versus time data to a file for PID loop tuning purposes. Table 5.1 shows all of the command-line arguments of the utility, the parameters they accept, and their functionality.

Table 5.1: Command-line arguments and functionality for the APC command-line utility.

Argument	Parameters	Functionality
-help	None	Prints a list showing the functionality of the command-line utility.
-status	None	Queries APC for status.
-target	Az. axis mode, Az. target position, Az. target velocity, Az. max-speed flag, El. axis mode, El. target position, El. target velocity, El. max-speed flag, Command bitmask	Sends a motion command to APC. Axis mode can be "s" (stop), "i" (idle) "v" (velocity), and "p" (position). The bitmask indicates to the APC which parameters, if any, to ignore.
-goto	Az. target position, El. target position	Sends a command to APC to move the antenna to the specified position using the maximum configured speed.
-setidle	None	Disables the power bridge circuit on the servo-drives.
-clearfaults	None	Clears any faults within APC.
-logresponse	Filename	Continuously queries APC for status and writes the time and position to a file until the target position is reached.

5.4 APC Calibration and Configuration

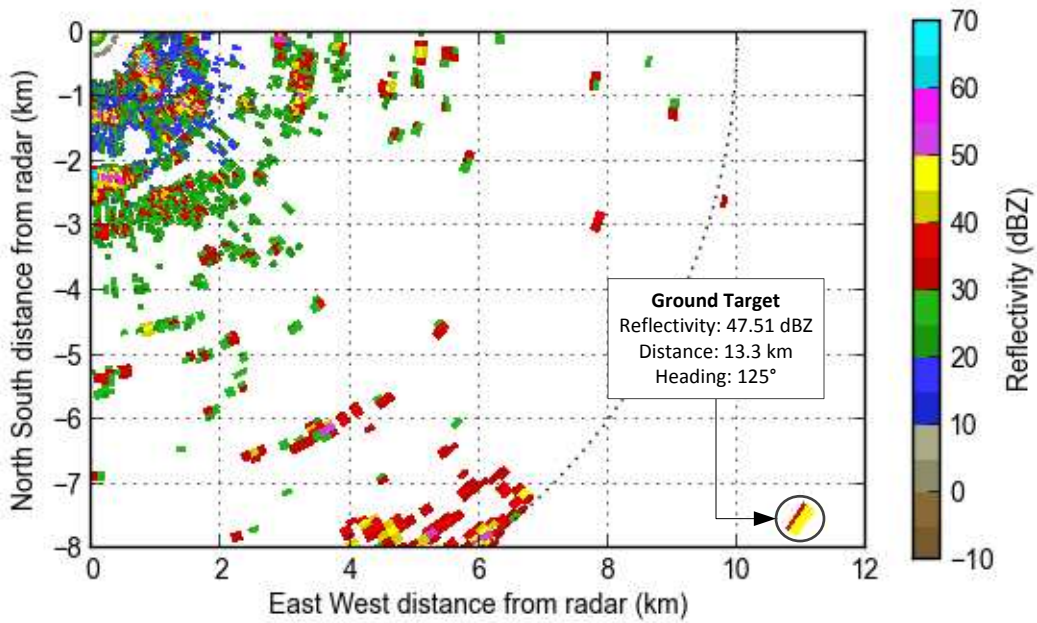
5.4.1 Encoder Offsets

Measuring and setting the azimuth and elevation encoder offsets is necessary because when the encoders are mechanically installed into the pedestal, their shafts are at an arbitrary position relative to the position of the antenna. Once the difference between the encoder shaft position and

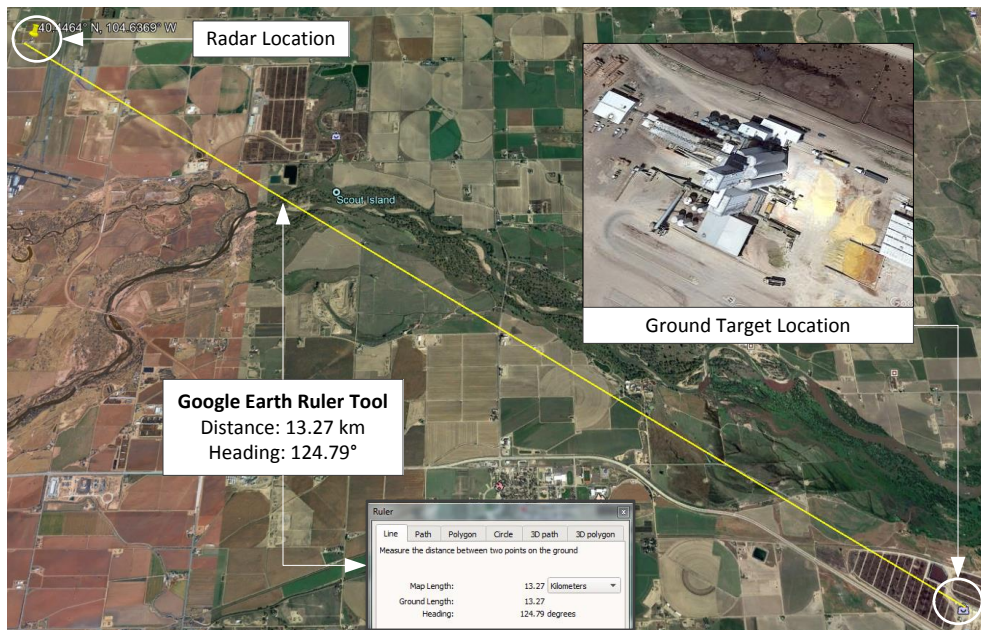
the angular position of the antenna is determined and accounted for, the real antenna position is known by the system. More sensitive radars can utilize a solar calibration method to measure the encoder offsets, however this system is not capable of observing X-band radio emissions from the sun and therefore other means are used to measure the azimuth and elevation offsets.

The azimuth encoder offset is initially estimated using a compass to determine the cardinal direction in which the antenna is pointing. Setting a rough estimate of the azimuth encoder offset facilitates fine-tuning of the offset which requires using a low elevation scan to find a known ground target. To fine-tune the azimuth encoder offset, a ground target is chosen such that it is reasonably isolated and relatively tall when compared to other nearby ground targets so that it is easy to distinguish, and narrow enough to appear in as few range bins as possible to maximize the precision of the measurement. Once the azimuth encoder offset is roughly set and a suitable ground target is found, a 1° to 2° elevation PPI scan is run over the sector in which the ground target is located. If the chosen ground target met the aforementioned criteria and the initial rough estimate of the offset was reasonable, it can be located in the radar display as a small target with high reflectivity and zero velocity. The apparent azimuth angle of the ground target can be compared against satellite imagery, and the difference between the measured and the actual azimuth angle can be set in the APC configuration file. Figure 5.7 demonstrates the verification of the azimuth encoder offset using Google Earth to locate an isolated ground target observed with the system and measure the heading and distance with respect to the radar location.

To measure the actual elevation angle of the antenna, an inclinometer with precision of at least 0.1° is placed against the face of the antenna. Note that when making this measurement, it is assumed that the radar platform has been leveled close to $\pm 0.1^\circ$ using the procedure discussed in Section 5.2.6. The difference between the inclinometer reading and the elevation angle reported by APC is the elevation encoder offset which should be set in the configuration file.



(a) Reflectivity plot showing the ground target.



(b) Satellite image (Google Earth) with distance and heading of the radar to the ground target.

Figure 5.7: Determining the azimuth encoder offset using a known ground target and comparing its heading from the radar calculated from reflectivity data collected with the system versus from the radar calculated from satellite imagery.

5.4.2 Position Control Loop

The response of the antenna position control loop implemented in APC can be adjusted by tuning the PID control loop parameters in the APC configuration file. In addition to tuning the PID gains, the response of the system can be further adjusted by changing the speed limit, maximum integrator error, and the at-target position tolerance.

The goal of tuning the PID control loop parameters is to create a control system which minimizes the following: the time it takes for the target position to be reached, or rise-time, the overshoot past the target position, subsequent oscillatory behavior, the amount of time it takes for the system to reach a stable state, or settling time, and the steady-state error. Increasing the P gain will decrease the rise-time and decrease the steady state error but increase the overshoot and exacerbate oscillatory behavior. Increasing the I gain will decrease rise-time and eliminate the steady-state error at the cost of increasing the overshoot, exacerbating oscillatory behavior, and increasing the settling time. Increasing the D gain will decrease the overshoot, decrease the settling time, and either improve or exacerbate oscillatory behavior [21]. Increasing the speed limit will increase the slope of the response, however caution must be taken as to not cause an over-current fault in the servo-drives and motors. The maximum integrator error limits the I term in the control signal so as to minimize sporadic steady-state corrections to the antenna position which may happen if the antenna is held at a target position for a long period of time. The at-target position tolerance is the amount of position error that APC will tolerate when setting the at-target position flag.

Two different methods were used to tune the PID control loop: the Ziegler-Nichols method and a P-only gain adjustment method. The Ziegler-Nichols method computes the PID gains, K_p , K_i , and K_d :

$$K_p = 0.6K_u \quad (5.10)$$

$$K_i = \frac{2K_p}{T_u} \quad (5.11)$$

$$K_d = \frac{K_p T_u}{8} \quad (5.12)$$

where K_u is the minimum P gain, with the I and D gains set to zero, at which the system produces sustained, steady-state oscillations and T_u is the period of these oscillations in seconds [22]. The P-only gain adjustment method simply sets the I and D gains to zero, and finds the maximum K_p where no overshoot occurs.

Figure 5.8 shows the responses of the two PID control systems, the Ziegler-Nichols and the P-only, used in the azimuth axis with a starting position of 0° , target position of 60° , and speed limit of 30° per second. Note that while the Ziegler-Nichols system reaches the target position

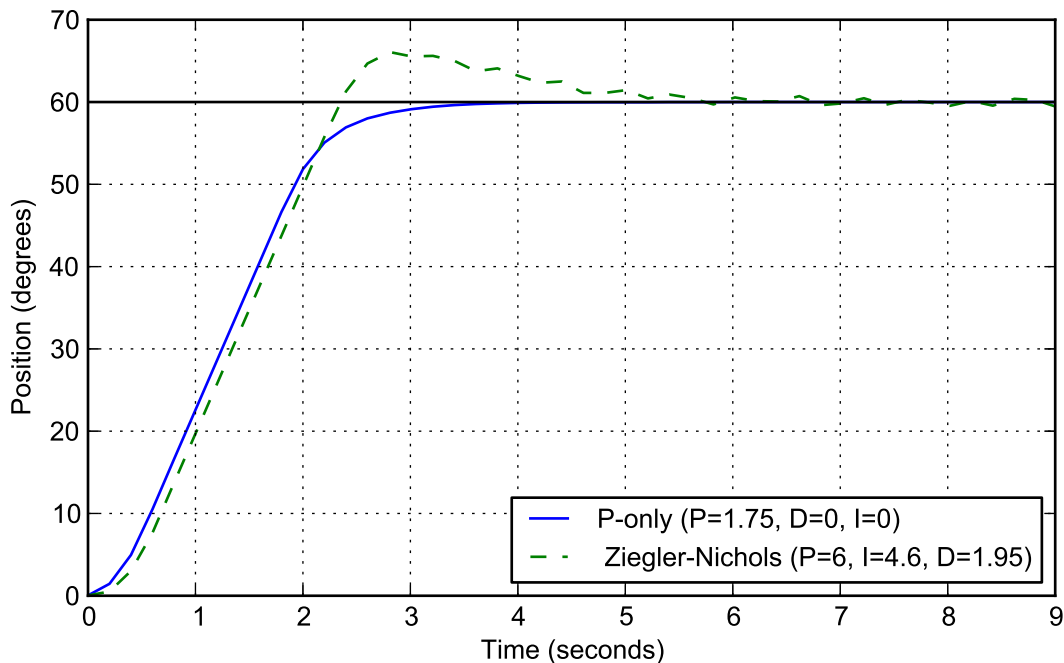


Figure 5.8: Responses of the P-only and Ziegler-Nichols control systems used for the azimuth position loop with a starting position of 0° and a target position of 60° .

faster than the P-only system, there is a significant overshoot of more than 5° followed by multiple oscillations and a long settling time of over 9 seconds. Although the P-only method resulted in a control system which has a slower rise-time, particularly when the antenna is within 5° of the target position, there is no overshoot and no oscillatory behavior, which are higher priorities when

holding a fixed position for electronic scans and when moving the antenna during a mechanical scan.

Chapter 6

Signal Processor

6.1 Introduction

The signal processor subsystem is responsible for calculating weather moment data from the raw IQ data output by the DXR, writing moment and timeseries data files to the system storage, and visually displaying the data to the user. A Linux machine with a multicore processor hosts the signal processing software which uses a thread pool based architecture to enable parallel processing of the data. Worker threads process work units in parallel, which each correspond to one coherent processing interval, using one of four autocovariance processing modes that have been implemented for the system: single polarization mechanical scan, single polarization electronic scan, alternating polarization mechanical scan, and alternating polarization electronic scan. Using these processing modes, the signal processor is capable of calculating signal-to-noise ratio, reflectivity, doppler velocity, normalized coherent power, spectral width, differential reflectivity, differential phase, and correlation coefficient for both mechanical and electronic scans.

The moment archiver, a TCP/IP client to the signal processing software, ingests the processed data and writes it to a high capacity RAID storage and a binary-to-NetCDF converter is used to convert the data files so that they can be read and plotted by the real-time display software. Furthermore, the signal processor subsystem can store and reprocess timeseries files using the timeseries archiver and offline signal processing software which is useful for regenerating moment data with altered calibration values and testing new processing modes.

Calibration values including the short-to-long pulse transition, radar constant, Z_{dr} bias, and power correction and phase rotation tables, are read from a configuration file and are used to correct reflectivity, differential phase, and differential reflectivity. The power and phase rotation tables are generated by running an electronic scan calibration mode, and are meant to correct for differences in horizontal and vertical power and phase for each electronic scan angle. Additionally, a noise

calibration mode is used to calculate the average noise floor of the receiver. Signal processing for electronic scans, compared to traditional mechanical scans, requires that trigger numbers for incoming timeseries data are monitored in order to associate a given ray with its corresponding electronic scan angle. This is crucial to ensure that the pointing angle information for each ray is correct, and that the power and phase differences due to electronic scanning are properly corrected for.

This chapter will provide an overview of the signal processing software, detail the implementation of the processing algorithms and downstream software, and discuss the procedures used to calibrate the radar and configure the signal processor subsystem.

6.2 Signal Processing Software Overview

6.2.1 Thread Pool Architecture

The signal processing software maximizes throughput by utilizing a thread pool architecture which takes advantage of the multi-core CPU of the signal processing computer to enable parallel processing of the digital IQ data output from the DXR. The thread pool consists of three types of threads: the assign thread which sets up processing modes and assembles work units, the worker threads which simultaneously process multiple work units using the algorithms specified by the processing modes, and the collect thread which orders the processed data and passes it to the connection handler threads for output over the network or to a file writer thread if using the offline signal processing software.

The assign thread reads metadata and IQ data packets on an input queue which is populated by an ingest thread that reads the DXR output over a 10 Gb/s fiber-optic link. Based on the radar system, or platform, for which the signal processing software is configured, the assign thread sets the appropriate processing mode in response to specific metadata packets and structures the raw IQ data into work units for processing by the worker threads. Once a work unit, corresponding to a single ray, has been created, it is passed to the next available worker thread along with a copy of the signal processing software's state which includes the processing mode to be used.

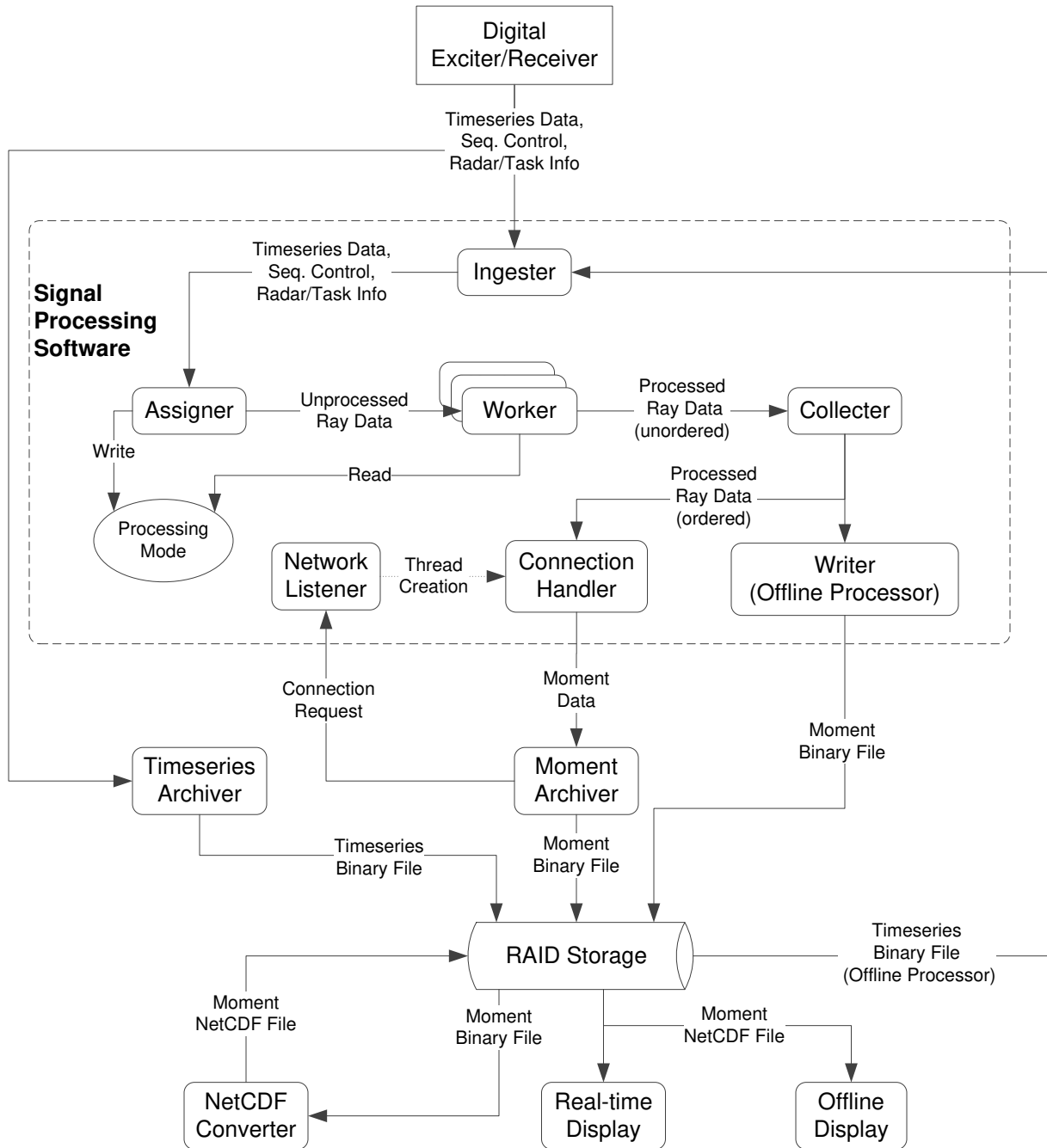


Figure 6.1: Block diagram of the signal processing, archiving, conversion, and display software.

The worker threads are responsible for processing work units in parallel using the algorithms which correspond to the processing mode it was passed. The number of worker threads spawned upon execution of the software is specified in the signal processor configuration file and is set such that there is one worker thread per CPU core in order to maximize the parallel processing capability of the hardware. Each worker thread is passed pointers to a semaphore indicating how many workers are idle and an idle condition variable which are used to indicate to the assign thread how many worker threads and which ones are ready to accept a new work unit. Additionally, each worker thread is passed a pointer to a semaphore which informs the collect thread how many worker thread have finished processing a work unit. The collect thread reads the output from the worker threads, reorders the data if necessary, and writes it to an output queue which is read by connection handlers to write the data to a network socket to be ingested and written to a file by a moment archiver or alternatively, read by a file writer thread if using the offline signal processing software.

6.2.2 Offline Signal Processing Software

The offline signal processing software is an independent program which utilizes the same thread pool architecture and processing modes as the online software but instead of reading a DXR data stream and writing the processed output to a network socket, it reads and processes timeseries data files and writes the result to a moment data file. The offline signal processing software is a useful utility for reprocessing IQ data in order to regenerate moment data with altered calibration values or processing modes, or to test entirely new processing modes. Only the main, ingest, and collect threads behave differently in the offline software in order to minimize any differences in the output compared to the online software.

The main thread of the offline signal processing software uses a flag to signal to the ingest and collect threads to slightly modify their behavior for offline processing. The offline ingest thread reads data from a file using the timeseries data filepath passed to it by the main thread and, as in the online software, adds the metadata and IQ data packets to an input queue which is read by

the assign thread. The assign thread and worker threads in the offline software then process the metadata and IQ data, behaving in the exact same way as in the online software. When the offline collect thread receives processed data from the worker threads it writes to an output queue which is read by the main thread that in turn writes the processed data to an output file. The result is signal processing software which can process timeseries data offline and independent of the rest of the system which is useful for reprocessing data with different calibration values and testing new processing modes.

6.2.3 Signal Processing Platforms

The signal processing software can be configured to process the system controller metadata and DXR IQ data for different radar platforms. A platform identification variable, which is set in the signal processor configuration file, is used to access the appropriate metadata parsing and initialization functions from a table. These functions are used by the assign thread to respond accordingly to system controller metadata packets from the DXR. A separate table is used to store platform-specific processing modes which contain pointers to the functions used for assembling work units and running the appropriate processing algorithms for a given scan. A processing platform was developed to handle metadata and process IQ data specifically for the Front-X radar system.

6.3 Front-X Signal Processing Platform

6.3.1 Thread Pool Functionality

The Front-X signal processing platform specifies the functions used by the assign thread to respond to DXR metadata packets originating from the system controller and assemble the raw IQ data into work units for processing by the worker threads. At the start of a task, the system controller sends scan mode and radar information packets to the DXR to inject into its output data stream which contain information about the type of scan used and the information needed to process it, including the number of integrations and samples per ray, pulse repetition time, range

gate spacing, polarization mode, electronic scan angles, etc. When the assign thread reads a scan mode packet from its input queue, it sets the processing mode to correspond to the type of scan used and stores the values used by the worker threads for processing. When a radar information packet is read, the assign thread injects a processing information packet into the output data stream of the signal processing software for use by archiving, file conversion, and display software.

After setting the signal processing software to the appropriate processing mode, the assign thread assembles the received IQ data into manageable work units, each representing one ray of unprocessed data, to be sent to the next available worker thread. Each packet of IQ data received from the DXR corresponds to a set of samples of the received signal for one transmitted pulse. The assign thread increments a pulse counter for each packet of IQ data received, stores the data into a work unit structure, and compares the value of the pulse counter to the stored pulses per frame field from the last received scan mode packet. If the number of packets received equals the number of pulses per frame, the assign thread resets the counter and sends the completed work unit to the next idle worker thread for processing. The assign thread accounts for the possibility of dropped data packets by monitoring the trigger number associated with each IQ data packet. If the trigger number for the most recently received data packet is different from the last data packet but the pulse counter is less than the pulses per frame field, this is an indication that one or more data packets from the DXR has been dropped and the assign thread abandons that particular work unit.

The worker threads use a different algorithm to calculate moment data depending on what processing mode was set by the assign thread in response to the type of scan that was used to generate the IQ samples. There are four autocovariance processing modes implemented for the Front-X signal processing platform, one for each combination of single and alternating polarization mode and mechanical and electronic scan mode: single polarization mechanical scan, single polarization electronic scan, alternating polarization mechanical scan, and alternating polarization electronic scan processing modes. The single polarization and alternating polarization processing modes use distinct autocovariance signal processing algorithms to calculate signal-to-noise ratio, reflectivity, doppler velocity, normalized coherent power, and spectral width. In addition to the single polar-

ization moments, the alternating polarization mode calculates differential reflectivity, differential phase, and correlation coefficient. Additionally, two calibration modes have been implemented: an electronic scan calibration mode used to calculate horizontal and vertical power and differential phase for beams using each electronic scan angle; and a noise calibration mode used to calculate the receiver noise floor in order to perform the noise subtraction used by the processing algorithms.

6.3.2 Single Polarization Autocovariance Processing Algorithm

The single polarization autocovariance processing algorithm operates on horizontal-only and vertical-only polarization samples collected in both the mechanical scan and electronic scan modes of the radar to calculate signal-to-noise ratio, reflectivity, doppler velocity, normalized coherent power, and spectral width [7]. The first stage of the algorithm calculates the lag 0, 1, and 2 autocovariances of the received signal for N samples at each range bin for both the short and long pulse subchannels:

$$R[0] = \frac{1}{N} \sum_{n=1}^N S[n]S^*[n] \quad (6.1)$$

$$R[1] = \frac{1}{N-1} \sum_{n=1}^N S[n+1]S^*[n] \quad (6.2)$$

$$R[2] = \frac{1}{N-2} \sum_{n=1}^N S[n+2]S^*[n] \quad (6.3)$$

where S is the complex form of the IQ sample of the received signal for a given subchannel and range bin. The diagram in Figure 6.2 shows the receive pulses in sample-time for one range bin which are used to calculate the autocovariances in the single polarization processing modes.



Figure 6.2: Receive pulses in sample-time for one range bin in the single polarization processing modes.

The second stage of the algorithm calculates the moments at each range bin using the autocovariances from (6.1), (6.2), and (6.3). A configurable short-to-long pulse transition variable specifies the range bin at which the algorithm switches from using the short pulse to the long pulse autocovariances to calculate the moments. Note that the short pulse data is used for range bins closer to the radar because of its smaller blind range and the long pulse data is used for the range bins farther from the radar because of its higher sensitivity. The signal-to-noise ratio is calculated by:

$$\text{SNR} = \frac{R[0]}{P_{noise}} \quad (6.4)$$

where P_{noise} is the noise floor power calculated from the noise calibration mode. The normalized coherent power is calculated by:

$$\text{NCP} = \frac{|R[1]|}{R[0]} \quad (6.5)$$

and the spectral width is calculated by:

$$w = \frac{v_{nyq} \sqrt{\sigma^2}}{\pi} \quad (6.6)$$

where v_{nyq} is the Nyquist velocity, calculated from the pulse repetition frequency PRF of the scan, and the wavelength λ of the center frequency of the transmitted pulse:

$$v_{nyq} = \frac{\text{PRF} * \lambda}{4} \quad (6.7)$$

and the variance, σ^2 , is calculated in two different ways based on a configurable threshold:

$$\sigma^2 = -2 \ln \frac{|R[1]|}{R[0]} \quad (6.8)$$

$$\sigma^2 = \frac{2}{3} \ln \frac{|R[1]|}{|R[2]|} \quad (6.9)$$

If the SNR is greater than the threshold, the variance is calculated using (6.8), otherwise (6.9) is used. The reflectivity in decibels is calculated using a noise floor subtraction:

$$\text{dBZ} = C + 10 \log_{10}(R[0] - P_{\text{noise}}) + 20 \log_{10} r + K[\theta_{\text{escan}}, \phi_{\text{escan}}] \quad (6.10)$$

where C is the radar constant set in the configuration file, r is the distance from the radar in meters, and $K[\theta_{\text{escan}}, \phi_{\text{escan}}]$ is the electronic scan angle dependent power correction, either horizontal or vertical, calculated from the electronic scan calibration mode for θ_{escan} and ϕ_{escan} off-boresight in elevation and azimuth, respectively, assuming a 2-dimensional electronic scanning antenna. The doppler velocity is calculated from the phase of the lag 1 autocovariance:

$$v_{\text{dopp}} = \frac{v_{\text{nyq}}}{\pi} \arg(R[1]) \quad (6.11)$$

6.3.3 Alternating Polarization Autocovariance Processing Algorithm

The alternating polarization autocovariance processing algorithm operates on alternating horizontal and vertical polarization samples in both the mechanical scan and electronic scan modes of the radar to calculate dual polarization moments including differential reflectivity, differential phase, and correlation coefficient [23] in addition to the signal-to-noise ratio, reflectivity, doppler velocity, normalized coherent power, and spectral width. The first stage calculates the horizontal and vertical lag 0, 1, and 2 autocovariances of the received signal for N samples at each range bin for both the short and long pulse subchannels under the assumption that the first sample, $S[0]$, corresponds to a horizontally polarized pulse:

$$R_h[0] = \frac{1}{N/2} \sum_{n=1}^{N/2} S[2n-1]S^*[2n-1] \quad (6.12)$$

$$R_v[0] = \frac{1}{N/2} \sum_{n=1}^{N/2} S[2n]S^*[2n] \quad (6.13)$$

$$R_h[1] = \frac{1}{N/2} \sum_{n=1}^{N/2} S[2n]S^*[2n-1] \quad (6.14)$$

$$R_v[1] = \frac{1}{N/2 - 1} \sum_{n=1}^{N/2-1} S[2n + 1]S^*[2n] \quad (6.15)$$

$$R_h[2] = \frac{1}{N/2 - 1} \sum_{n=1}^{N/2-1} S[2n + 1]S^*[2n - 1] \quad (6.16)$$

$$R_v[2] = \frac{1}{N/2 - 1} \sum_{n=1}^{N/2-1} S[2n + 2]S^*[2n] \quad (6.17)$$

where S is the complex form of the IQ sample of the received signal for a given subchannel and range bin. The diagram in Figure 6.3 shows the horizontal and vertical receive pulses in sample-time for one range bin which are used to calculate the autocovariances in the alternating polarization processing modes.

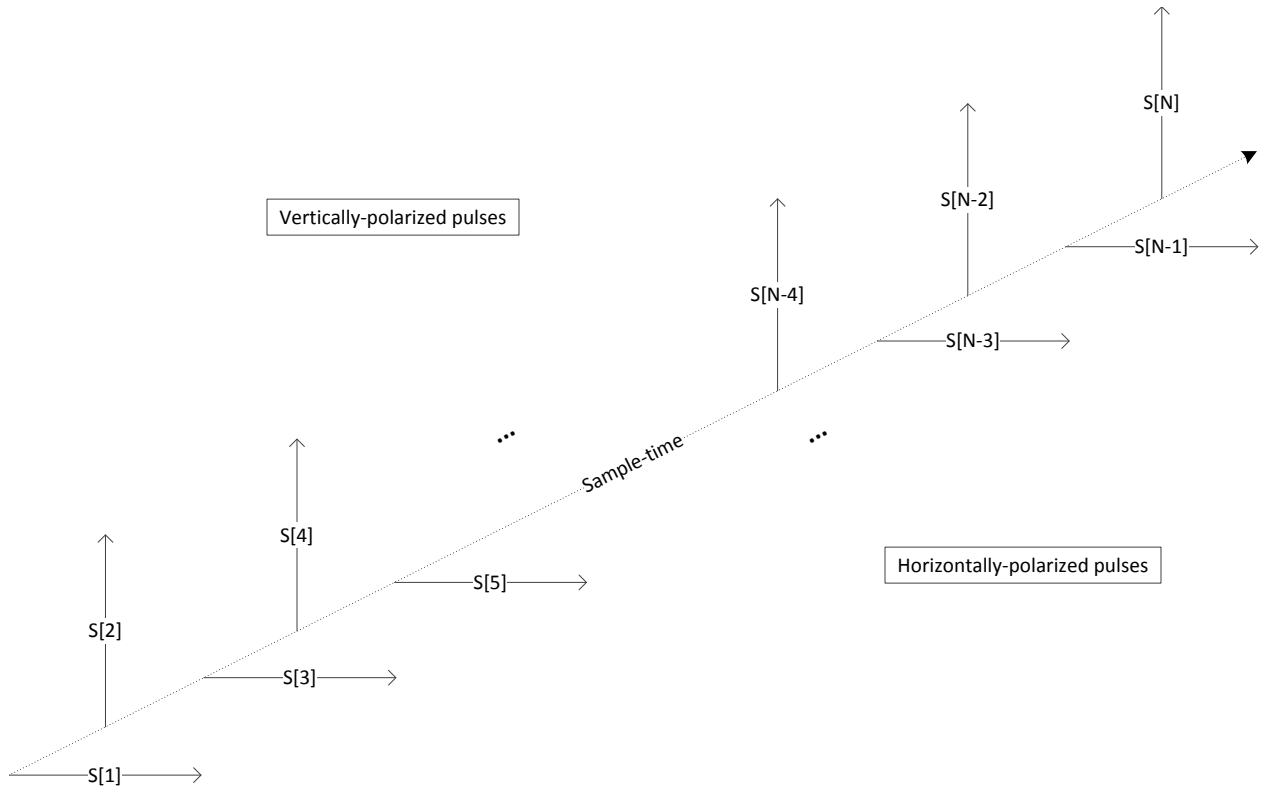


Figure 6.3: Horizontal and vertical receive pulses in sample-time for one range bin in the alternating polarization processing modes.

The second stage of the algorithm calculates the moments at each range bin using the autocovariances from (6.12), (6.13), (6.14), (6.15), (6.16), and (6.17). As with the single polarization autocovariance processing algorithm, a configurable short-to-long pulse transition variable is used to specify at which range bin the algorithm switches from using IQ data from the short pulse to the long pulse subchannel for the moment calculations. The horizontal and vertical signal-to-noise ratios are calculated from (6.4) using the respective horizontal and vertical lag 0 autocovariances, $R_h[0]$ and $R_v[0]$. The normalized coherent power and correlation coefficient are calculated by:

$$\text{NCP} = \frac{|R_h[2]| + |R_v[2]|}{2\sqrt{R_h[0]R_v[0]}} \quad (6.18)$$

$$\rho_{hv} = \frac{|R_h[1]| + |R_v[1]|}{2\sqrt{R_h[0]R_v[0]}\left(\frac{R_h[0]+R_v[0]}{|R_h[2]+R_v[2]|}\right)^{1/4}} \quad (6.19)$$

and the variance and the spectral width are calculated by:

$$\sigma^2 = \ln \frac{R_h[0]R_v[0]}{|R_h[2]R_v[2]|} \quad (6.20)$$

$$w = \frac{v_{nyq}\sqrt{\sigma^2}}{2\pi} \quad (6.21)$$

The calculation for reflectivity is the same as in (6.10) using the horizontal lag 0 autocovariance $R_h[0]$ by convention. Differential reflectivity, Z_{dr} , is calculated by:

$$Z_{dr} = 10 \log_{10} \left(\frac{R_h[0]}{R_v[0]} \right) + B_{boresight} + K_h[\theta_{escan}, \phi_{escan}] - K_v[\theta_{escan}, \phi_{escan}] \quad (6.22)$$

where $B_{boresight}$ is the configurable Z_{dr} bias that corrects for differences between the horizontal and vertical transmit/receive paths measured for the boresight electronic scan angle, and K_h and K_v are the electronic scan angle dependent horizontal and vertical power corrections calculated from the electronic scan calibration mode for θ_{escan} and ϕ_{escan} off-boresight in elevation and azimuth, respectively, assuming a 2-dimensional electronic scanning antenna. The doppler velocity and differential phase, Φ_{dp} , are calculated by:

$$v_{dopp} = \frac{v_{nyq}}{2\pi} \arg[R_v[1]\Phi_{dpRot}[\theta_{escan}, \phi_{escan}]] \arg[R_h[1]\Phi_{dpRot}^*[\theta_{escan}, \phi_{escan}]] \quad (6.23)$$

$$\Phi_{dp} = -\frac{1}{2} \arg[R_h[1]\Phi_{dpRot}^*[\theta_{escan}, \phi_{escan}](R_v[1]\Phi_{dpRot}[\theta_{escan}, \phi_{escan}])^*] \quad (6.24)$$

where $\Phi_{dpRot}[\theta_{escan}, \phi_{escan}]$ is an electronic scan angle dependent phase rotation, calculated from the electronic scan calibration mode, that shifts the initial differential phase close to -90° in order to maximize the amount that Φ_{dp} can increase through a weather target without aliasing.

6.3.4 Electronic Scan Calibration Mode

The electronic scan calibration mode is used to generate the electronic scan angle dependent horizontal and vertical power corrections and phase rotations used in (6.10), (6.22), and (6.24). The assign thread sets the electronic scan calibration mode when it receives the electronic scan calibration scan mode packet from the DXR, originating from the system controller. Pulses are transmitted and received using an electronically steered beam, at a range of electronic scan angles, which is pointed at the same stationary calibration target by offsetting the electronic scan angle with an equal and opposite mechanically pointing angle. For each electronic scan angle, θ_{escan} in elevation and ϕ_{escan} in azimuth, the signal processing software calculates the received horizontal and vertical power at a user specified range using (6.12) and (6.13), and the differential phase using (6.24). The electronic scan angle dependent horizontal and vertical power corrections in decibels, K_h and K_v , are computed with respect to the boresight electronic scan angle:

$$K_h[\theta_{escan}, \phi_{escan}] = (P_h[0, 0])_{dB} - (P_h[\theta_{escan}, \phi_{escan}])_{dB} \quad (6.25)$$

$$K_v[\theta_{escan}, \phi_{escan}] = (P_v[0, 0])_{dB} - (P_v[\theta_{escan}, \phi_{escan}])_{dB} \quad (6.26)$$

The electronic scan angle dependent phase rotation Φ_{dpRot} is calculated such that the starting phase for a given ray will be -70° in order to maximize the amount that Φ_{dp} can increase through a weather target without aliasing, but also high enough that any noise in the calibration will not cause aliasing:

$$\Phi_{dpRot}[\theta_{escan}, \phi_{escan}] = -70^\circ - (\Phi_{dp}[\theta_{escan}, \phi_{escan}])_{uncorrected} \quad (6.27)$$

The computed K_h , K_v , and Φ_{dpRot} values for the given electronic scan angle are stored in three tables for use when calculating reflectivity, differential reflectivity, and differential phase data collected in electronic scan mode. For each table, a linear interpolation is computed to fill in any entries which do not have a measured value, using the two nearest points:

$$Y[\theta] = Y[\theta_a] + \frac{\theta - \theta_a}{\theta_b - \theta_a}(Y[\theta_b] - Y[\theta_a]) \quad (6.28)$$

6.3.5 Noise Calibration Mode

The noise calibration mode is used by the signal processing software to measure the noise floor power P_{noise} used in (6.4) to calculate the signal-to-noise ratio and in (6.10) to calculate the noise-subtracted reflectivity. The assign thread sets the noise calibration mode when it receives a noise calibration scan mode packet from the DXR, originating from the system controller which sets up a high elevation scan to avoid echo from ground targets. The scan mode packet contains the number of samples per range bin that are to be averaged. As the assign thread receives the subsequent IQ data packets, it sums the lag 0 autocovariances for each subchannel and range bin. When it has counted the number of samples specified in the scan mode packet, it computes the average uncalibrated power by dividing each sum by the number of samples. Then, for each subchannel, the sums corresponding to each range bin are sorted by value and stored into an array. The first and last 25% of the array are discarded in order to reject any outliers from the calculation. Finally, the average uncalibrated power across the range bins for each subchannel is computed, resulting in the noise floor power for both the short and the long pulse subchannels. The two values are updated in the signal processing software and are written to a log file along with the date and time.

6.4 Downstream Software

6.4.1 Archiver

The archiver is a program used to write both processed moment data and raw timeseries data files. For standard execution, the archiver will connect using TCP/IP to the signal processing software running on the host computer which is specified on the command-line. Otherwise, when given the "--timeseries" command-line argument the archiver will connect to the acquisition daemon software running on the DXR. In both instances the archiver sets up the connection with its respective server which includes setting an appropriate input buffer size, opening a socket with the server, and sending a command to use the appropriate data format. If connection to the server is lost, the archiver will retry the connection until it is reestablished. After the connection to the server has been established, functionality between the standard moment archiving and timeseries archiving modes is essentially identical.

The archiver functionality is divided between two threads: the main thread which, after setting up the TCP/IP connection to the server, is responsible for reading the incoming data and adding it to a queue, and the writer thread which reads the data from the queue and responds accordingly by either opening, writing to, or closing a file. When the writer thread encounters a "Start Task" event packet originating from the system controller, it will close the current file if it exists, and open a new file in a command-line specified directory using the current date and time as the filename. All subsequently received data and headers are written to this file. The writer thread will close the file when an "End Task" event packet is received.

6.4.2 Binary-to-NetCDF Converter

The binary-to-NetCDF converter reads a moment data file output by the archiver and rewrites it in NetCDF format for use by the display software and other plotting and analysis tools which rely on NetCDF. When the converter opens the moment data file, specified on the command-line, it searches the file for three headers: a radar info packet, a processing info packet, and a task info packet. The radar info packet originates from the system controller and contains general

information about the system including the radar name, longitude, latitude, and altitude. The processing info packet is emitted by the signal processing software at the start of a task and contains the values specific to the scan used for moment processing including pulse repetition time, range gate spacing, and number of range bins per ray. The task info packet also originates from the system controller and contains information specific to the task including task name, number of sweeps, sweep mode, and fixed angles. The converter stores the information from the three headers which is used to initialize the NetCDF file which includes setting the time, range, sweep, and string length dimensions, and populating the NetCDF file header data. In addition to the value itself, populating a header data field involves setting various other corresponding fields including name, description, units, and dimensions which are read from a table for easy maintenance of the software.

After initializing the NetCDF file, the converter reads the data in the binary file ray by ray, counting the number of rays read. At the start of each ray, the corresponding time, elevation, and azimuth are written, followed by the moment data. As with the header data, the moment data is added to the file using a table which stores the variable name, description, units, and polarization mode. The converter writes the following fields for each range bin of a scan: signal-to-noise ratio, normalized coherent power, horizontal power, vertical power, reflectivity, velocity, spectral width, differential reflectivity, differential phase, linear depolarization ratio, specific differential phase, and correlation coefficient. When an "End Sweep" event packet is encountered in a volume scan, the number of rays is used to compute the end ray index of the current sweep and the start ray index of the next sweep, which it writes to the NetCDF file. When the converter reaches the end of the moment file and finishes writing the last ray to the NetCDF file, it closes both and terminates.

A real-time binary-to-NetCDF converter bash script is used to automatically create NetCDF files from newly created moment data files for use by the real-time display. Using inotifywait to detect when a new moment file is written to the RAID storage system, the script will call the converter to convert it to NetCDF and store it back in the RAID storage for use by the real-time display.

6.4.3 Real-Time Display

The real-time display software is used to plot moment data as it is generated by the system in order to provide the user with immediate visual weather observations. The software monitors the directory used by the real-time binary-to-NetCDF converter script to store NetCDF files converted from the moment data files output by the archiver. When a new NetCDF file appears in the direc-

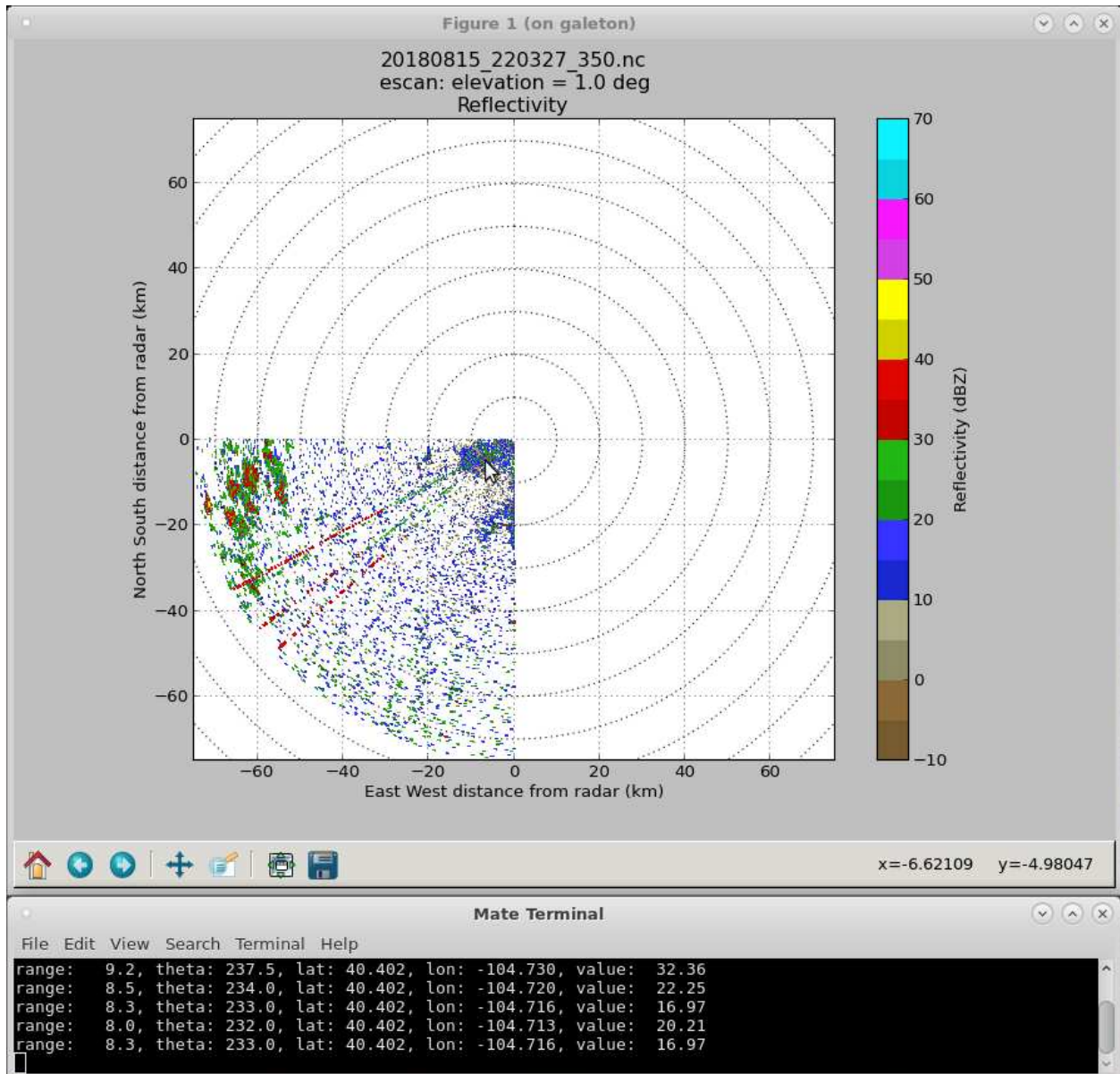


Figure 6.4: Screenshot of the real-time display and command-line outputting data corresponding to a range bin pointed at with the cursor.

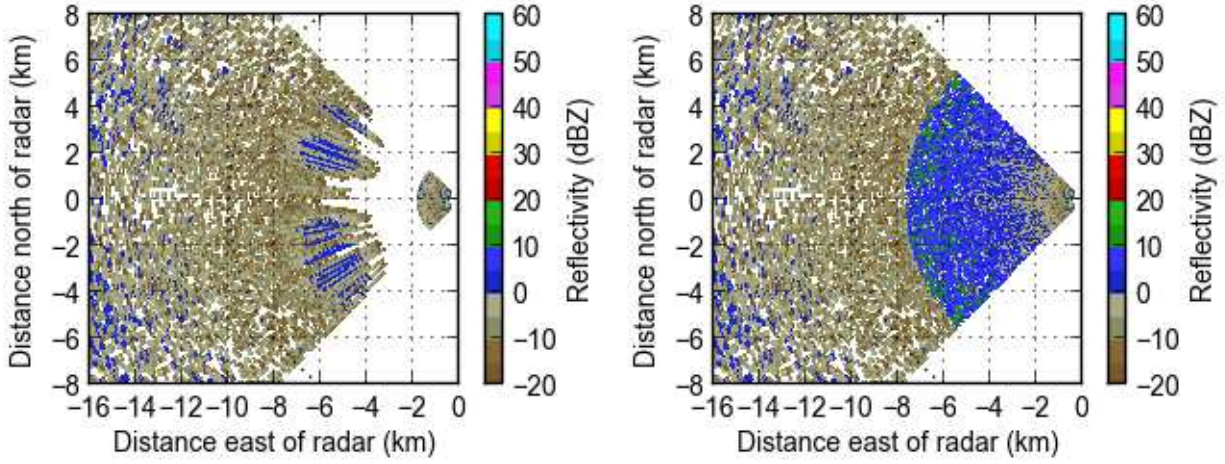
tory, the software automatically reads the data from the file and plots the moment field specified on the command-line using an NCP filter to reject noise. The title of the plot includes the filename of the NetCDF file, the task name specified in a scan file, the fixed angle used for the scan, and the moment field that is plotted. After a scan is plotted, the user can hover the mouse cursor over different range bins in the plot to display the range, pointing angle, latitude and longitude, and gate value on the command-line. Additionally, the software can be used to plot NetCDF files offline by specifying a filepath on the command-line.

6.5 Signal Processor Calibration and Configuration

6.5.1 Short-to-Long Pulse Transition

The short-to-long pulse transition variable specifies the range bin at which the processing algorithms switch from using the IQ data from the short pulse to the long pulse to calculate moment data. Because the long pulse has higher sensitivity than the short pulse due to higher average power, it is important to set the short-to-long pulse transition small enough in order to maximize the number of range bins that use the long pulse in order to increase the signal-to-noise ratio. However if the transition is set too small, IQ data taken from the long pulse subchannel during subchannel muting by the DXR will be used by the signal processing software and produce invalid data at short ranges.

Figure 6.5 shows two reflectivity plots for a single scan with no targets and no thresholding in order to show the noise floor only. In Figure 6.5a the short-to-long pulse transition has been set too small such that no reflectivity data can be calculated 2 to 4 km from the radar. In Figure 6.5b the transition has been set large enough to suppress the invalid long pulse data but small enough to maximize the usage of valid long pulse data resulting in a smooth transition which increases the sensitivity of the system at short ranges.



(a) Short-to-long pulse transition set too small.

(b) Short-to-long pulse transition set appropriately.

Figure 6.5: Comparison of reflectivity for uncalibrated versus calibrated short-to-long pulse transition for a single scan showing only noise.

6.5.2 Radar Constant

The radar constant specified in the signal processor configuration file is used to calibrate reflectivity for the system based on the radar equation. The radar equation can be rewritten to relate reflectivity, digitized received power, and range in decibels:

$$\text{dBZ} = (P_{rx})_{dBm} + 20 \log_{10}(R) + C \quad (6.29)$$

where C is the radar constant containing the system-specific parameters, physical constants, and unit conversion:

$$C = 10 \log_{10} \left(\frac{1024(10^{18}) \ln(2) \lambda^2 L_r}{c \tau P_{tx} G_a^2 \theta_{bw} \phi_{bw} \pi^3 K_w^2 G_r} \right) \quad (6.30)$$

Table 6.1 contains the values of the system parameters and physical constants [15] used to compute C with exception to the receiver gain, G_r , which is defined as the gain applied to the received signal from the antenna output port to the output of the receiver [9]. Note that θ_{bw} , the electronic scan

axis beamwidth depends on the electronic scan angle which is computed using the equation from Table 3.1.

Table 6.1: System parameters and physical constants used to calculate the radar constant.

Parameter/Constant	Value	Description
$(P_{tx})_{dB}$	48.6 dBm	Transmit power
$(G_a)_{dB}$	35.4 to 37.4 dBi	Antenna gain (min.–max.)
λ	3.2 cm	Transmit wavelength
θ_{bw}	0.026 to 0.044 <i>rad</i>	E-Scan axis beamwidth (1.5° to 2.5°)
ϕ_{bw}	0.045 <i>rad</i>	Non-E-Scan axis beamwidth (2.5°)
τ_l	49 μs	Long pulse width
τ_s	1 μs	Short pulse width
NF	7 to 9 dB	System noise figure (min.–max.)
f_s	2.5 MHz	Sampling frequency (60 m gate spacing)
$(L_r)_{dB}$	3.5 dB	Finite receiver bandwidth loss factor
$(P_{noise-out})_{dB}$	32 dBu	Uncalibrated DXR output for thermal noise
c	299792458 m/s	Speed of light
K_w	0.93	Dielectric factor for water

For traditional receivers with one input to the RF chain, the gain can be computed by injecting a known signal into the input of the RF chain, observing the receiver output, and using the following relationship with the measured values[24]:

$$(G_r)_{dB} = (P_{out})_{dB} - (P_{in})_{dB} \quad (6.31)$$

However the FRF166 phased array antenna does not have the means to inject a test signal into each one of the elements to characterize the RF receive chain of the antenna. Instead, the receiver gain is computed by using the minimum detectable signal of the system and the noise floor of the DXR as respective inputs P_{in} and P_{out} to (6.31). The minimum detectable signal is calculated by [25]:

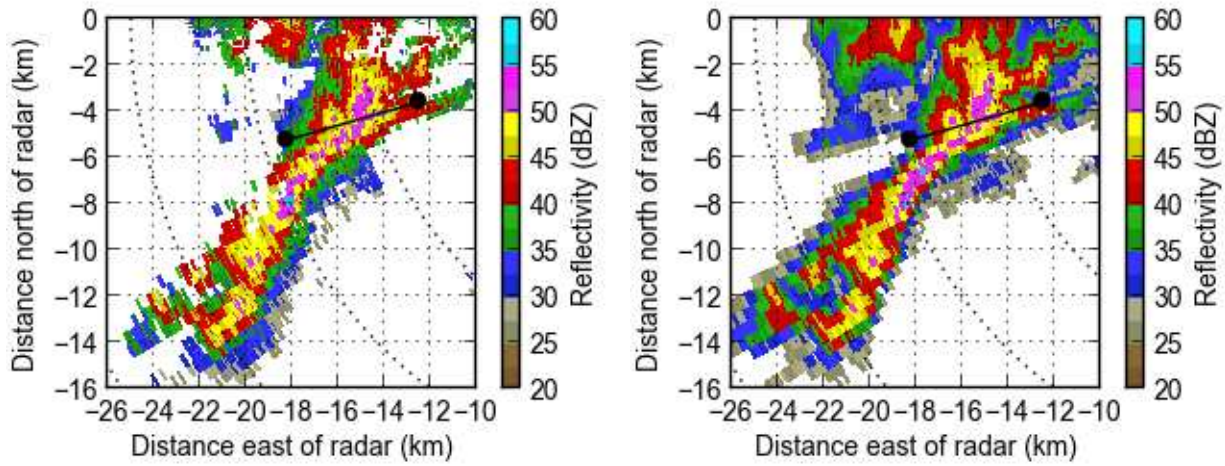
$$\text{MDS} = -174\text{dBm} + \text{NF} + 10 \log_{10}(f_s) \quad (6.32)$$

where the noise figure NF, and the sampling frequency f_s , can both be found in Table 6.1.

Using the method described with the values specified in Table 6.1, converted to linear and SI units, ranges for the radar constant for the boresight electronic scan angle were computed: -86 to -80 dBZ for the short pulse and -103 to -97 dBZ for the long pulse. Figure 6.6 compares two PPIs showing reflectivity data: the Front-X mechanical scan mode using a radar constant of -81.5 dBZ for the short pulse and -98.5 dBZ for the long pulse, and the proven CHILL X-band radar, in addition to a smoothed line plot comparing the two for the highlighted ray at an azimuth of 254 degrees. This particular ray was chosen because at this azimuth the core of the storm occurs both in the short and long pulse ranges of Front-X, allowing for the examination of both the short and long pulse radar constants. The line plot uses a Savitzky Golay filter in order to filter out high frequency noise and preserve the shape of the curve [18]. Both curves in the line plot have an equivalent maxima and share the same rough shape in both the short and long pulse regions which shows that the Front-X radar constants are reasonable. Additionally, the two PPIs show an overall good visual agreement. Note that the CHILL X-band data was averaged in elevation between 2.4° and 3.4° to approximate the 3° elevation used by Front-X, and in azimuth across 1.5° to approximate the azimuth beamwidth of Front-X. Also, both PPIs use an NCP threshold of 0.5 and a reflectivity threshold of 25 dBZ.

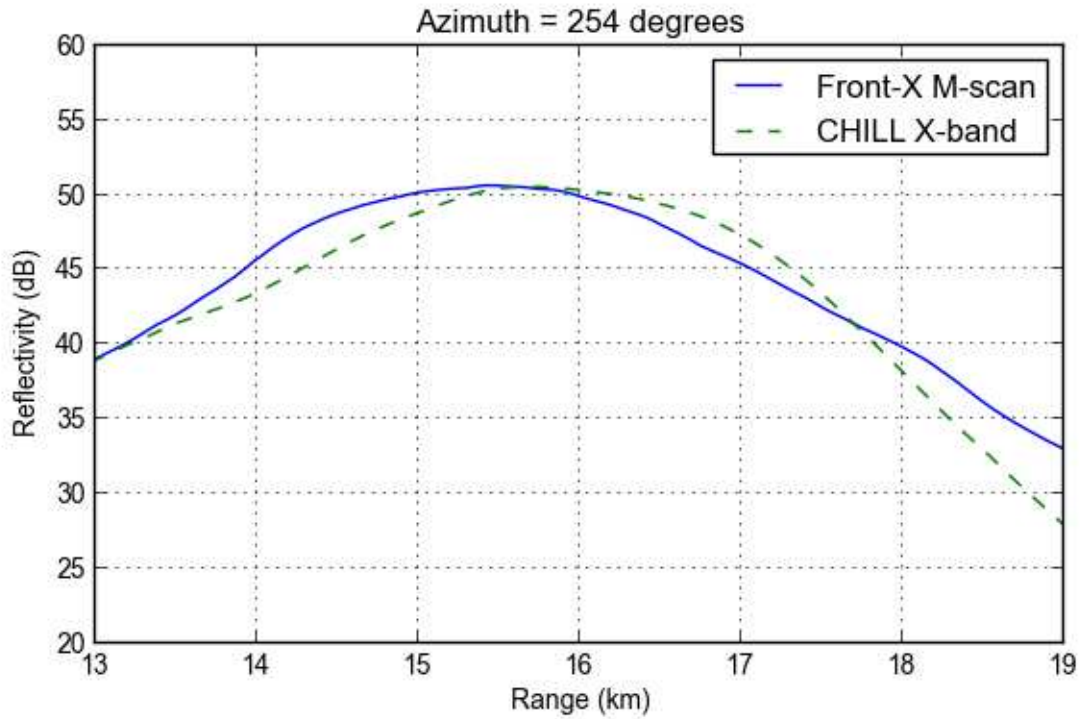
6.5.3 Z_{dr} Bias Correction

The Z_{dr} bias correction configuration variable is used to correct for any differences between the horizontal and vertical paths of the system which cause a bias in differential reflectivity. Traditionally, a method of using vertically pointing scans is used to measure the Z_{dr} bias in radar systems [26]. However, due to the tendency for this system's flat radome to collect water during vertically pointing scans causing unreliable measurements, different methods are used: a light rain method, and a comparison to the CHILL X-band radar.



(a) Front-X mechanical scan.

(b) CHILL X-band.



(c) Line plot of reflectivity for Front-X mechanical scan and CHILL X-band at 254 degrees in azimuth.

Figure 6.6: Comparison of PPIs and a single ray showing reflectivity for Front-X mechanical scan, using a radar constant of -81.5 dBZ for the short pulse and -98.5 dBZ for the long pulse, and the CHILL X-band radar.

The shape of water drops in drizzle and light rain can be approximated as a sphere, and thus their differential reflectivity is close to 0 dB [27]. This property of light rain can be used to measure the Z_{dr} bias in order to set the appropriate Z_{dr} bias correction in the signal processor configuration file. The corresponding uncorrected and corrected differential reflectivity plots are shown in Figure 6.7. The Z_{dr} bias evident in Figure 6.7a was calculated by averaging both the differential reflectivity and the reflectivity, using a maximum reflectivity threshold of 20 dBZ and a minimum NCP threshold of 0.35. The result was an average differential reflectivity of 1.0 dB ($\sigma = 0.9$ dB) for an average reflectivity of 15.6 dBZ ($\sigma = 3.0$ dBZ), which was used to set the Z_{dr} bias correction to -1 dB. The average differential reflectivity for the corrected data in Figure 6.7b is 0.0 dB, the desired result for light rain.

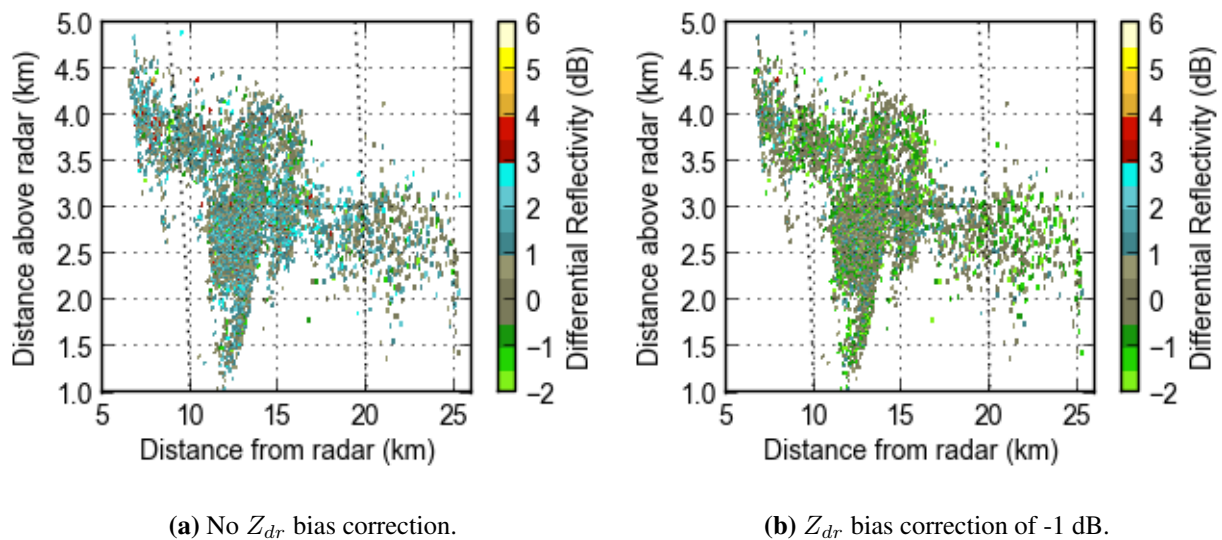


Figure 6.7: Comparison of RHIs showing differential reflectivity for light rain with and without the calculated bias correction.

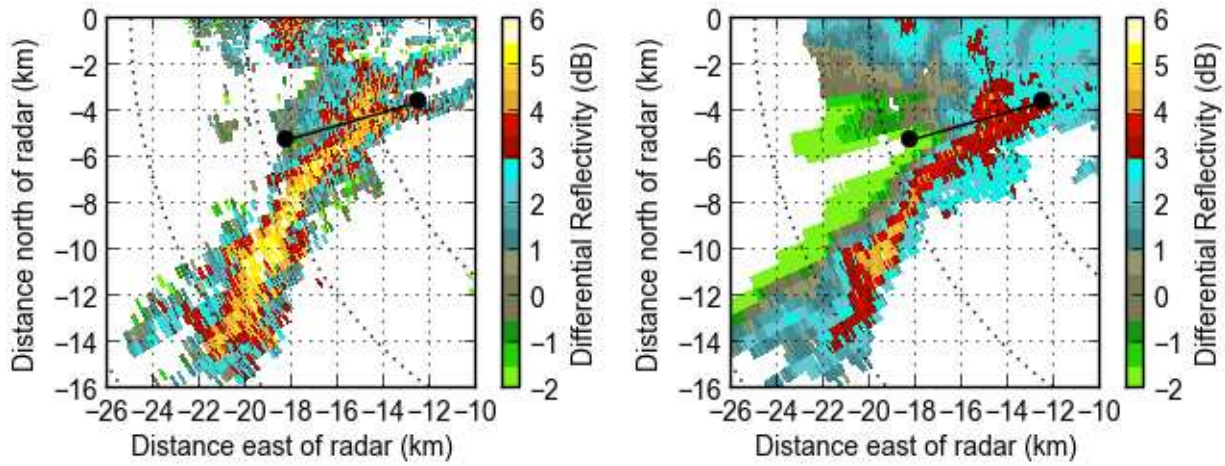
Figure 6.8 compares two PPIs showing differential reflectivity data, one collected with the Front-X mechanical scan mode using the -1 dB Z_{dr} bias correction calculated from the light rain method and the other with the CHILL X-band radar, in addition to a line plot, smoothed with a Savitzky Golay filter, comparing the two for the highlighted ray at an azimuth of 254 degrees.

The Front-X differential reflectivity looks biased high, relative to the CHILL X-band data, by approximately 1 dB according to the line plot, and confirmed visually by the PPIs. Figure 6.8 shows the same data, but with the Front-X data using a -2 dB Z_{dr} bias correction. Here, the maxima of the curves match closely, although the shape of the curves deviate by at least 2 dB at the edges of the storm. The Front-X data in figure 6.9 demonstrates better visual agreement with the CHILL X-band data in 6.9 which suggests that the light rain method of produced a Z_{dr} bias correction that is 1 dB too low. Note that the CHILL X-band data has been averaged in elevation and azimuth in order to approximate the elevation angle used by Front-X in addition to the Front-X beamwidth. Additionally, both PPIs use an NCP threshold of 0.5 and a reflectivity threshold of 25 dBZ.

6.5.4 Power Correction and Phase Rotation Tables

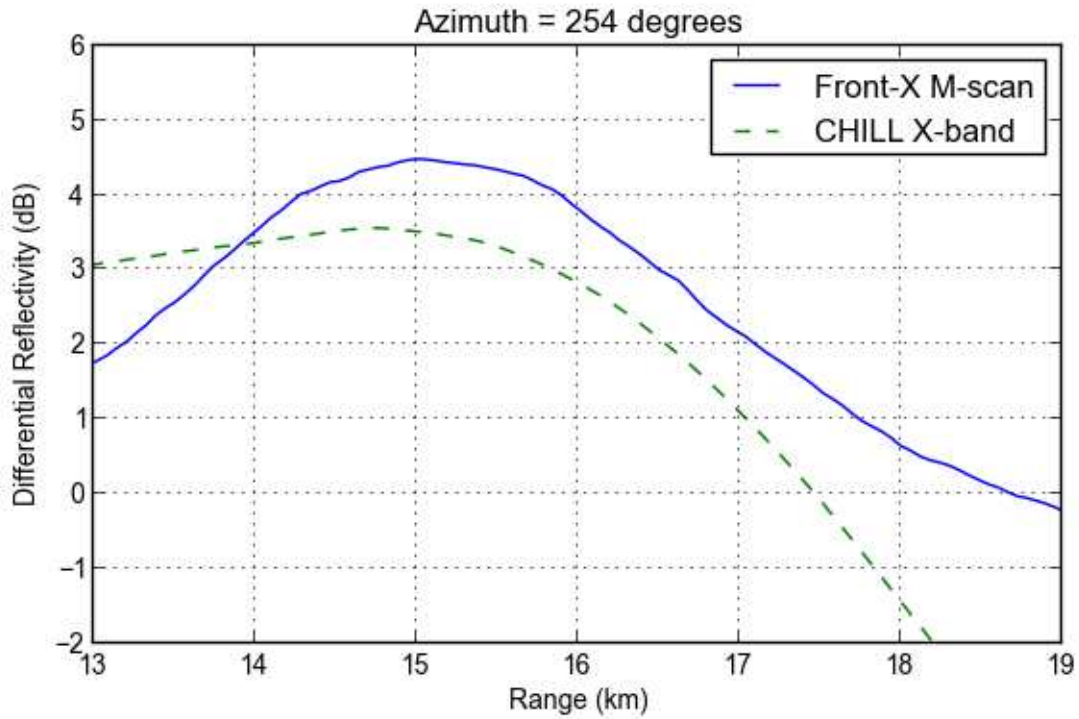
The horizontal and vertical power correction and phase rotation tables were populated by executing two iterations of the electronic scan calibration mode, using a corner reflector as a calibration target, and averaging and smoothing the results of the two scans. The trihedral corner reflector was placed in a flat, empty field approximately 3 meters above the ground and 870 meters away from the radar and was precisely located using an electronic volume scan to determine its azimuth, elevation, and range. Two calibration scans were executed, using opposite beam steering directions, specifying the determined azimuth and range of the corner reflector. An elevation angle of 1.5° was used in order to reduce multipath effects [28] while still illuminating the target with the main lobe of the beams. Furthermore, the scans were configured to use 30 meter gate spacing to refine the range resolution and also reduce contamination from multipath echo.

The results from the two calibration scans were averaged and smoothed using a Savitzky Golay filter in order to better visualize the shape of the curve across electronic scan angles. Figures 6.10 and 6.11 show the results, with smoothing, from the two calibration scans for the horizontal and vertical power corrections, respectively. Additionally, the theoretical power correction, provided by the manufacturer of the FRF166 phased array antenna, has been plotted for reference [15]:



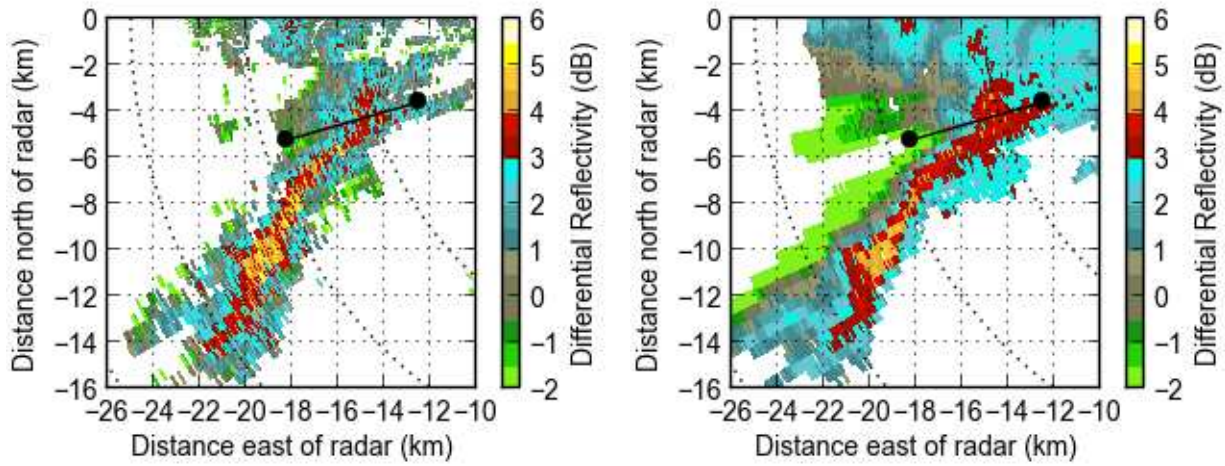
(a) Front-X mechanical scan.

(b) CHILL X-band.



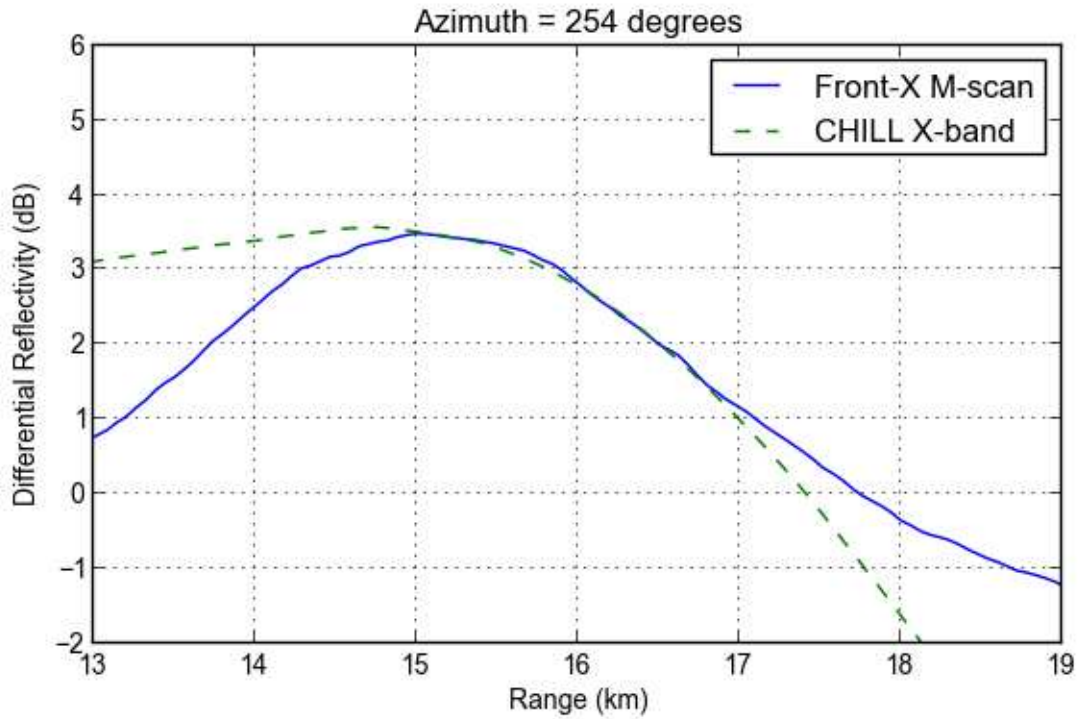
(c) Line plot of differential reflectivity for Front-X mechanical scan and CHILL X-band at 254 degrees in azimuth.

Figure 6.8: Comparison of PPIs and a single ray showing differential reflectivity for Front-X mechanical scan, using the -1 dB bias correction calculated from the light rain method, and the CHILL X-band radar.



(a) Front-X mechanical scan.

(b) CHILL X-band.



(c) Line plot of differential reflectivity for Front-X mechanical scan and CHILL X-band at 254 degrees in azimuth.

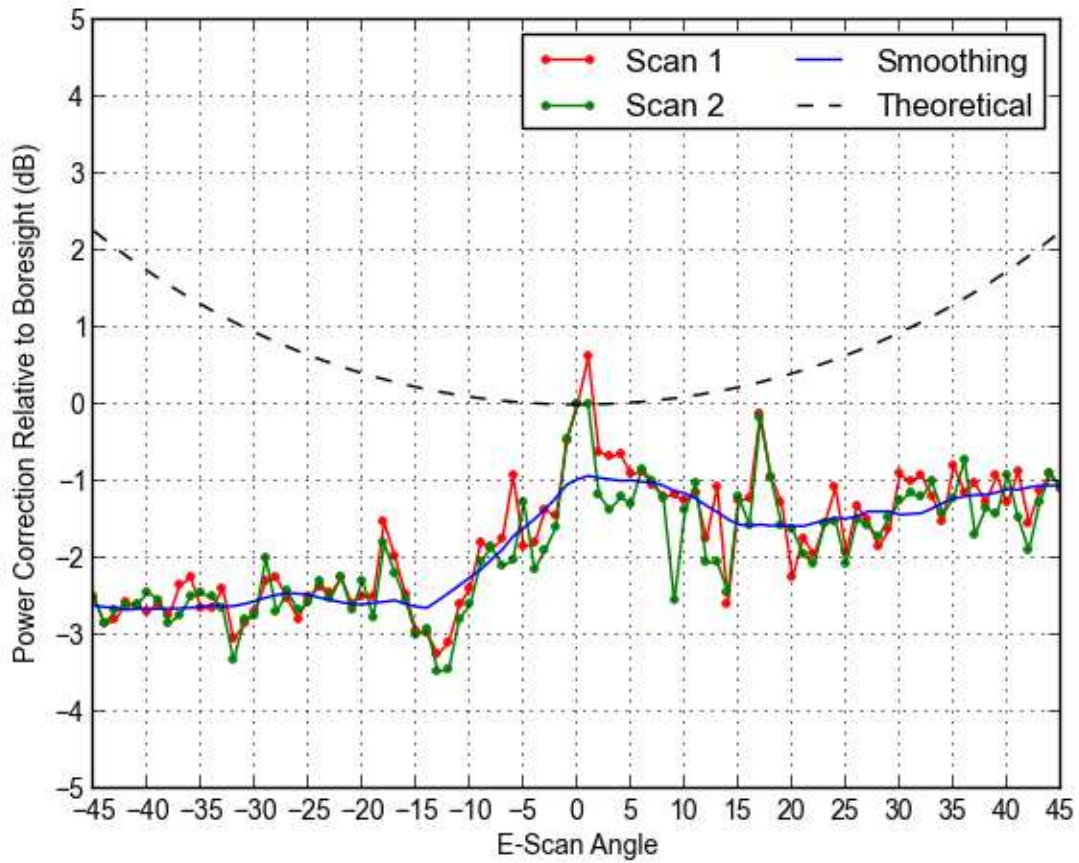
Figure 6.9: Comparison of PPIs and a single ray showing differential reflectivity for Front-X mechanical scan, using a -2 dB bias correction, and the CHILL X-band radar.

$$K[\theta_{escan}, \phi_{escan}] = \cos(\theta_{escan}, \phi_{escan})^{3/2} \quad (6.33)$$

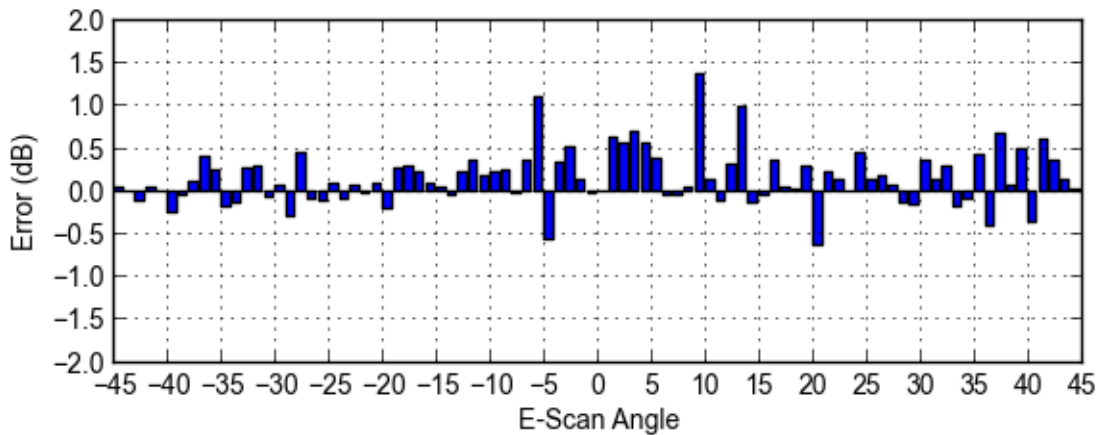
The curve generated by the calibration results differs greatly from the theoretical curve, deviating up to 4 dB. While the theoretical curve predicts more power loss for electronic scan beams further off from boresight, the calibration results show the opposite, with the power corrections negative with respect to the boresight beam. The errors between the two calibration scans reasonably agree with each other, with the differences between the two no greater than 1.5 dB.

Figure 6.12 shows the phase rotation results, with smoothing, from the two calibration scans. The consistently increasing phase rotation across the range of electronic scan angles implies that the system phase differs depending on the electronic scan angle. Note that the measured phase rotation values follow the smoothed curve reasonably well, and the error between the two scans does not exceed 10 degrees.

The weather data generated by Front-X using the power correction and phase rotation tables described above are discussed in detail in Chapter 7.

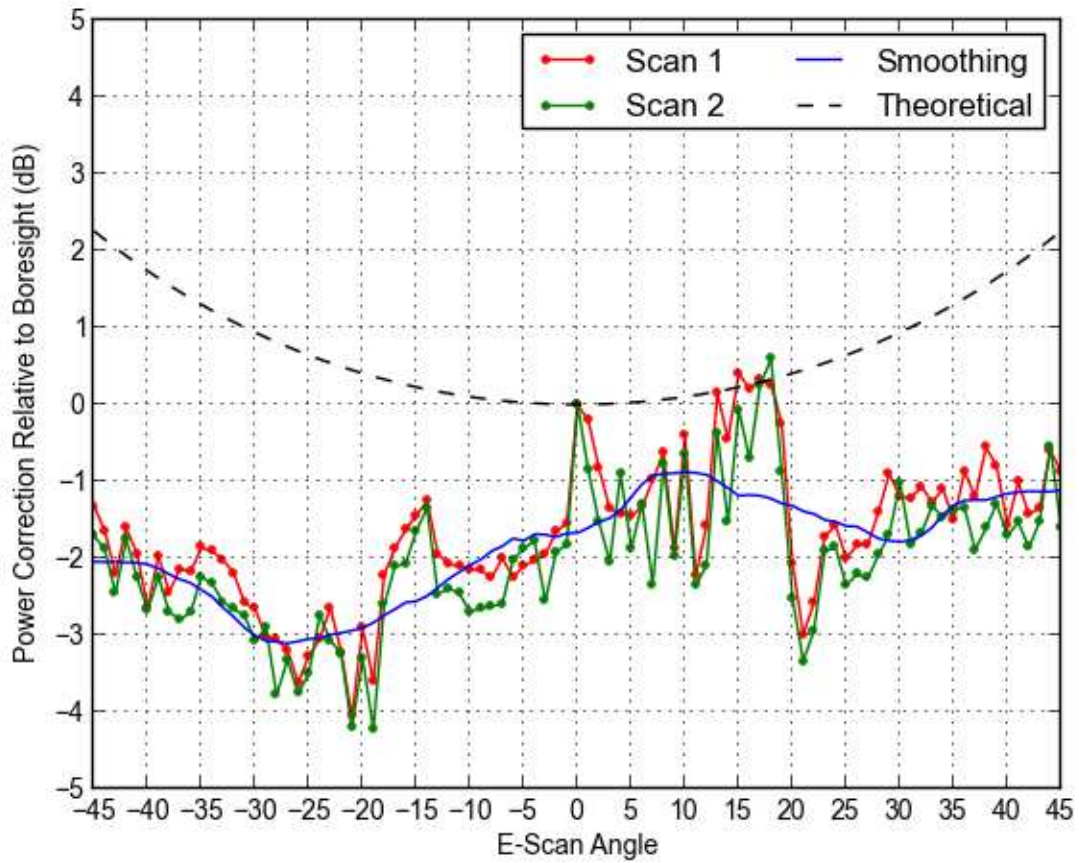


(a) Horizontal power correction results with smoothing compared to theoretical correction.

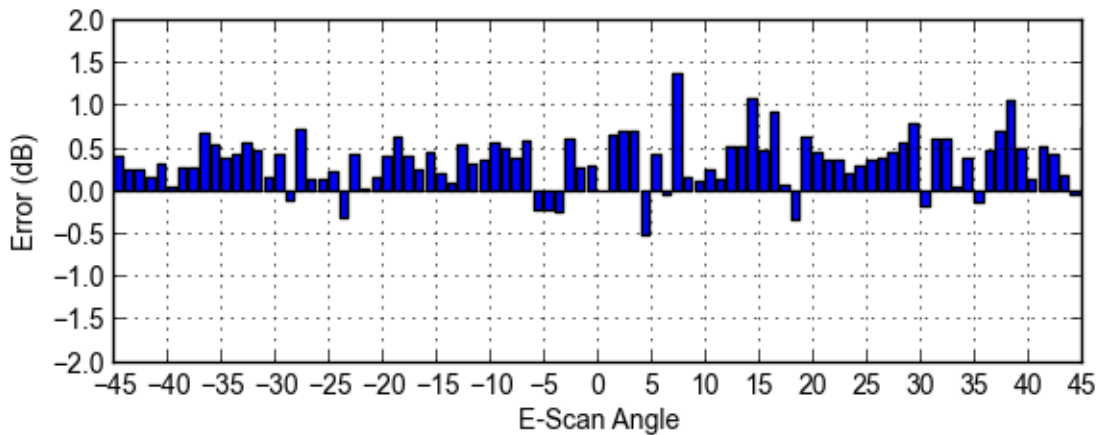


(b) Error between two successive calibration scans.

Figure 6.10: Results from two calibration scans showing the calculated horizontal power correction versus electronic scan angle.

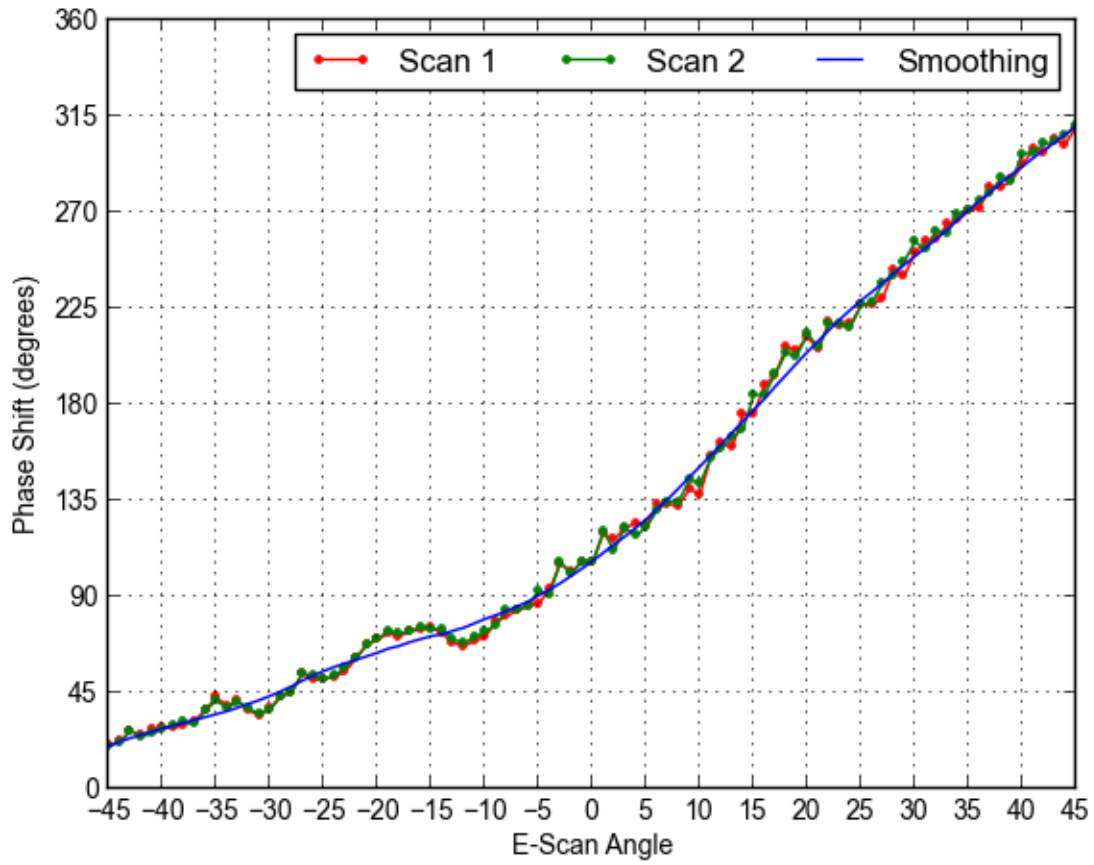


(a) Vertical power correction results with smoothing compared to theoretical correction.

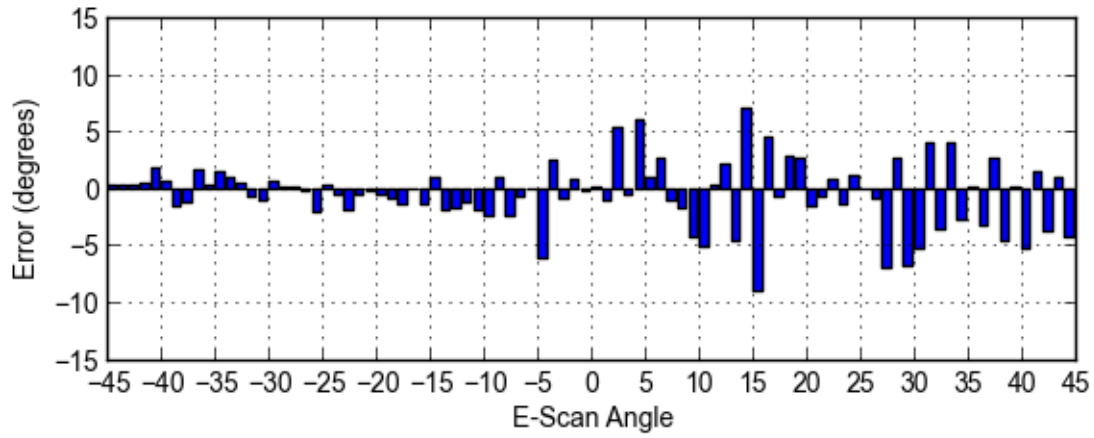


(b) Error between two successive calibration scans.

Figure 6.11: Results from two calibration scans showing the calculated vertical power correction versus electronic scan angle.



(a) Phase rotation results with smoothing.



(b) Error between two successive calibration scans.

Figure 6.12: Results from two calibration scans showing the calculated phase rotation versus electronic scan angle.

Chapter 7

System Operation and Demonstration

7.1 Introduction

Data collected with Front-X from two weather events at the CSU-CHILL radar facility near Greeley, Colorado were chosen to examine the differences between mechanical and electronic scan using different correction methods and to visually verify the data by comparing it against data collected with the proven CHILL X-band radar.

A hailstorm on July 27, 2018 which occurred near the radar site is used to compare the Front-X mechanical scan and electronic scan data, processed using both the electronic scan calibration results and the theoretical correction discussed in Section 6.5.4. This event was chosen because a strong echo was observed at every azimuth in the scan, which provides an opportunity to analyze measurements made with the full range of electronic scan angles.

Another hailstorm on June 16, 2018 is used to visually compare Front-X electronic and mechanical scan data to CHILL X-band data. This event was chosen because it occurs in the short and long pulse regions of Front-X, so both could be verified, and also because the Front-X and CHILL scans were completed within a reasonably small amount of time from one another using similar elevation angles.

This chapter discusses the differences in electronic and mechanical scan data collected with Front-X using different correction methods, in addition to visual comparisons with the CHILL X-band radar for verification.

7.2 July 27th, 2018: Electronic Scan versus Mechanical Scan

A hailstorm event on July 27, 2018 observed by Front-X is used to compare reflectivity, differential reflectivity, and differential phase data from the electronic scan mode using the power correction and phase rotation tables, theoretical power correction, and no correction, and the me-

chanical scan mode. The core of storm was as close as 10 km to the radar and extended across the full range of electronic scan angles which makes it ideal for analyzing the effectiveness of the power and phase correction tables generated by the electronic scan calibration mode. Note that the PPIs use an NCP threshold of 0.2. Table 7.1 shows how the electronic and mechanical scans were configured.

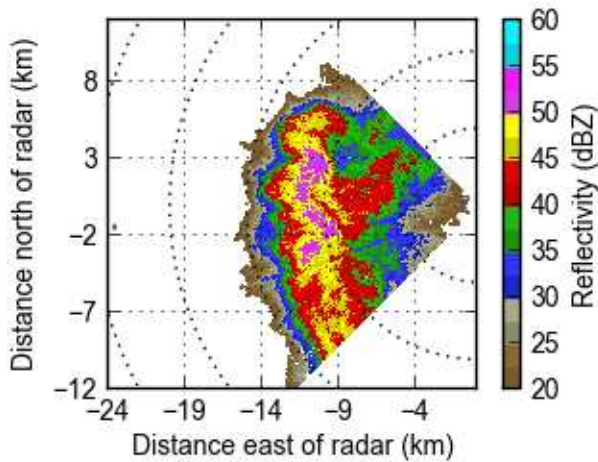
Table 7.1: Electronic and mechanical scan parameters used to collect data for the July 27 case.

Parameter	Electronic Scan	Mechanical Scan
Start time	02:28:51 UTC	02:29:13 UTC
Elevation angle	3°	3°
Electronic scan angles	-45° to 45° (0.5° incr.)	0°
Mechanical scan speed	N/A	15°/sec
PRF	1250 Hz	1250 Hz
Integration cycle length	90	90
Range gate spacing	60 m	60 m
Polarization Mode	Alternating H/V	Alternating H/V
Beamshape	Uniform	Uniform

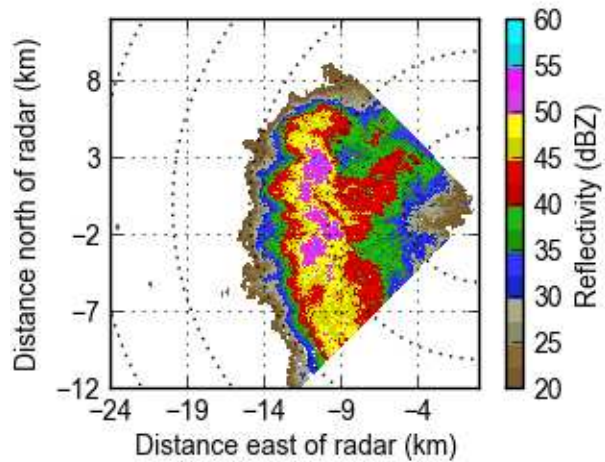
7.2.1 Reflectivity

Figure 7.1 shows PPIs of reflectivity for electronic scan using the horizontal power correction table, theoretical power correction, and no correction, compared to mechanical scan for the July 27 hailstorm. Visually, the PPIs show that the theoretical correction electronic scan data has generally higher reflectivities than the mechanical scan data, while the table corrected and uncorrected electronic scan data appears to be both higher and lower than the mechanical scan data, depending on the range and azimuth.

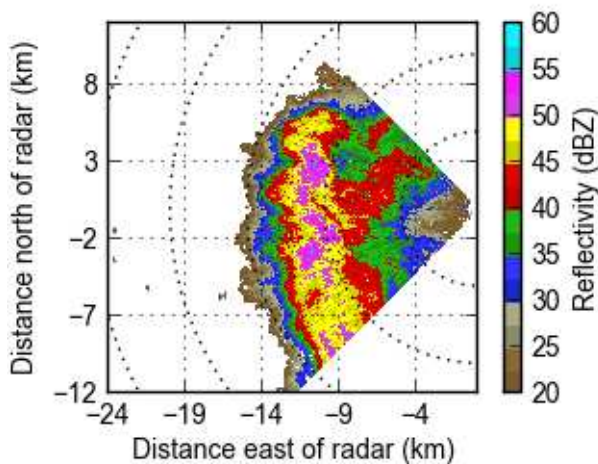
Figures 7.2 and 7.3 show the differences in reflectivity, smoothed with a Savitzky Golay filter, between electronic scan, using the different correction methods, and mechanical scan versus az-



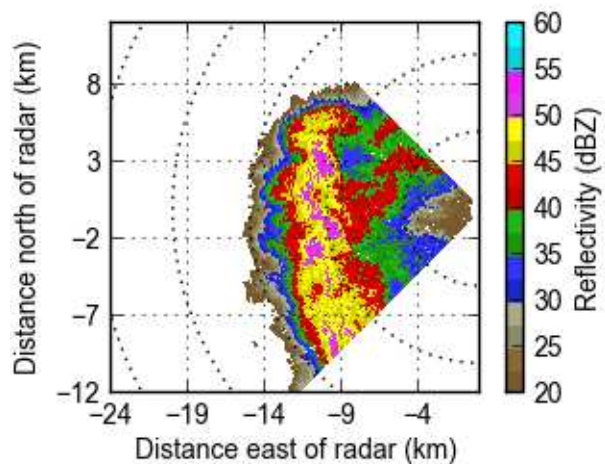
(a) Electronic scan using power correction table.



(b) Electronic scan using no correction.



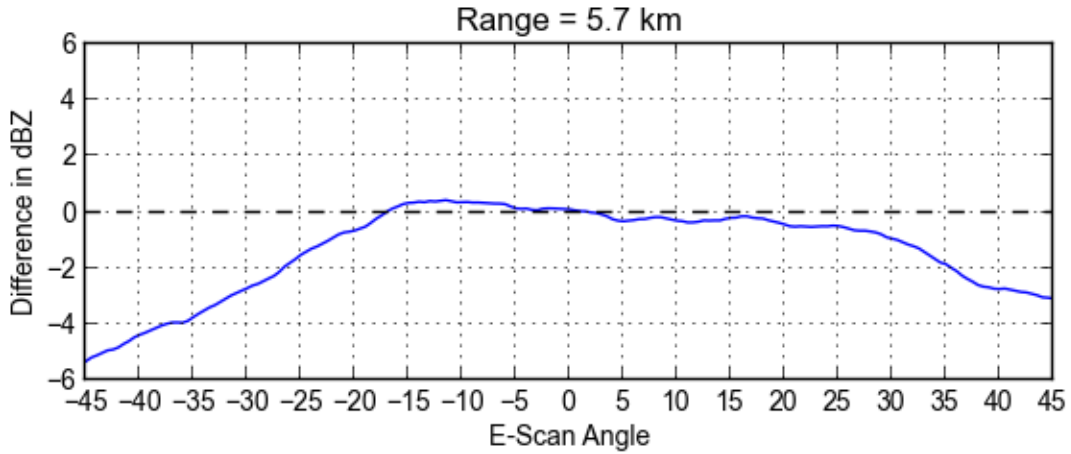
(c) Electronic scan using theoretical power correction.



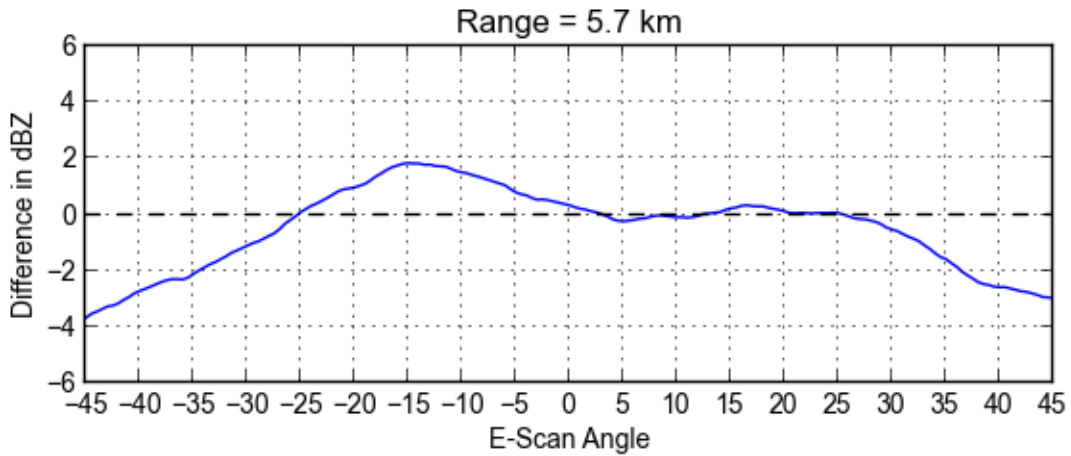
(d) Mechanical scan.

Figure 7.1: PPIs showing reflectivity for electronic scan using the horizontal power correction table, theoretical power correction, and no correction, compared to mechanical scan for the July 27 case.

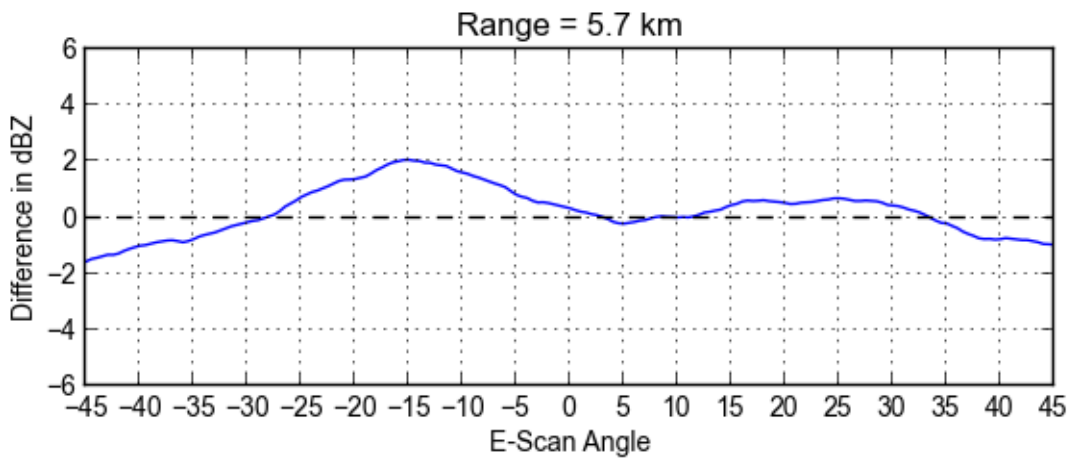
imuth at 5.7 km and 12.1 km, respectively. At 5.7 km where the reflectivities range from 30-45 dBZ, the electronic scan data with no correction reveals two peaks where the electronic scan reflectivities are larger, by up to 2 dBZ, than mechanical scan. The power correction table effectively reduces the reflectivity difference for electronic scan angles between -20° and 30° to less than 0.5 dBZ. However, at the electronic scan angles further off-boresight, the electronic scan reflectivities



(a) Electronic scan using power correction table.

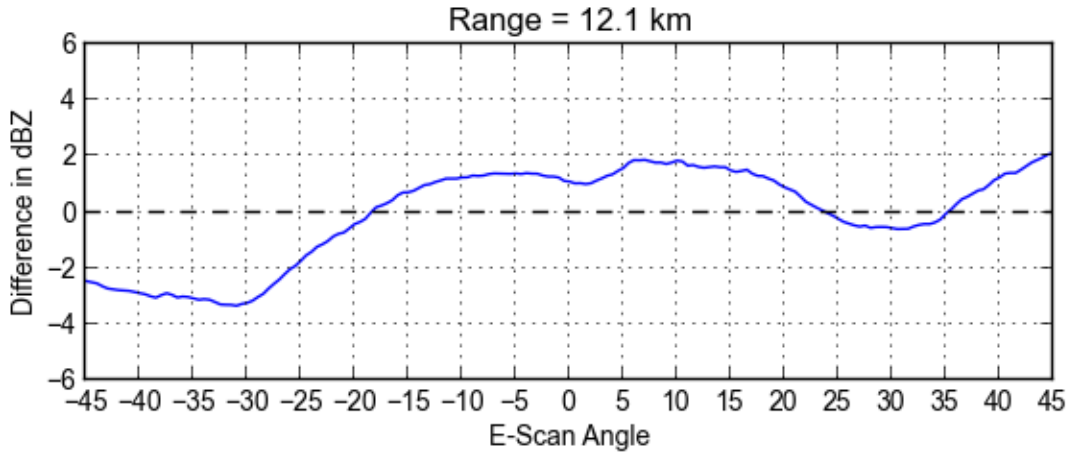


(b) Electronic scan using no correction.

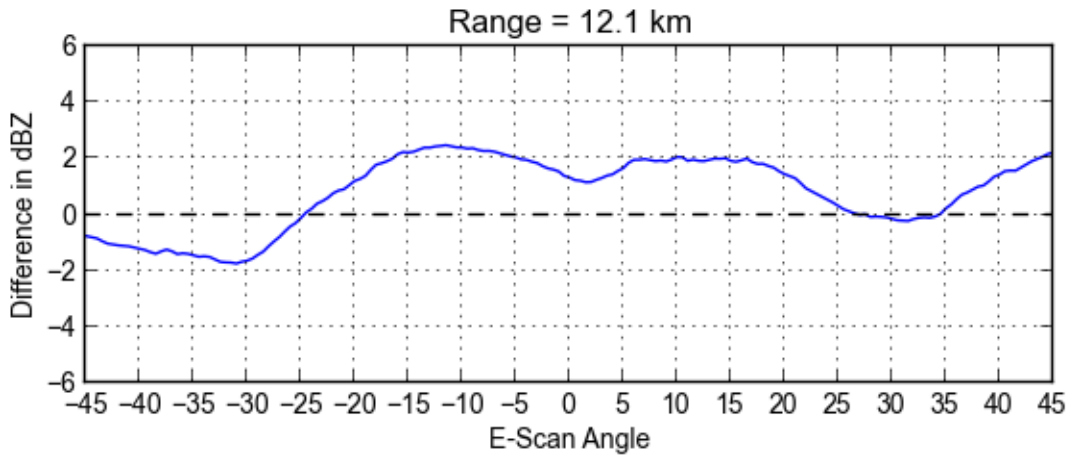


(c) Electronic scan using theoretical power correction.

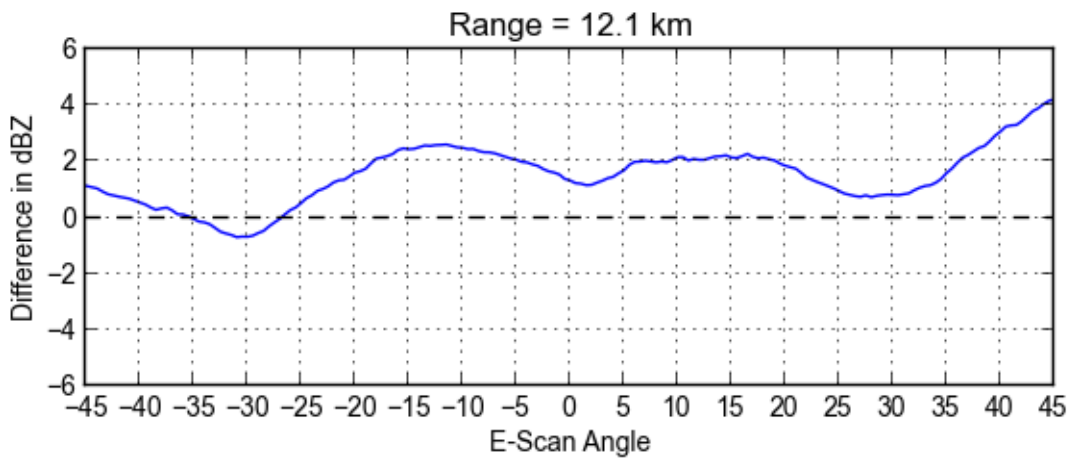
Figure 7.2: Difference in reflectivity between electronic scan, using the horizontal power correction table, theoretical power correction, and no correction, and mechanical scan at 5.7 km for the July 27 case.



(a) Electronic scan using power correction table.



(b) Electronic scan using no correction.



(c) Electronic scan using theoretical power correction.

Figure 7.3: Difference in reflectivity between electronic scan, using the horizontal power correction table, theoretical power correction, and no correction, and mechanical scan at 12.1 km for the July 27 case.

are lower than mechanical scan, down to -5 dBZ. The opposite is true for the theoretical correction, where the reflectivity difference is increased for electronic scan angles nearer to boresight by up to 2 dBZ, while at the furthest angles off-boresight the difference is closer to zero but up to -1.5 dBZ.

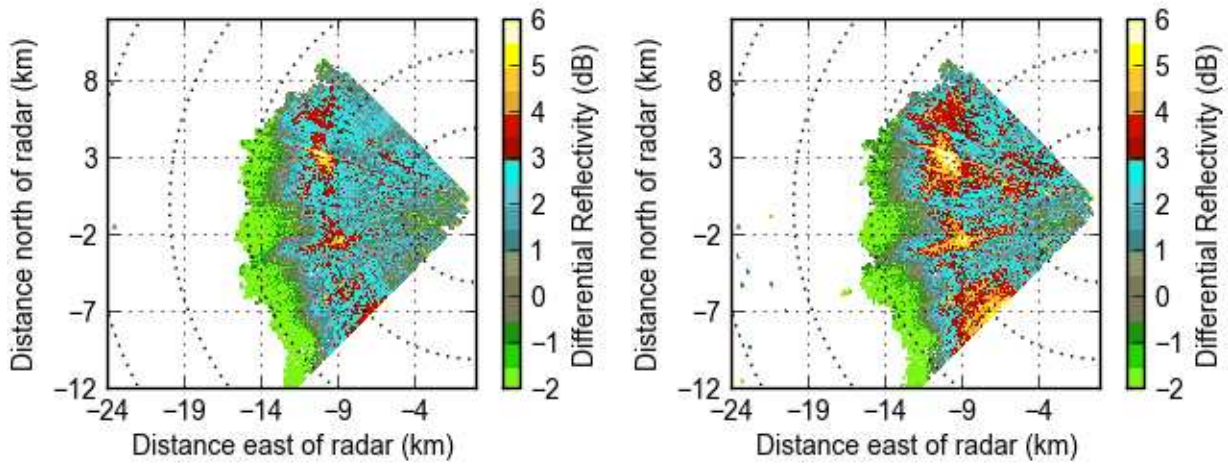
At 12.1 km where the reflectivities range from 40-55 dBZ, as with the 5.7 km range the uncorrected electronic scan data shows two peaks in reflectivity difference, which are reduced by the table correction, and exacerbated by the theoretical correction for electronic scan angles from -20° to 30°. However beyond these angles, the electronic scan reflectivities increase as the electronic scan angle points further off-boresight, with the table correction producing lower reflectivities by as much as 3 dBZ and the theoretical correction producing reflectivities comparable to mechanical scan within about 1 dBZ.

The variation in shape of the difference plots show that the reflectivities at different electronic scan angles change depending on the range and/or target reflectivity, which may imply that the beamshape changes depending on the electronic scan angle. More specifically, the reflectivities for the electronic scan angles furthest off-boresight being lower than mechanical scan for the edge of the storm, but higher than mechanical scan at the core of the storm, may be explained by the beams with electronic scan angles further off-boresight having higher antenna side-lobes. How the beamshape changes depending on electronic scan angle could be explored further by varying the beamshape parameter of the antenna.

7.2.2 Differential Reflectivity

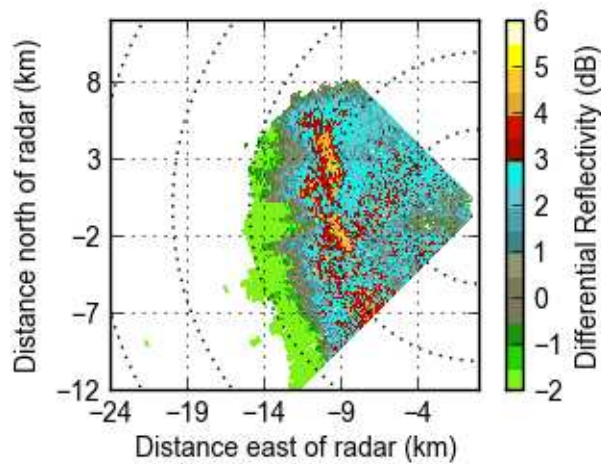
Figure 7.4 shows PPIs of differential reflectivity for electronic scan using the power correction tables and no correction, compared to mechanical scan for the July 27 hailstorm. Visually, the PPIs show that the uncorrected electronic scan data has generally higher differential reflectivities than the mechanical scan data, while the table corrected electronic scan data appears to be lower overall, but agrees more closely with the mechanical scan data.

Figures 7.5 and 7.6 show the differences in differential reflectivity, smoothed with a Savitzky Golay filter, between electronic scan, using the table correction and no correction, and mechanical



(a) Electronic scan using power correction tables.

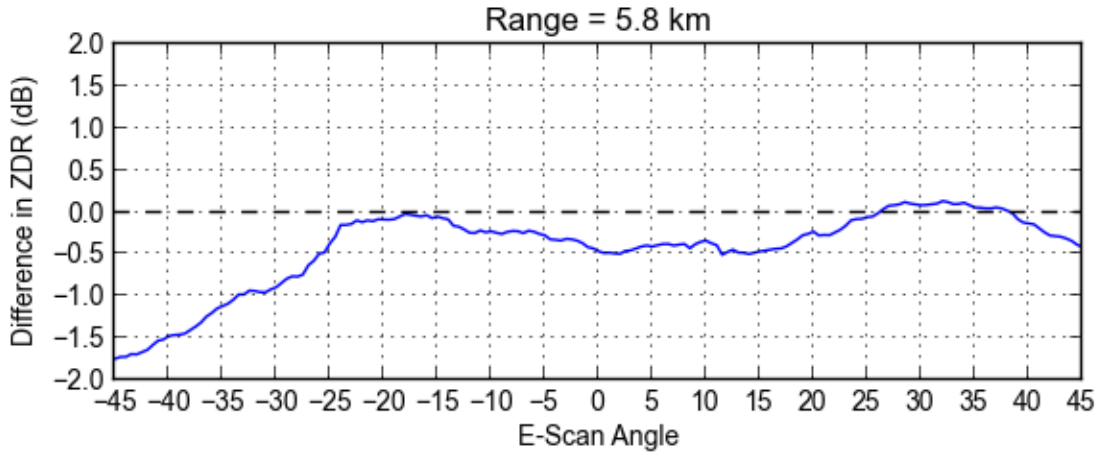
(b) Electronic scan using no correction.



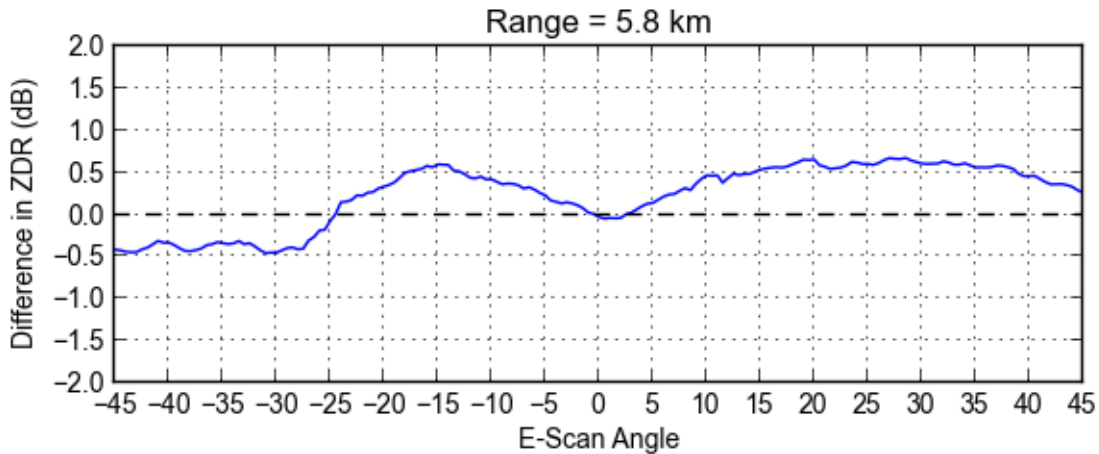
(c) Mechanical scan.

Figure 7.4: PPIs showing differential reflectivity for electronic scan, using the power correction tables and no correction, compared to mechanical scan for a weather event on July 27.

scan versus azimuth at 5.8 km and 10.0 km, respectively. At 5.8 km where the differential reflectivities range from 0-3 dB and the reflectivities range from 30-45 dBZ, the electronic scan data with no correction reveals two peaks where the electronic scan differential reflectivities are larger, more than 0.5 dB, than mechanical scan. The power correction tables reduce the differential reflectivity difference for electronic scan angles at the peaks, however, for the electronic scan angles between



(a) Electronic scan using power correction tables.

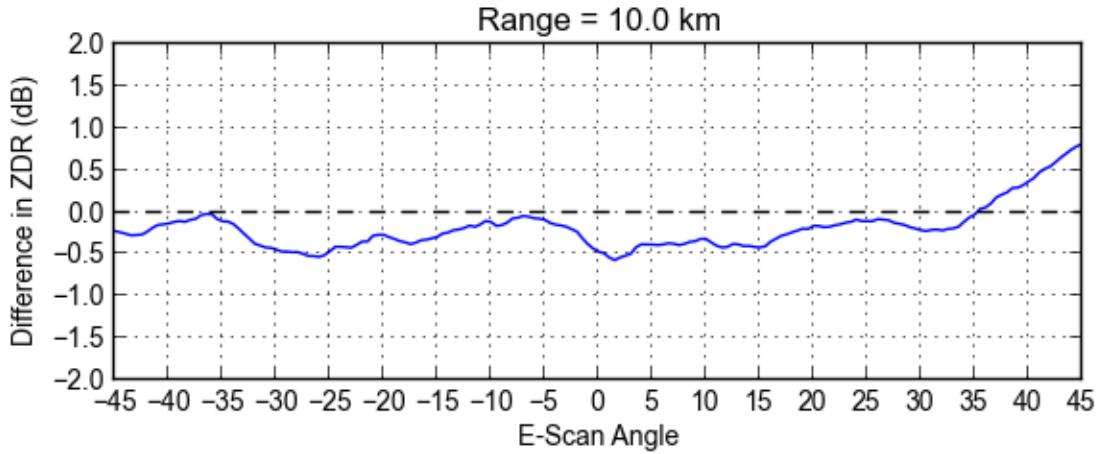


(b) Electronic scan using no correction.

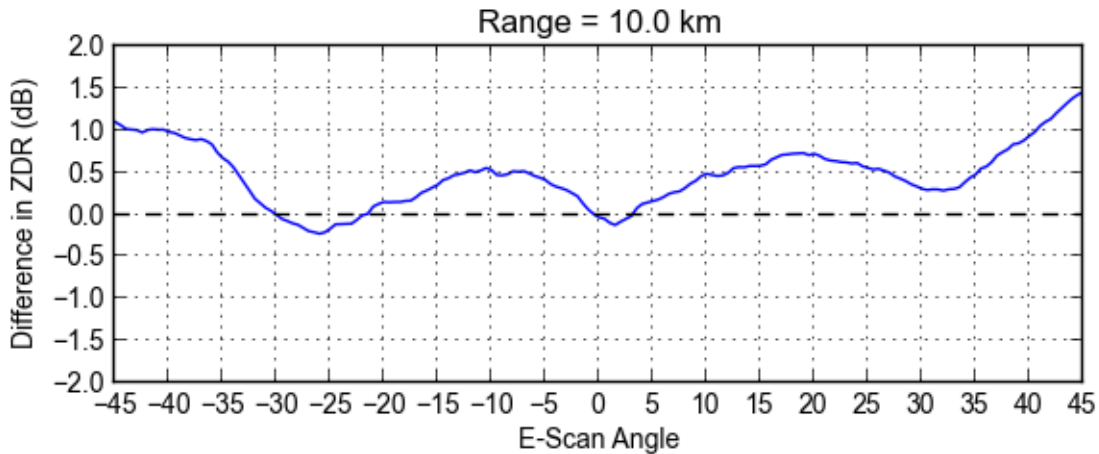
Figure 7.5: Difference in differential reflectivity between electronic scan, using the power correction tables and no correction, and mechanical scan at 5.8 km for the July 27 case.

and further off-boresight from the peaks, the electronic scan differential reflectivities are lower than mechanical scan, down to almost -2 dB at -45° off-boresight.

At 10.0 km where the differential reflectivities range from 1-5 dB and the reflectivities range from 40-55 dBZ, as with the 5.8 km range the uncorrected electronic scan data shows two peaks in differential reflectivity difference, in addition to increasing the difference at the electronic scan angles furthest off-boresight. The correction tables reduce the overall variation in differential re-



(a) Electronic scan using power correction tables.



(b) Electronic scan using no correction.

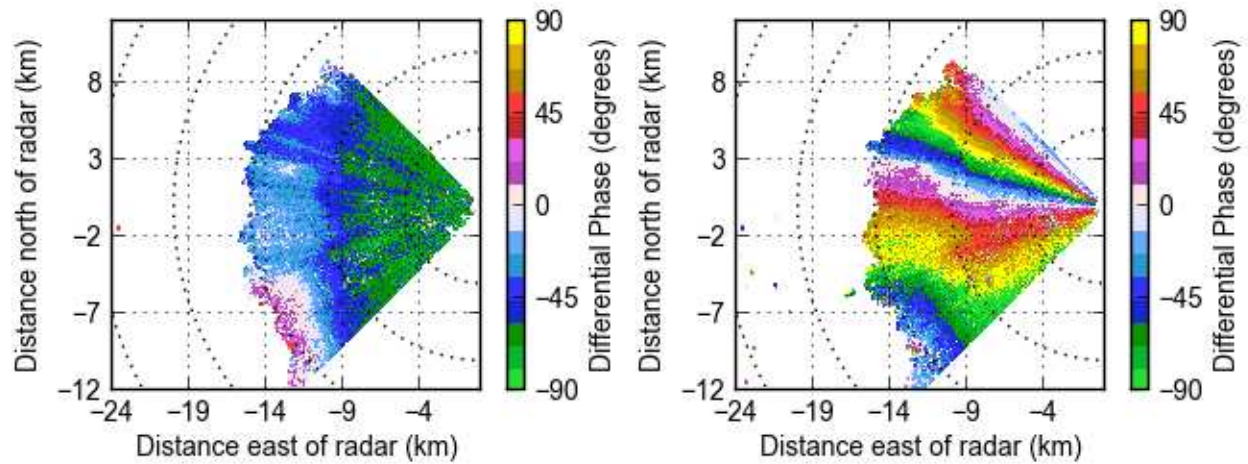
Figure 7.6: Difference in differential reflectivity between electronic scan, using the power correction tables and no correction, and mechanical scan at 10.0 km for the July 27 case.

flectivity across electronic scan angles, although it also introduces a bias with respect to mechanical scan varying from 0 to -0.5 dB.

As with reflectivity, the variation in shape of the difference plots show that the differential reflectivities at different electronic scan angles change depending on the range and/or target reflectivity, which may imply that the beamshape changes depending on the electronic scan angle with the added complexity of having two beamshapes, horizontal and vertical, that can vary.

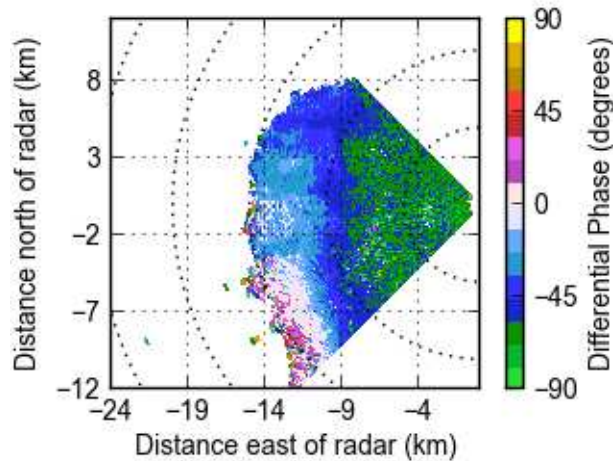
7.2.3 Differential Phase

Figure 7.7 shows PPIs of differential phase for electronic scan using the phase rotation table and no rotation, compared to mechanical scan for the July 27 hailstorm. Visually, it is clear that the electronic scan mode which does not use the rotation table produces a differential phase which is electronic scan angle dependent and vastly differs from the mechanical scan data. The starting



(a) Electronic scan using phase rotation table.

(b) Electronic scan using no rotation.

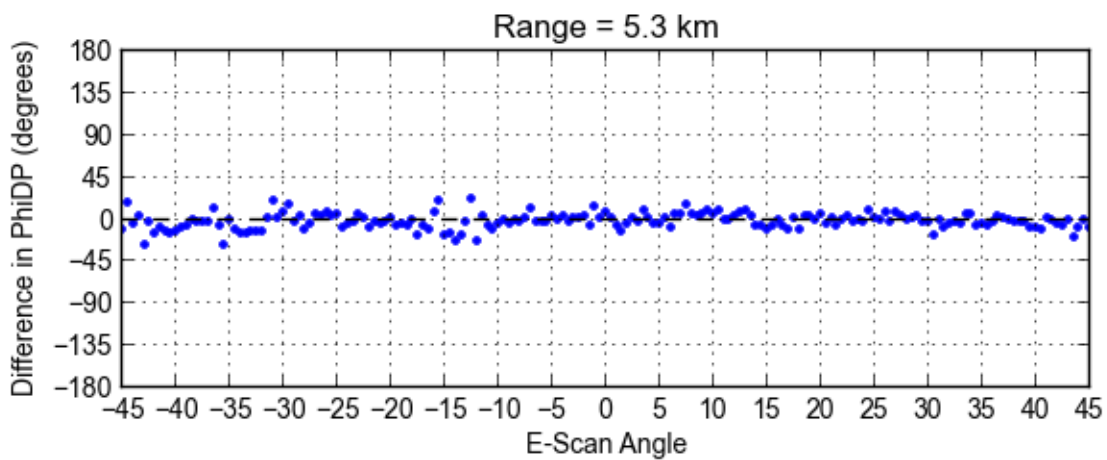


(c) Mechanical scan.

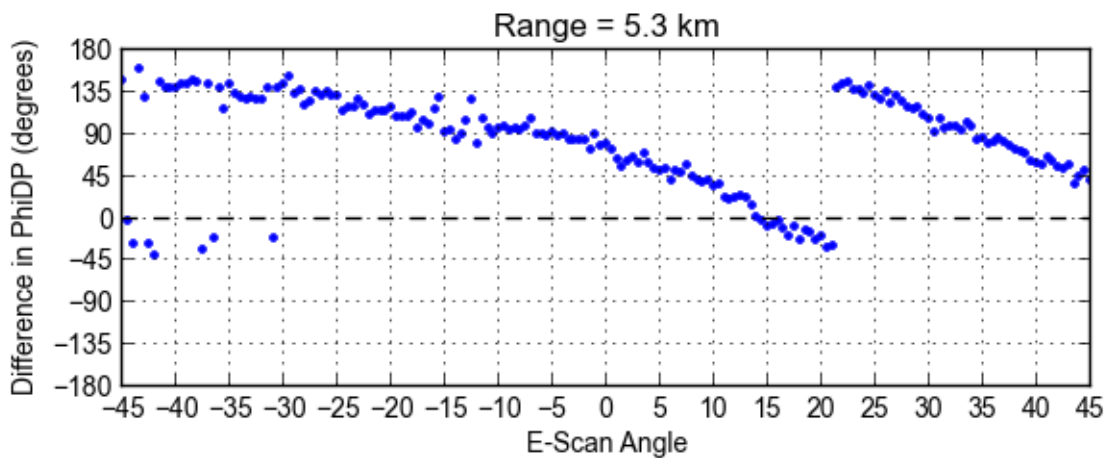
Figure 7.7: PPIs showing differential phase for electronic scan, using the phase rotation table and no rotation, compared to mechanical scan for a weather event on July 27.

phase differs greatly across electronic scan angles and results in a striped pattern in azimuth for the weather target. Furthermore, aliasing occurs at multiple electronic scan angles because the starting phase is close to 90° .

The phase rotation table removes the obvious discrepancies between uncorrected electronic scan and mechanical scan. Figure 7.8 shows the differences in differential phase between electronic scan, using the table correction and no correction, and mechanical scan versus azimuth at 5.3 km. While the unrotated differential phase shows differences with mechanical scan up to 160° , for the



(a) Electronic scan using phase rotation table.



(b) Electronic scan using no rotation.

Figure 7.8: Difference in differential phase between electronic scan, using the phase rotation table and no rotation, and mechanical scan at 5.3 km for the July 27 case.

rotated differential phase the difference rarely exceeds 20° .

The vast differences in starting phase for electronic scan suggests that the reference against which differential phase is measured in the FRF166 changes depending on the electronic scan angle. Although the phase rotations generated by the electronic scan calibration do not perfectly account for differences between electronic scan angles, evident by the thin streaks in 7.7a, the rotations keep the starting differential phases far enough from 90° for every electronic scan angle to avoid aliasing for the entire scan.

7.3 June 16, 2018: Front-X versus CHILL X-Band

A hailstorm event on June 16, 2018 observed both by Front-X and the CHILL X-band radar is used to compare the reflectivity, differential reflectivity, differential phase, and velocity data produced by Front-X using the electronic scan mode, with power correction and phase rotation tables and no correction, and the mechanical scan mode against the CHILL X-band radar for visual verification. The storm extends from 10 km to 30 km which makes it useful for examining the data produced by both the short and long pulses because the short to long pulse transition for Front-X occurs near 16 km for these scans. Furthermore, the CHILL X-band radar was coordinated with Front-X to collect data closely spaced in time and at similar elevation angles. Note that the CHILL X-band data was averaged in elevation between 2.4° and 3.4° to approximate the 3° elevation used by Front-X, and in azimuth across 1.5° to approximate the azimuth beamwidth of Front-X. Also, the PPIs use an NCP threshold of 0.5 and a reflectivity threshold of 25 dBZ. Table 7.2 shows how the Front-X and CHILL X-band scans were configured.

Figure 7.9 shows PPIs of reflectivity for electronic scan using the horizontal power correction table and no correction, mechanical scan, and the CHILL X-band for the June 16 hailstorm. Relative to the CHILL X-band data, the electronic scan data has both higher and lower reflectivities, depending on azimuth, range, and/or reflectivity, which is expected based on the results shown in Figures 7.2 and 7.3 due to possible differences in beamshape between electronic scan angles. The mechanical scan data shows reasonable visual agreement with the CHILL X-band data and

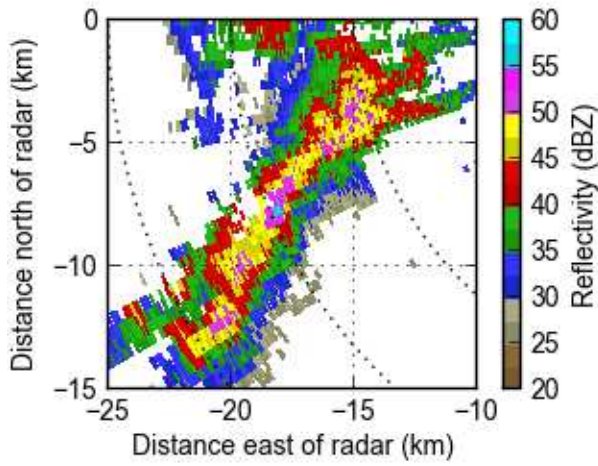
Table 7.2: Electronic and mechanical scan parameters used to collect data on the June 19 weather event.

Parameter	Electronic Scan	Mechanical Scan	CHILL X-band
Start time	18:32:09 UTC	18:31:49 UTC	18:31:25 UTC
Elevation angle	3°	3°	2.4 and 3.4 (avg.)
Electronic scan angles	-45° to 45° (1° incr.)	0°	N/A
Mechanical scan speed	N/A	15°/sec	5°/sec
PRF	1250 Hz	1250 Hz	1000/1500 Hz (dual)
Integration cycle length	90	90	94
Range gate spacing	60 m	60 m	90 m
Polarization Mode	Alternating H/V	Alternating H/V	Simultaneous H/V
Beamshape	Uniform	Uniform	N/A

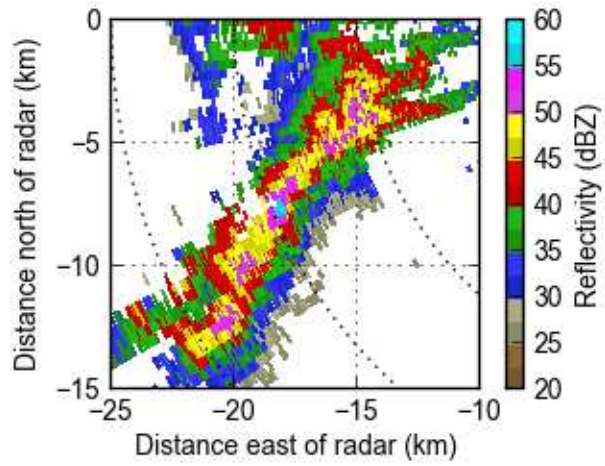
visually, there is good continuity for both mechanical and electronic scan data between the short and long pulse regions.

Figure 7.10 shows PPIs of differential reflectivity for electronic scan using the power correction tables and no correction, mechanical scan, and the CHILL X-band for the June 16 hailstorm. The uncorrected electronic scan data compared to the CHILL X-band data is generally biased high up to 2 dB while the table corrected electronic scan data is generally biased low down to -1 dB, depending on azimuth and range, which is expected based on the results shown in Figures 7.3 and 7.3. The mechanical scan data shows mixed visual agreement with the CHILL X-band: in regions with high differential reflectivity, ~3 dB, the mechanical scan data is biased as high as 0.5 dB, whereas in low differential reflectivity regions, ~0 dB, the mechanical scan data is biased as low as -0.5 dB. Visually, there is good continuity for both mechanical and electronic scan data between the short and long pulse regions.

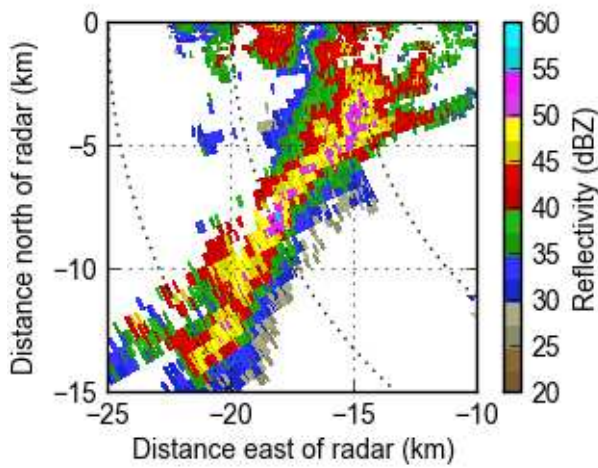
Figure 7.11 shows PPIs of differential phase for electronic scan using the phase rotation table and no rotation, mechanical scan, and the CHILL X-band for the June 16 hailstorm. The unrotated electronic scan data, as expected based on Figure 7.8, has a starting differential phase which differs depending on the electronic scan angle, and exhibits aliasing at electronic scan angles with starting



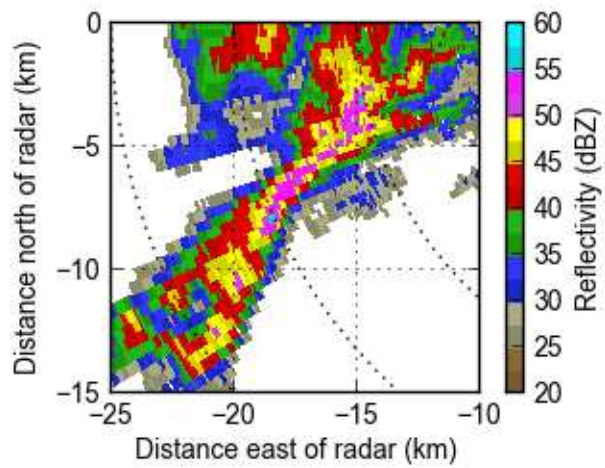
(a) Electronic scan using power correction table.



(b) Electronic scan using no correction.

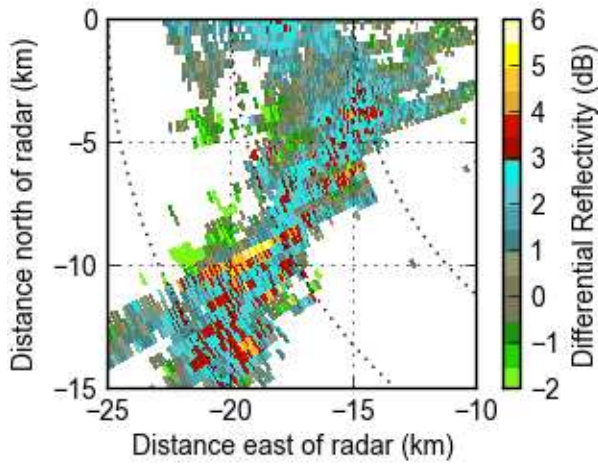


(c) Mechanical scan.

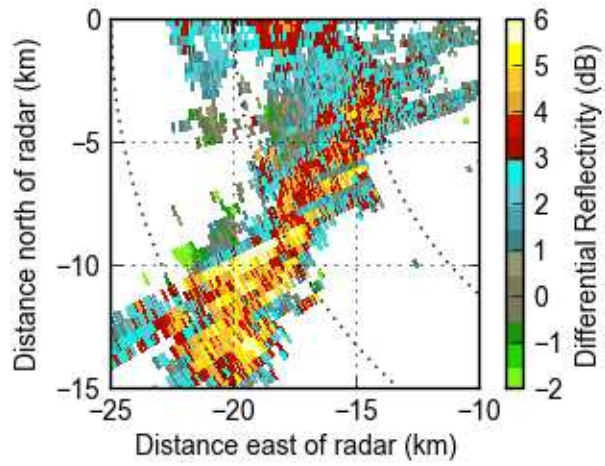


(d) CHILL X-Band.

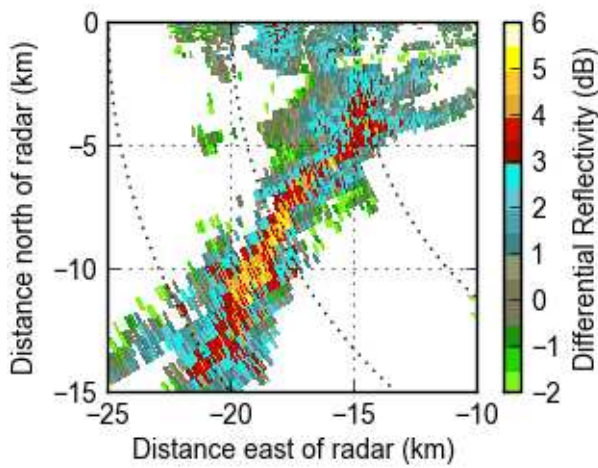
Figure 7.9: PPIs showing reflectivity for Front-X electronic scan, using the horizontal power correction table and no correction, Front-X mechanical scan, and CHILL X-band for the June 19 case.



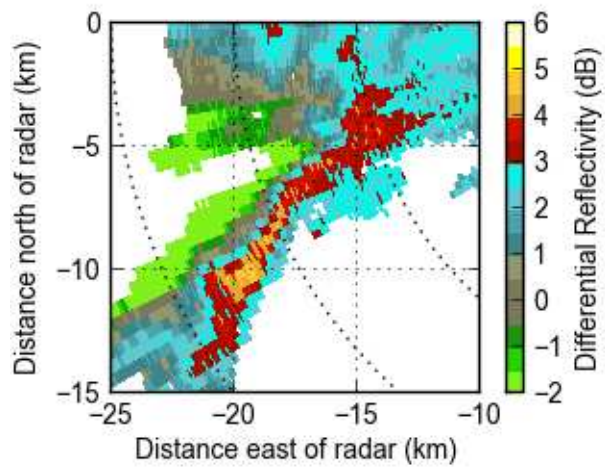
(a) Electronic scan using power correction tables.



(b) Electronic scan using no correction.

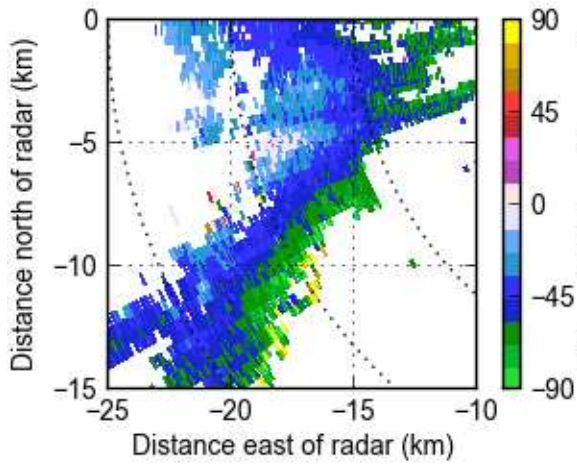


(c) Mechanical scan.

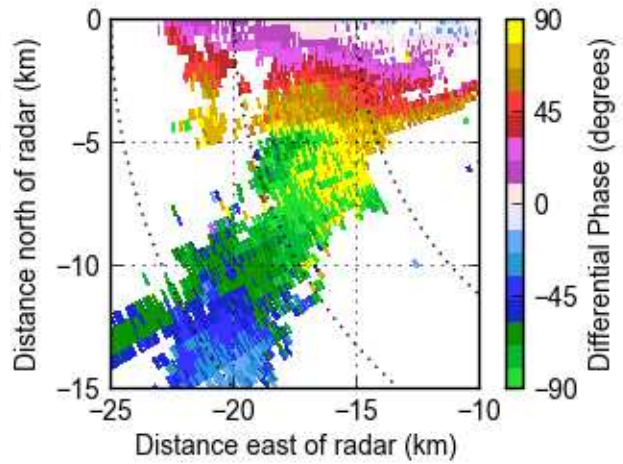


(d) CHILL X-Band.

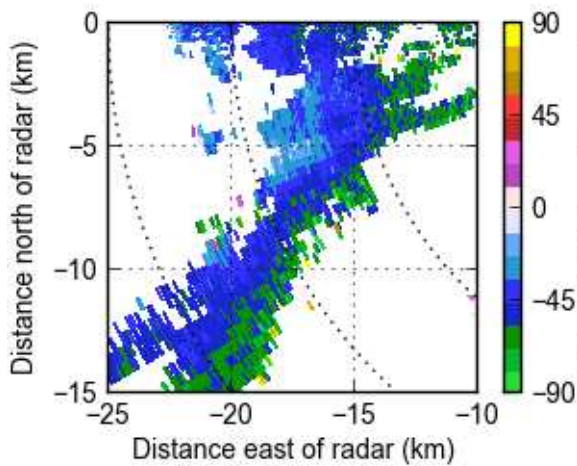
Figure 7.10: PPIs showing differential reflectivity for Front-X electronic scan, using the power correction tables and no correction, Front-X mechanical scan, and CHILL X-band for the June 19 case.



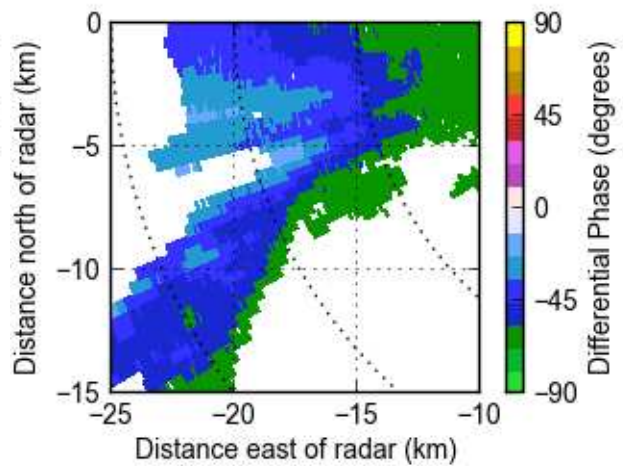
(a) Electronic scan using phase rotation table.



(b) Electronic scan using no rotation.

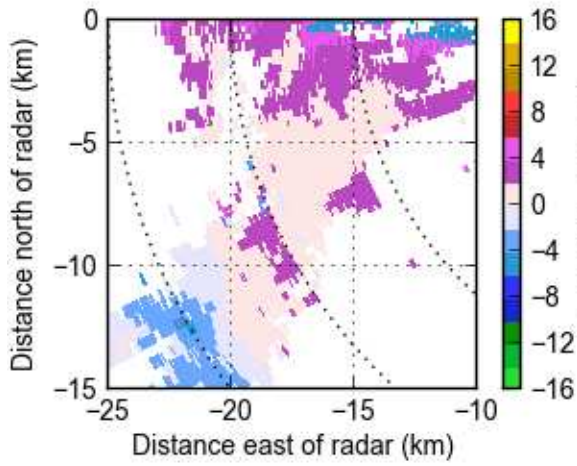


(c) Mechanical scan.

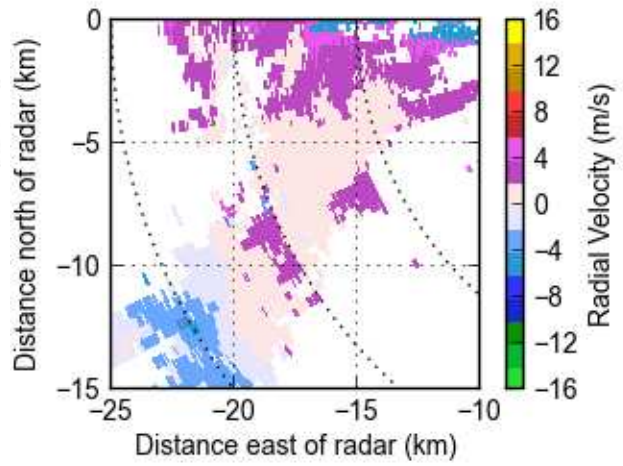


(d) CHILL X-Band.

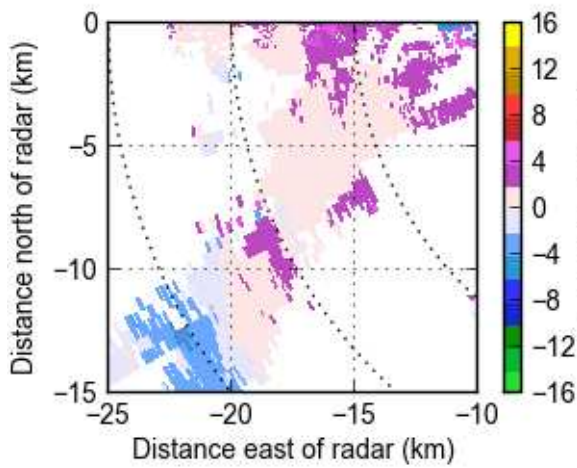
Figure 7.11: PPIs showing differential phase for Front-X electronic scan, using the phase rotation table and no rotation, Front-X mechanical scan, and CHILL X-band for the June 19 case.



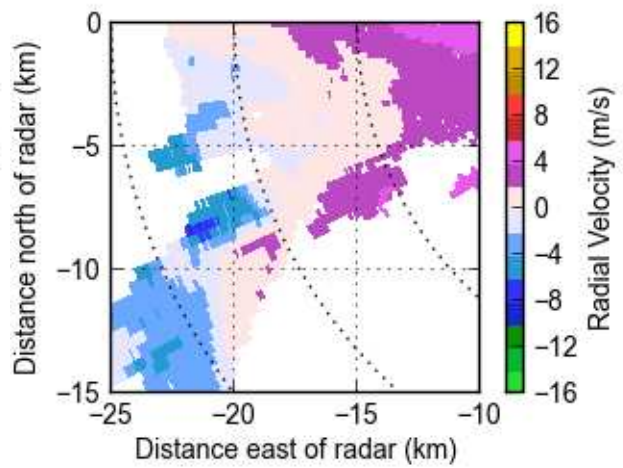
(a) Electronic scan using phase rotation table.



(b) Electronic scan using no rotation.



(c) Mechanical scan.



(d) CHILL X-Band.

Figure 7.12: PPIs showing velocity for Front-X electronic scan, using the phase rotation table and no rotation, Front-X mechanical scan, and CHILL X-band for the June 19 case

phase near 90° . The electronic scan data using the phase rotation table effectively sets a reasonably consistent starting differential phase for the electronic scan angles shown, such that there is no aliasing and decent visual agreement with the mechanical scan data. Although the starting phases differ by up to 10° , the change in differential phase for the electronic and mechanical scans visually agree with the CHILL X-band data.

Figure 7.12 shows PPIs of velocity for electronic scan using the phase rotation table and no rotation, mechanical scan, and the CHILL X-band for the June 16 hailstorm. Both the unrotated and rotated electronic scan data agree visually with the mechanical scan data, and there is reasonable visual agreement of the Front-X data with the CHILL X-band data.

Chapter 8

Summary and Future Work

8.1 Summary

The objective of this thesis was to present the system design and development of a dual-polarization X-band phased array weather radar, Front-X, and demonstrate the system through a comparison of data collected using both electronic and mechanical beam steering. The subsystems of the radars were described and the software design, implementation, and calibration/configuration of the system controller, antenna positioner, and signal processor were discussed in detail. To demonstrate the system, weather cases were presented which compare polarimetric data collected with the electronic and mechanical scan modes, using various correction methods, and with the proven CHILL X-band radar as verification.

The system controller software coordinates the phased array radar subsystems in order to execute commands from a client to configure the system, manage a task-list, and run scans using several different scan modes. The software design uses a multi-threaded architecture to maintain asynchronous connections to the radar subsystems, including the FRF166 phased array antenna, Digital Exciter/Receiver, and antenna positioner. A master thread receives high-level commands from a client through a network interface and breaks them down into coordinated, subsystem specific commands that are sent to subsystem handler threads which each manage an independent subsystem connection. Two data collection scan modes have been implemented, including an electronic scan mode which uses the electronic beam steering capability of the phased array antenna, and a mechanical scan mode which uses the mechanical beam steering capability of the antenna positioner. Additionally, two calibration modes were implemented: an electronic scan calibration mode which maintains a fixed pointing angle towards a calibration target for each electronic scan angle in order to characterize amplitude and phase differences caused by electronic beam steering,

and a noise calibration mode which measures the noise floor of the system in order to perform noise subtractions and calculate signal-to-noise ratio.

The antenna positioner subsystem uses a servo-mechanism to precisely control the position and velocity in azimuth and elevation of the phased array antenna for scan repositioning and mechanical beam steering. The antenna positioner hardware consists of a pedestal which houses the gearboxes and to which the antenna is mounted, the mobile radar platform, platform leveling measurement system, encoders for antenna position feedback, servo-drives/motors to actuate the positioner, and the motion control computer which hosts the Antenna Positioner Controller software that controls the subsystem. APC communicates with the system controller, receiving commands to position and sweep the antenna and returning the status of the antenna positioner. A multi-threaded architecture is used to manage the antenna positioner hardware, including a servo-drive handler thread for each axis which implements a PID control algorithm and sends velocity commands to a servo-drive, and an encoder handler thread which ingests the encoder output to calculate position and velocity which is used as input to the PID control algorithm. The methods used to configure and calibrate the antenna positioner were discussed, including tuning the PID control system and determining the azimuth and elevation encoder offsets.

The signal processor subsystem processes the timeseries and metadata output by the Digital Exciter/Receiver to generate, store, and display weather data in real-time. The signal processing software uses a thread-pool design in order to process the polarimetric meteorological moments in parallel, leveraging the multicore processor of the host computer for faster processing. Downstream software is used to archive both the timeseries and moment data, and display the moment data in real-time. Four processing modes have been implemented, including single and alternating polarization modes for both electronic and mechanical scanning; in addition to an electronic scan calibration mode for calculating electronic scan corrections for reflectivity, differential reflectivity, and differential phase, and a noise calibration for calculating the noise floor of the system. The methods used to calibrate the radar to configure the signal processor were discussed, including

specification of the short-to-long pulse transition, calculation of the radar constant, measurement of the Z_{dr} bias, and example results from the electronic scan calibration mode.

The Front-X radar was demonstrated by presenting two weather cases: one which compares polarimetric data collected with an electronic scan mode and a mechanical scan mode, and the other which uses polarimetric data from the CHILL X-band data as visual verification of the Front-X data. PPIs of reflectivity, differential reflectivity, and differential phase collected with the mechanical and electronic scan modes, with a theoretical correction, an experimental correction using the electronic scan calibration mode, and no correction, are plotted side-by-side. Furthermore, the difference between mechanical scan and electronic scan data versus azimuth are plotted to show the apparent dependence on electronic scan angle as well as the performance of the correction methods. Polarimetric data from the proven and well-calibrated CHILL X-band radar, collocated with the Front-X radar, was used to visually verify reflectivity, differential reflectivity, differential phase, and velocity data collected with the electronic and mechanical scan modes, demonstrating that there is reasonable visual agreement of the data collected with the two systems.

The result of this thesis is a phased array weather radar capable of performing automated scans and a demonstration of the system through a comparison of polarimetric weather data collected using electronic and mechanical beam steering. Front-X can serve as a research test-bed for implementing adaptive scan strategies using electronic and mechanical beam steering and investigating phased array radar calibration methods.

8.2 Future Work

Future work on Front-X which are outside of the scope of this thesis are suggested in this section. This includes improvements and additions to the system controller, antenna positioner, signal processor, and further analysis of the weather data output of the radar.

New scan modes in the system controller which combine electronic and mechanical beam steering and use adaptive scan strategies could be developed in order to reduce scan times and improve the temporal resolution of the data collected by the system. Currently, in order to perform

a 360° volume scan using the electronic scan mode, a radar task must be executed for each quadrant which requires four reposition moves. It is possible that a scan mode which uses the electronic beam steering in the electronic RHI configuration of the antenna and mechanical beam steering in azimuth would greatly reduce time needed to complete a volume scan. Additionally, implementing a scan mode which could allocate more time to sample regions of interest could further improve temporal resolution of the data, perhaps by reducing the number of integrations or increasing the electronic scan angle increment in areas more likely to have clear air.

A more sophisticated control system in APC and the integration of the radar with the platform described in Section 5.2.5 and would improve the performance of the antenna positioner. Possibilities for an improved control system in APC would be a multi-tiered PID system, which uses different sets of PID gains depending on the distance of the antenna from the target position, or a feedforward system. This would allow more control over the position loop tuning and potentially reduce reposition times while avoiding position overshoot. Additionally, integrating into the system the platform described in Section 5.2.5, which uses outriggers and an all steel design, would improve stabilization and rigidity of the positioner compared to the current platform, allowing for more precise positioning and ease of leveling for remote deployments.

Possible additions and improvements to the signal processor include the implementation of spectral processing algorithms, new processing modes to accompany new scan modes, and improved calibration values. Spectral processing algorithms would enable the implementation of ground clutter filtering and new processing modes would likely be necessary for processing the timeseries data collected in scan modes which combine electronic and mechanical beam steering and which use adaptive scan strategies. To improve the accuracy and quality of the data output by the signal processor, the calibration and correction values could be further refined by using more iterations of the calibration methods discussed in Section 6.5 or using new methods altogether. Furthermore, more quantitative analysis of electronic and mechanical scan data, and quantitative verification with the CHILL X-band radar and potentially other radars would provide more insight

as to how to improve the calibration and correction methods and the system as a whole, as well as on the feasibility of phased array weather radars in general.

Bibliography

- [1] D. Zrníc *et al.*, “Agile-beam phased array radar for weather observations,” *Bulletin of the American Meteorological Society*, vol. 88, pp. 1753–1766, November 2007.
- [2] C. Nguyen and V. Chandrasekar, “A space-time model for electronic scan for phase array weather radar,” *2011 IEEE RadarCon*, pp. 1086–1090, May 2011.
- [3] M. Weber, J. Y. N. Cho, J. S. Herd, J. M. Flavin, W. E. Benner, and G. Torok, “The next-generation multimission U.S. surveillance radar network,” *Bulletin of the American Meteorological Society*, vol. 88, pp. 1739–1751, November 2007.
- [4] A. Ryzhkov, S. Giangrande, V. Melnikov, and T. Schuur, “Calibration issues of dual-polarization radar measurements,” *Journal of Atmospheric and Oceanic Technology*, vol. 22, pp. 1138–1155, August 2005.
- [5] G. Zhang, R. Doviak, D. Zrníc, and J. Crain, “Phased array radar polarimetry for weather sensing,” *IEEE International Geoscience and Remote Sensing Symposium*, pp. 449–452, July 2008.
- [6] R. Serafin and R. Strauch, “Meteorological radar signal processing in air quality meteorology and atmospheric ozone’,” *American Society for Testing and Materials*, pp. 159–182, 1977.
- [7] R. Doviak and D. Zrníc, *Doppler Radar and Weather Observations*. Academic Press, 1984.
- [8] R. Rinehart, *Radar for Meteorologists*. Rinehart Publications, 2010.
- [9] V. Bringi and V. Chandrasekar, *Polarimetric Doppler Weather Radar: Principles and Applications*. Cambridge University Press., 2001.
- [10] M. Skolnik, *Radar Handbook*. McGraw Hill, 2008.
- [11] D. Zrníc, “Weather radar polarimetry: Trends toward operational applications,,” *Bulletin of the American Meteorological Society*, vol. 77, pp. 1529–1534, 1996.

- [12] C. Balanis, *Antenna Theory: Analysis and Design*. John Wiley & Sons, Inc., 1997.
- [13] R. Mailloux, *Phased Array Antenna Handbook*. Artech House, 2005.
- [14] S. Orfanidis, *Electromagnetic Waves and Antennas*. Rutgers University, 2016.
- [15] L. Sankey, *FRF-166 Prototype PTWR Antenna User's Guide*. First RF Corporation, December 2012.
- [16] J. George, "CSU solid-state digital exciter/receiver," tech. rep., Colorado State University, March 2018.
- [17] Advanced Motion Controls, 3805 Calle Tecate, Camarillo, CA 93012-5068, *DriveWare 7 Setup Software Quick Reference*, February 2015.
- [18] A. Savitzky and M. J. E. Golay, "Smoothing and differentiation of data by simplified least squares procedures," *Analytical Chemistry*, vol. 36, pp. 1627–1639, July 1964.
- [19] A. Fan, "How to improve the accuracy of inclination measurement using an accelerometer," *Analog Dialogue*, vol. 52, pp. 1–2, February 2018.
- [20] K. J. Astrom and R. M. Murray, *Feedback Systems*. Princeton University Press, 2 ed., February 2009.
- [21] K. H. Ang, G. Chong, and Y. li, "Pid control system analysis, design, and technology," *IEEE Transactions on Control Systems Technology*, vol. 13, p. 560, July 2005.
- [22] J. Ziegler and N. Nichols, "Optimum settings for automatic controllers," *Transactions of the A.S.M.E.*, pp. 764–765, November 1942.
- [23] A. Zahrai and D. Zrnica, "The 10-cm-wavelength polarimetric weather radar at noaa's national severe storms laboratory," *Journal of Atmospheric and Oceanic Technology*, p. 655, October 1993.

- [24] J. Hubbert, V. Bringi, and D. Brunkow, “Studies of the polarimetric covariance matrix. part i: Calibration methodology,” *Journal of Atmospheric and Oceanic Technology*, p. 697, May 2003.
- [25] K. McClaning and T. Vito, *Radio Receiver Design*. SciTech Publishing, Inc., 1959.
- [26] T. Seliga, V. Bringi, and H. Al-Khatib, “Differential reflectivity measurements in rain: First experiments,” *IEEE Transactions on Geoscience Electronics*, pp. 240–244, October 1979.
- [27] R. Bechini, L. Baldini, and E. G. R. Cremonini, “Differential reflectivity calibration for operational radars,” *Journal of Atmospheric and Oceanic Technology*, p. 1543, September 2008.
- [28] W. Patterson *et al.*, “Engineer’s refractive effects prediction systems (EREPS),” tech. rep., Naval Command, Control, and Ocean Surveillance Center TD 2648, May 1994.